Auðkenning próteina sem tengjast Aquaporin 4 próteininu

Marteinn Þór Snæbjörnsson

Ritgerð til meistaragráðu

Leiðbeinandi: Pétur Henry Petersen

Meistaranámsnefnd: Eiríkur Steingrímsson og Sigurður Víðir Smárason

Lífvísindasetur Læknagarðs

Læknadeild

Heilbrigðisvísindasvið Háskóla Íslands

Ágúst 2010

Identification of proteins interacting with Aquaporin 4

Marteinn Þór Snæbjörnsson

Thesis submitted for the degree of Master of Science

Supervisor: Pétur Henry Petersen

Masters committee: Eiríkur Steingrímsson and Sigurður Víðir Smárason

Biomedical center

Faculty of Medicine

School of Health Sciences University of Iceland

August 2010

Prentun: Háskólaprent ehf.

Reykjavík, Ísland 2010

Ágrip

Aquaporin 4 (AQP4) próteinið er helsta vatnsflutningsprótein í miðtaugakerfi spendýra. AQP4 finnst í mestu magni á þeim stöðum þar sem heilavefur liggur að blóði eða heilahimnuvökva, eins og t.d í stjarnfrumum sem umlykja háræðar heilans og ependymal frumum við heilahol. Staðsetning AQP4 innanfrumu er skautuð, í stjarnfrumum finnst það fyrst og fremst við blóð-heila múrinn í endafótum við háræðar og í ependymal frumum er það einungis staðsett basolateral. Margar rannsóknir benda til þess að AQP4 sé staðsett í endafótunum af dystrophin prótein flókanum, það er hins vegar ekki vitað hvernig AQP4 tengist honum.

Á innanfrumu C-enda sínum hefur AQP4 röð sem er þekkt fyrir að bindast PDZ (PSD-95, DLG, ZO-1) hneppum en velþekkt hlutverk próteina sem innihalda PDZ hneppi er að staðsetja himnuprótein á ákveðnum svæðum í himnum fruma. Sú tilgáta hefur verið sett fram að α-Syntrophin, sem er PDZ prótein og tilheyrir dystrophin prótein flókanum, bindist AQP4. Þetta er byggt á því að AQP4 tapar staðsetningu sinni í heilum α-Syntrophin$^{-/-}$ músa. Það hefur hins vegar ekki verið sýnt fram á það hingað til að AQP4 bindist α-Syntrophin né nokkru öðru PDZ próteini.

Í þessari rannsókn sem er byggð á niðurstöðum sem áður fengust með Y2H (Yeast two hybrid) skimun, var notast við *in vitro* greiningaraðferðina GST (Glutathione-S-Transferase) niðurtog sem og ónæmislitanir til að auðkenna prótein sem bindast við innanfrumu C-enda AQP4. Auk þess var þróað samræktunarmódel með stjarnfrumum úr músum og HUVEC (Human Umbilical Vein Endothelial Cells) frumum með það að markmiði að líkja eftir myndun endafóta stjarnfruma *in vivo*.

Með því að nota Syntrophin mótefni sem þekkir α, β1 og β2 Syntrophin ísóformin til að skoða niðurstöður GST niðurtogs sem framkvæmt var á frumulysati 293T fruma á western blotti kom í ljós að Syntrophin úr 293T frumum binst AQP4 PDZ háð en í Y2H skimuninni sýndi α-Syntrophin ekki bindingu við AQP4. Hugsanlegt er að AQP4 bindist α-Syntrophin beint en bindingin greindist ekki í Y2H mögulega vegna rangra breytinga á próteininu eftir þýðingu. Einnig gæti AQP4 bundist α-Syntrophin óbeint gegnum áður óþekktan millilið eða bundist β1 eða β2 Syntrophin beint en bæði próteinin eru hluti af dystrophin prótein flókanum líkt og α-Syntrophin.

Sýnt var fram á að AQP4 binst sértækt við tíunda PDZ hneppi Mupp1 (Multiple PDZ domain protein 1). Engu að síður sýndu AQP4 og Mupp1 ekki sömu staðsetningu *in vitro* í frumurækt né *in vivo* í heila og nýrnasneiðum. Hins vegar var áður óþekkt binding AQP4 við PDZ próteinið Patj, sem er náskylt Mupp1, uppgötvuð með GST niðurtogi. Patj og AQP4 sýndu sömu staðsetningu í frumuhimnum í frumurækt og í kringum háræðar heilans í heilasneiðum úr músum. Þessar niðurstöður benda til þess að AQP4 og Patj bindist hvort öðru í endafótum stjarnfruma.

Þetta er í fyrsta skipti sem sýnt er fram á PDZ háða bindingu AQP4 við önnur prótein og gæti mögulega aukið skilning á virkni AQP4 og varpað ljósi á það hvernig það er staðsett í endafótum stjarnfruma.

Abstract

The Aquaporin 4 water channel is the primary aquaporin in the mammalian central nervous system. The highest concentration of AQP4 is observed where the brain interfaces with blood and cerebrospinal fluid such as in astrocytes surrounding brain capillaries and ependymal cells lining the ventricles. AQP4 displays a polarized subcellular distribution. In astrocytes it is chiefly found in perivascular endfeet at the blood brain barrier and in ependymal cells it is located basolaterally. Strong evidence indicate that AQP4 is anchored at the perivascular endfeet by the dystrophin complex, it is however not known how AQP4 is linked to the dystrophin complex.

At its cytoplasmic C-terminal AQP4 contains a sequence motif known to interact with PDZ domains. A well known function of proteins containing PDZ domains is to localize membrane proteins to specific subcellular domains. It has been hypothesized that α-Syntrophin, which is a PDZ protein and a member of the dystrophin complex, interacts with AQP4, based on the observation that AQP4 is mislocalized in the brains of α-Syntrophin mutant mice. However to date AQP4 has not been shown to interact with α-Syntrophin or any other PDZ domain protein.

In this study, which is based on a previously performed Y2H screen, the *in vitro* protein interaction assay GST pulldown as well as immunostaining of tissue sections and cell cultures were used to identify proteins interacting with the cytoplasmic C-terminal of AQP4. Additionally, a coculture model of primary mouse astrocytes and HUVECs was developed to model the formation of astrocyte endfeet *in vivo*.

Using a Syntrophin antibody that recognizes the α, β1 and β2 Syntrophin isoforms to visualize the results of a GST pulldown carried out on 293T cell lysate on western blot revealed that a Syntrophin, endogenous to 293T cells, interacts with AQP4 in a PDZ specific manner. However, in the Y2H screen α-Syntrophin did not interact with AQP4. It is possible that AQP4 interacts directly with α-Syntrophin and the Y2H result is a false negative possibly due to incorrect post translational modification. However, assuming that the Y2H result is true this indicates that AQP4 interacts either with α-Syntrophin indirectly through an unknown intermediate protein or directly with β1 or β2 Syntrophin that are both part of the dystrophin complex.

It was demonstrated that AQP4 interacts specifically with the 10th PDZ domain of Mupp1 a PDZ scaffolding protein, yet AQP4 and Mupp1 did not show any colocalization *in vitro* in cell culture or *in vivo* in brain and kidney sections. However, a novel PDZ dependent interaction of AQP4 with the PDZ scaffolding protein Patj, a paralogue of Mupp1, was identified using GST pulldown. Moreover Patj and AQP4 colocalized at the cell membrane of 293T cells and around capillaries in mouse brain sections. These results strongly suggest that AQP4 and Patj interact in astrocyte perivascular endfeet.

This is the first time AQP4 is shown to interact with other proteins in a PDZ specific manner and has the potential to shed a new light on the function of AQP4 and reveal how it is localized to the astrocyte endfeet.

Acknowledgements

I am truly grateful for the opportunity given to me to work in the fields of neurobiology and molecular biology in the Laboratory for neurobiology at Læknagarður. I would like to thank several people for their support and contributions to this project.

I am first and foremost thankful to my supervisor **Dr. Pétur H. Petersen** for giving me the opportunity to conduct this masters project. He has been a great mentor and I have benefited greatly from his guidance.

I would also like to express my gratitude to **Dr. Finnbogi R. Þormóðsson** at the Laboratory for neurobiology for his help and guidance through the past years.

Dr. Torgeir Holen at the Department of medicine of the University of Oslo, also deserves my deepest gratitude for his guidance when I stayed at his laboratory during the summer of 2009.

I am also grateful to my co-workers and friends at the Laboratory for neurobiology and at læknagarður for their help and companionship, especially my fellow students at the Laboratory for neurobiology **Anna Þ. Pétursdóttir, Bjarni Þ. Sigurðsson, Indíana E. Ingólfsdóttir** and **Guðrún Jónsdóttir**.

I would also like to acknowledge the following individuals for their contributions to my project:

Brynhildur Thors M.Sc at the Department of Pharmacology and toxicology for providing HUVECs.

Dr. Alexander Schepsky at the Department of Biochemistry and Molecular Biology for his assistance during my initial GST pulldown experiments and for providing the HEK 293T cells.

Dr. Eiríkur Steingrímsson at the Department of Biochemistry and Molecular Biology and a member of my masters committee who has assisted me in many ways during my studies.

Finally I am very grateful to my girlfriend **Wally Bluhm** and my family for their invaluable support and encouragement during my studies.

Table of Contents

Ágrip **3**
Abstract **4**
Acknowledgements **5**
Table of Contents **7**
Figures and Tables **9**
Abbreviations **10**
1 Introduction **13**
1.1 Aquaporins 13
1.2 Astrocytes and the neurovascular unit 14
1.3 Aquaporin 4 16
1.3.1 Expression of AQP4 16
1.3.2 The ultrastructure of AQP4 17
1.3.3 The functions of AQP4 in the CNS 18
1.3.4 The localization of AQP4 19
1.4 PDZ domain proteins 20
2 Aims of the study **23**
3 Materials and Methods **25**
3.1 Cell culture 25
3.1.1 HEK 293T cells 25
3.1.2 CRL-2006 25
3.1.3 Primary astrocytes 25
3.1.4 HUVECs 26
3.2 Transfection 26
3.3 Coculture of primary astrocytes and HUVECs 26
3.4 Immunohistochemistry 26
3.5 Immunocytochemistry 27
3.6 Confocal microscopy 27
3.7 Bacterial Transformation 27
3.8 Preparing the GST, AQP4-GST and 3A-GST beads for GST pulldown 28
3.9 GST pulldown 28
3.10 Western blotting 29
3.11 Coomassie staining 30
3.12 Cloning 30
4 Results **35**
4.1 Validation of the GST fusion proteins 35
4.2 GST pulldown of Mupp1 35
4.2.1 Optimization of Mupp1 GST pulldown and pulldown of endogenous Mupp1 35
4.2.2 GST pulldown of Mupp1 7xMyc, Mupp1 9+10 and Mupp1 7+8 36
4.3 Coimmunostaining of tissue sections for AQP4 and Mupp1 38
4.4 GST pulldown of Patj and in vitro coimmunosaining of Patj and AQP4 40
4.5 Coimmunostaining of tissue sections for AQP4 and Patj 42

4.6 Establishing primary astrocyte-HUVEC cocultures ... 45
4.7 Patj in primary astrocyte-HUVEC cocultures ... 49
4.8 GST pulldown of Syntrophin ... 49
4.9 GST pulldown of Sephs1-Myc and Ubiquitin ... 50
5 Discussion ... 53
5.1 The interaction of AQP4 with Mupp1 ... 53
5.2 The interaction of AQP4 with Patj ... 53
5.2.1 Colocalization and interaction of Patj and AQP4 in vitro ... 53
5.2.2 Immunostaining of tissue sections for Patj ... 54
5.2.3 Establishing primary astrocyte-HUVEC cocultures and Patj immunostaining of cocultures ... 54
5.2.4 Possible roles of the AQP4-Patj interaction ... 55
5.3 The interaction of AQP4 with a Syntrophin endogenous to 293T cells ... 55
5.4 The interaction of AQP4 with Sephs1 and Ubiquitin ... 56
5.5 Future perspectives ... 57
5.5.1 Patj ... 57
5.5.2 Syntrophin ... 57
6 Concluding remarks ... 59
Appendix ... 61
References ... 63
Published paper ... 71

Figures and Tables

Figure 1. The complex morphology of astrocytes 14
Figure 2. AQP4 and AQP1 expression in the brain 16
Figure 3. Square arrays 17
Figure 4. Validation of the GST beads 35
Figure 5. Mupp1 endogenous to 293T cells interacts with AQP4 36
Figure 6. Schematic picture of Mupp1 37
Figure 7. The 10th PDZ domain of Mupp1 interacts with AQP4 37
Figure 8. AQP4 and Mupp1 do not colocalize around brain capillaries 38
Figure 9. AQP4 and Mupp1 do not colocalize in ependymal cells 39
Figure 10. AQP4 and Mupp1 do not colocalize in the kidney 39
Figure 11. Schematic picture of Patj 40
Figure 12. Patj interacts with AQP4 41
Figure 13. Patj colocalizes with AQP4 *in vitro* 42
Figure 14. Patj and AQP4 colocalize with Syntrophin around brain capillaries 43
Figure 15. Patj and AQP4 colocalize around brain capillaries 44
Figure 16. Patj and AQP4 do not colocalize in kidney 44
Figure 17. Cocultures of primary astrocytes and HUVECs 45
Figure 18. GFAP and CD31 immunostaining of cocultures 46
Figure 19. AQP4 is polarized around HUVEC colonies 47
Figure 20. Syntrophin colocalizes with AQP4 and Patj in astrocytes 48
Figure 21. Syntrophin endogenous to 293T cells interacts with AQP4 49
Figure 22. GST pulldown of Sephs1-Myc 50
Figure 23. GST pulldown of Ubiquitin endogenous to 293T cells 51
Table 1. Classification of PDZ ligands 21
Table 2. Preparation of acrylamide gels for protein electrophoresis 29
Table 3. Primers used to clone the AQP4 cytoplasmic tail and Sephs1 31
Table 4. Comparison of PDZ domains amino acid sequence 41
Table 5. List of antibodies used in this study 61
Table 6. List of plasmids used in this study 61

Abbreviations

AQP	Aquaporin
NPA	asparagine-proline-alanine motif
CNS	Central nervous system
eGFP	enhanced Green Fluorescent protein
BBB	Blood Brain Barrier
ISF	Interstitial fluid
HUVEC	Human Umbilical Vein Endothelial Cells
fMRI	functional Magnetic Resonance Imaging
MIWC	Mercury Insensitive Water Channel
DMD	Duchenne Muscular Dystrophy
CSF	Cerebral Spinal Fluid
SON	Supra Optic Nucleus
PKC	Protein Kinase C
CHO	Chinese Hamster Ovary
ECS	Extra Cellular Space
DAP´s	Dystrophin Associated Proteins
MDX	X chromosome linked Muscular Dystrophy
MDCK	Madine Darby Canine Kidney (cell line)
CKII	Casein Kinase II
PDZ	PSD 95 DLG ZO-1
HEK 293T	Human Embryonic Kidney 293 T antigen (cell line)
SSV	Serine Serine Valine
Y2H	Yeast Two Hybrid
GST	Gluthathione-S-Transferase
BN Page	Blue Native Page
DMEM	Dulbecco´s Modified Eagle Medium
FBS	Fetal Bovine Serum
PBS	Phosphate Buffered Saline

EGM	Endothelial Growth Medium
hEGF	human Epidermal Growth Factor
hFGF-B	human Fibroblast Growth Factor B
VEGF	Vascular Endothelial Growth Factor
R_3-IGF-1	human Recombinant Insuline like Growth Factor 1
RT	Room Temperature
NGS	Normal Goat Serum
ON	Over Night
IPTG	Iso Propyl Thio Galactose
PMSF	Phenyl Methane Sulfonyl Fluoride
DTT	Dithiothreitol
BSA	Bovine Serum Albumine
LTB	Lower Tris Buffer
UTB	Upper Tris Buffer
ECL	Enhanced Chemi Luminescence
PCR	Polymerase Chain Reaction

1 Introduction

1.1 Aquaporins

Water is a major component of all cells and the transmembrane transfer of water in and out of cells is important for maintaining their volume, shape and metabolism. How water travels across the plasma membrane was for decades a matter of debate, the prevailing hypothesis being that water travels across the plasma membrane via passive diffusion. However a minority of the scientific community favoured the idea that water travels across the membrane via hypothetical water pores as well as by passive diffusion (1). Several observations supported this hypothesis. The high water permeability of red blood cells and renal tubules compared to other cells suggested a direct mechanism, and the fact that this high water permeabilty can be reversibly inhibited by mercuric ions (2) could not be explained by passive diffusion alone. Same is true for the changes in water permeabilty of the mammalian renal collecting duct and the amphibian bladder in response to the hormone vasopressin (1, 3). The water transport debate was put to rest in 1992 with the discovery of the CHIP28 protein as a water transport molecule, later to be named Aquaporin 1 (AQP1) (4, 5).

Aquaporins are water channels which allow the passage of water in response to osmotic pressure. They are divided into two groups based on their permeability; water specific aquaporins and aquaglyceroporins. Aquaporins can be found in all kingdoms of life, eubacteria usually have only one water specific aquaporin and one aquaglyceroporin while more compartmentalized orgnisms such as plants express many more, the plant *Arabidopsis thaliana* for example has at least 37 aquaporins (6). To date 13 Aquaporins have been discovered in mammals, AQP0-AQP12, each of them with specific subcellular and tissue distribution. In mammals the water specific aquaporins are AQP0, 1, 2, 4, 5, 6 and 8. With the exception of AQP6 and 8, which in addition to water are also permeated by anions and free radicals respectively, these channels are very specific for water transport denying even the hydronium ion passage. The aquaglyceroporins AQP3, 7, 9 and 10 are all highly permeable by glycerol in addition to water (7). AQP11 and 12 are the most recent members of the mammalian aquaporin family to be discovered and it is not known to what extent they are permeated by water or any solutes (8).

Based on primary amino acid sequence it was predicted that AQP1 and AQP0 consisted of six transmembrane helices and five connecting loops (A-E) with loops A,C and E on the extracellular side of the membrane but loops B and D on the cytoplasmic side (4, 9). Loops B and E which are hydrophobic both contain an asparagine-proline-alanine (NPA) motif that is highly conserved among AQPs. Using site directed mutagenesis Jung and colleagues showed that the NPA motifs are essential for the water transport function of AQP1 and proposed the so called „Hourglass model“ for AQP structure (10). This model proposes that the NPA containing loops E and B dip into the membrane from the extracellular and cytoplasmic sides respectively and form the pore. Later studies on AQP structure confirmed this model (11, 12) and showed that the NPA motifs

plays a crucial role in the selectivity of AQP´s for water (13, 14). All Aquaporins studied to date form a tetramer in the cell membrane and are unstable as monomer (15). The helices of each AQP monomer which face the membrane are hydrophopic but those who face the center of the tetramer are hydrophilic (7).

1.2 Astrocytes and the neurovascular unit

Glial cells are the nonneuronal cells of the CNS (Central Nervous System); astrocytes, oligodendrocytes and microglia. These cells have diverse and important roles in the CNS; oligodendrocytes provide axons with the insulating myelin sheath, the microglia are the immune cells of the CNS and astrocytes are the primary support cells of neurons providing them with nutrients, removing their waste, clearing excess neurotransmitters at synapses and maintaining local ion and pH homeostasis (16). Glial cells are generally considered the housekeeping cells of the CNS and earlier generations of neuroscientists found them rather unexciting in comparison to the complexity of neurons and their networks. However, it is becoming clear that the situation is not quite that simple and the role of glia, especially astrocytes, in the CNS is much more important than previously thought.

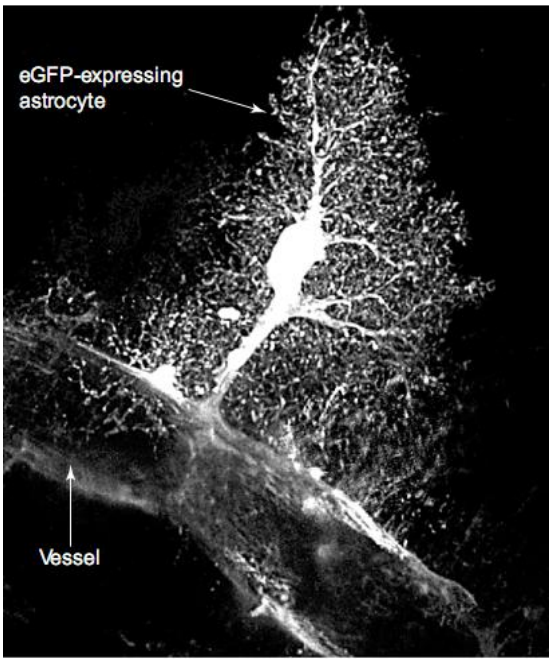

Figure 1. The complex morphology of astrocytes.

A two-photon confocal image of an astrocyte in a cortical slice expressing eGFP (enhanced green fluorescent protein). Notice the complex branching of perisynaptic processes and how the perivascular endfeet envelopes an adjoining capillary. Nedergaard M, et al.(16).

Astrocytes extend numerous processes which branch repeatedly into finer processes defining a specific astrocytic domain which overlaps with the domains of other astrocytes only to a very limited extent (17). These processes, termed perisynaptic processes extend to and are in close contact with all synapses within the astrocytic domain which are estimated to be around 100.000-160.000 for each astrocyte. This highly branched network can clearly be seen in transgenic mice expressing eGFP only in astrocytes (Fig. 1). Astrocytes furthermore extend other larger processes called perivascular endfeet which contact and envelop the capillaries and arterioles of the CNS (18) (Fig. 2). It has recently been shown that the astrocyte endfeet form a continuous sheath covering the brain capillaries leaving no slits between them (19).

In contrast to the endothelial cells found in the capillaries of pheripheral tissues the endothelial cells of brain capillaries form complex tight

junctions between each other, preventing most molecules and also small ions such as Na^+ and Cl^- from going the paracellular route. Only small gaseous molecules such as CO_2 and O_2 as well as small lipophilic agents can diffuse unrestricted through the lipid membranes and into the CNS, all other molecules must rely on specific transcellular transport mechanisms to pass. Small hydrophillic molecules are transferred across by specific ion transporters and transport proteins such as the transport of glucose by the Glut1 transporter, while large peptides such as insulin depend on receptor mediated transcytosis (20). This selective barrier quality of the endothelial lining of brain capillaries is called the blood brain barrier (BBB) (20). The BBB is crucial for the normal function of the CNS, it maintains the chemical composition of the brain interstitial fluid (ISF), which has lower concentration of proteins, Ca^{2+} and K^+ than blood plasma, but higher Mg^{2+} concentration. It also prevents entrance of neuroactive chemicals from the blood to the CNS and clears them out of the brain, against opposing concentration gradient (20, 21).

The ability of the brain capillary endothelial cells to form the BBB is not cell-inherent, instead it seems to be the consequence of induction by their adjacent microenvironment in the brain. Several experiments have shown that this induction is primarily mediated by astrocytes (22). In a critical experiment purified astrocytes injected into the anterior eye chamber of rats formed aggregates, which were quickly vascularized by surrounding tissue with capillaries showing typical BBB characteristics (23). Later experiments have shown that astrocytes induce BBB qualities such as junctional tightening and upregulation of BBB markers in coculture with endothelial cells that do not originate from the CNS such as HUVECs (Human Umbilical Vein Endothelial Cells) and bovine aorta endothelium (21).

It has been suggested that because of their interdependence neurons, astrocytes and endothelial cells of local blood vessels linked together by the astrocytic perisynaptic processes and perivascular endfeet, compose a functional unit called the neurovascular unit, which fulfills several important needs. Functional hyperemia or neurovascular coupling, which is a precise spatial and temporal coupling of neural activity and blood flow in the CNS that makes up the the conceptual basis of fMRI (functional Magnetic Resonance Imaging), seems to be controlled, at least in part, by the neurovascular unit (24, 25). Studies performed *in vitro* on cortical slices (26) and *in vivo* in mice (27) have shown that during neuronal activity glutamate from active synapses binds metabotropic glutamate receptors on perisynaptic processes. The binding of glutamate results in Ca^{2+} release from intracellular stores in waves that spread along the astrocyte to the perivascular endfeet and to other astrocytes via gap junctions where it stimulates the release of vasodilating prostaglandins which act on smooth muscle cells in arterioles and possibly pericytes in capillaries (16). It has also been suggested that glucose metabolism is coupled to neuronal activity. Glucose is transported from the bloodstream through the brain capillary endothelial cells and astrocyte endfeet which both contain large amounts of the glucose transporter Glut1, converted to lactate and then distributed to neurons by astrocytes (28). Evidence exist, which suggest that astrocytes respond to increased neuronal activity by increasing their glycolytic activity and releasing more lactate to neurons (29). Astrocytes also remove excess K^+ generated

by neuronal activity through potassium channels and redistribute it back to neurons (28). However uptake of K^+ by astrocytes causes reduction in extracellular osmolarity so water as well flows into the cell. It has been proposed that the potassium channel Kir4.1 and the water channel AQP4 which are both found in astrocyte perivascular endfeet and perisynaptic processes work in concert to remove K^+ (30).

1.3 Aquaporin 4

Aquaporin 4 (AQP4) was first identified in 1994 and originally named MIWC (mercurial insensitive water channel) as it is the only member of the aquaporin family in mammals that is not inhibited by $HgCl_2$ (31, 32). It is the most highly expressed AQP in the CNS.

1.3.1 Expression of AQP4

AQP4 is expressed in several organs in mammals but predominantly in the brain. It is expressed in the sarcolemma of type II muscle fibers in skeletal muscle (33) and its expression in muscle is significantly reduced in several degenerative muscle diseases including Duchenne muscular dystrophy (DMD) (34). In the kidney AQP4 is expressed in the basolateral membrane of principal cells in the inner medullary collecting duct and $AQP4^{-/-}$ mice display a four-fold decrease in transepithelial water permeability in the inner medullary collecting duct and have a mild urine concentrating defect (35, 36). AQP4 is also expressed in the non-pigmented ciliary epithelium which contributes to the movement of aqueous humor into the anterior chamber of the eye and $AQP4^{-/-}$ mice display reduced intraocular pressure compared to the wild type (37). The Müller cells of the retina express AQP4 as well and $AQP4^{-/-}$ mice exhibit mild impairment in light-neural transduction (38).

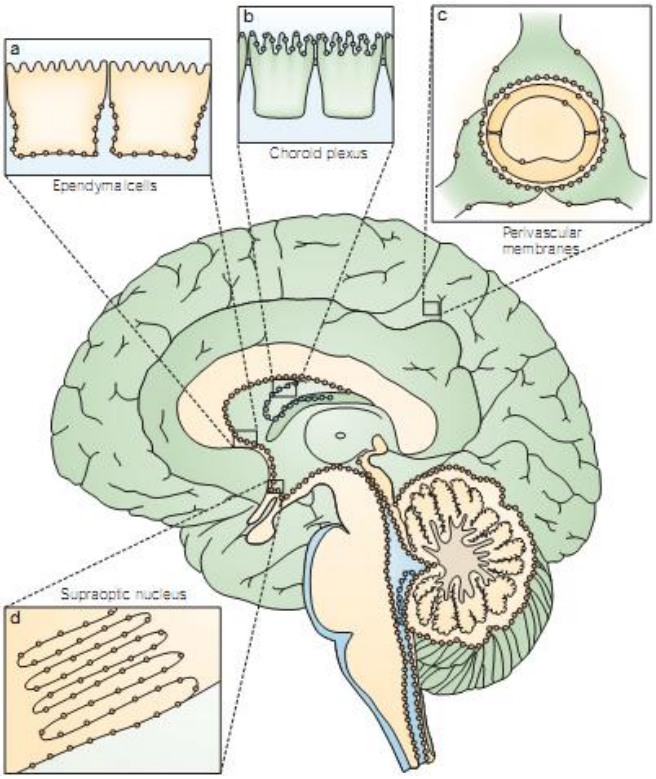

Figure 2. AQP4 and AQP1 expression in the brain. (A) AQP4 is localized basolaterally in ependymal cells lining the ventricles. (B) AQP1 expression in the brain is limited to the choroid plexus. (C) AQP4 is heavily concentrated in the endfeet membranes facing the basal lamina and the BBB. (D) In the supraoptic nucleus AQP4 shows a non-polarized distribution in glial lamellae which ensheath dendrites of local neurons. Amiry-Moghaddam M, et al.(30).

AQP4 is the prime aquaporin in the brain, the other three being AQP1 which within the brain is only known to be expressed in the choroid plexus (30) (Fig 2), AQP9 which is expressed in ependymal cells lining the ventricles

and tanycytes of the hypothalamus (39) and AQP11 which is expressed intracellularly in neurons (40). AQP4 is primarily expressed in subtypes of macroglia in the CNS (astrocytes, and ependymal cells), the highest concentration of AQP4 is observed where the CNS interfaces with blood and cerebrospinal fluid (CSF) such as in astrocyte endfeet by the blood brain barrier, astrocyte endfeet in glia limitans and basolaterally in ependymal cells lining the ventricles (30, 41) (Fig 2). Notably AQP4 is also expressed in glia located in the osmosensitive organs such as the supraoptic nucleus (SON) (Fig 2). SON neurons release the peptide hormone vasopressin which regulates blood osmolality by controlling AQP2 localization in collecting duct cells and consequently the water permeability of the collecting duct (42). Hence it has been suggested that AQP4 might play a role in the osmosensitivity of these organs (43). Interestingly the osmosensitive organs are the only known brain structures where AQP4 localization in glia is nonpolarized with AQP4 uniformly spread across the plasma membrane (44). It has been claimed that brain endothelial cells express AQP4 (45) but this is controversial (46).

1.3.2 The ultrastructure of AQP4

Like most aquaporins, AQP4 forms tetramers in the cell membrane but AQP4 tetrames are unique in their ability to form square arrays which are large assemblies of interconnected tetramers (Fig. 3). Studies on square arrays precede the discovery of the aquaporins, they were discovered in the 70´s using freeze fracture electron microscopy (47, 48) and their composition eluded scientist until the mid 90´s when it was discovered that AQP4 is the basic structural unit of square arrays (49, 50).

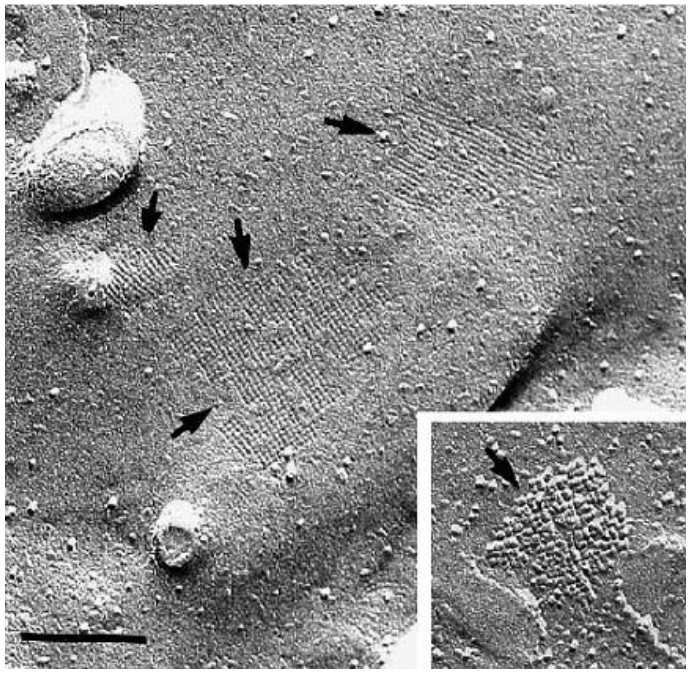

Figure 3. Square arrays.
Freeze fracture electron microscopy image of chinese hamster ovary (CHO) cells stably transfected with AQP4. Large image E face, inset P face. Arrows indicate the location of square arrays. Verbavatz JM, et al.(50).

There are at least three functional isoforms of AQP4 the M1, M23 and Mz isoforms (51) which differ only in the length of their cytoplasmic N-terminal, M23 is shorter than M1 but Mz is longer. M23 is the dominant isoform in the brain and is essential to initiate the formation of square arrays, it can form square arrays alone, the N-terminals of the M1 and Mz isoforms however, inhibit the initiation of square array formation and they can only become part of square arrays if M23 is included (52). The functional role of square arrays is not

well understood although a recent study on *Xenopus* eggs injected with the different AQP4 isoforms showed that upon protein kinase C (PKC) phosphorylation AQP4 is internalized. Cells injected with the M23 isoform exhibit significantly more reduction in water permeability than those injected with the other two isoforms and the M23 isoform is internalized much faster than the longer M1 and Mz isoforms after phosphorylation (53). This indicates that entire square arrays of M23 are being internalized but only individual tetramers of the M1 and Mz isoforms. It is therefore possible that at least one of the roles of square arrays is to provide a fast and efficient way to terminate water flow through AQP4.

1.3.3 The functions of AQP4 in the CNS

No AQP4 deficient humans have been identified but the $AQP4^{-/-}$ mouse has been extensively studied. Under normal circumstances the $AQP4^{-/-}$ mouse does not display any distinct phenotype in the CNS but studies on the $AQP4^{-/-}$ mouse under pathological conditions have revealed potential roles for AQP4 in the CNS which could be of clinical importance (30).

There are two types of edema, cytotoxic and vasogenic, in cytotoxic edema water flows from the vascular compartments through the intact BBB and perivascular endfeet into the neuropil and accumulates primarily in astrocytes, in vasogenic edema the BBB becomes leaky and blood plasma flows into the CNS (54). The $AQP4^{-/-}$ mice fare much better than wild type mice in models of cytotoxic edema 40% vs. 90% death rate after water intoxication and ischemic stroke (55, 56), seemingly because water has limited access to the CNS when AQP4 is missing from the perivascular endfeet. The exact opposite takes place in models of vasogenic edema presumably because AQP4 is needed for clearence of water from the CNS (57).

AQP4 also seems to play an important role in glial cell migration, migrating astrocytes form protrusions with AQP4 concentrated at the leading edge and *in vitro* experiments using transwell migration assay and wound healing assay show that primary astrocytes from wild type mice migrate significantly faster than those from $AQP4^{-/-}$ mice or wild type astrocytes treated with AQP4 RNAi (58). Greatly impaired migration of $AQP4^{-/-}$ astrocytes compared to wild type astrocytes has also been seen *in vivo* by measuring migration rate of GFP labeled wild type and $AQP4^{-/-}$ astrocytes towards site of injury after implantation in mouse brain (59). Although presently it is not understood how AQP4 facilitates cell migration a model has been proposed to explain its role (60). It is known that changes in actin polymerization and ion movements via the Na^+/H^+ exchanger across the cell membrane take place at the leading edge of migrating cells (60) and astrocyte migration speed can be altered by changing the osmolality of the external medium (58). Possibly the formation of protrusions is initiated by influx of ions through ion exchangers at the leading edge of the cell. Water then follows the increased osmolality in the cell through AQP4 and the leading edge expands forming a protrusion which is subsequently stabilized by actin repolymerization.

Active neurons relase K^+ into the extracellular space (ECS) during neural signal transduction. Too high K^+ levels in the ECS lowers the activation threshold for neural signal transduction

increasing the probability of inappropriate neural activity. The removal of K^+ from the ECS, which is performed by astrocytes, is therefore critical for normal brain function. Evidence suggest that AQP4 plays a role in K^+ uptake from the brain ECS. AQP4$^{-/-}$ mice show slower K^+ uptake from ECS by astrocytes than wild type mice (54) and studies on hippocampal slices from α-syntrophin$^{-/-}$ mice demonstrate reduced K^+ clearance following neural activity compared to wild type mice (61). In support of these data it has been shown that AQP4$^{-/-}$ mice have stronger and more prolonged seizures in response to convulsants and electrical stimulation compared to wild type although the seizure threshold is higher (62, 63). Finally, hippocampal samples from patients suffering from mesial temporal lobe epilepsy show redistribution of AQP4 away from the perivascular endfeet of astrocytes (64).

1.3.4 The localization of AQP4

How AQP4 achieves its polarized distribution in the sarcolemma of muscle fibers, astrocyte perivascular endfeet and ependymal cells has been a subject of intensive research. DMD (Duchenne muscular dystrophy) is a recessive X-linked degenerative muscle disease caused by a mutation in the DMD gene which expresses the protein Dystrophin (65). In the sarcolemma of normal muscle fibers Dystrophin exist in a complex with several proteins called dystrophin associated proteins (DAPs) and mutations in many of the DAPs can lead to muscular dystrophy. The main role of the dystrophin complex is to link the extracellular matrix with the cell cytoskeleton (65, 66). The X-chromosome linked muscular dystrophy (MDX) mouse is an animal model for DMD and has a genetic defect in the region homologous to the human DMD gene (67). In both MDX mice and DMD patients square arrays vanish from the muscle fibers (68, 69). Furthermore the MDX mice exhibit a significant loss of the AQP4 protein from skeletal muscle, ependymal cells and perivascular endfeet. AQP4 mRNA level is not reduced indicating that Dystrophin is necessary for the stability of AQP4 and not its expression (70). However in MDX mice there is no loss of AQP4 in lung, kidney and the gastrointestinal tract (70).

The cytoplasmic C-terminal tail of AQP4 is of importance for the functional regulation and stability of the AQP4 protein. Several reports indicate that phosphorylation of the AQP4 cytoplasmic tail influence its localization and water permeability. Phosphorylation by PKC at Ser 180 (M23 isoform) reduces the water permeability of *Xenopus* eggs expressing AQP4 (53, 71) (section 1.3.2) which, seems to take place via internalization of square arrays. Phosphorylation of Ser 276 (M1 isoform) by caseine kinase II (CKII) results in lysosomal targeting and destruction of AQP4 in Madine-Darby Canine Kidney (MDCK) cells by promoting the interaction of a tyrosine-based motif at residues 277-280 (M1 isoform) with the AP2 clathrin-adaptor complex (72). Additionally the tyrosine-based motif and a di-leucine based motif at residues 288-292 (M1 isoform) are both required for the basolateral targeting of AQP4 in MDCK cells (72).

At the end of it´s C-terminal AQP4 has a Serine-Serine-Valine (SSV) sequence which is a potential class I ligand for PDZ domains (Table 1). The α, β1, β2, γ1 and γ2 Syntrophins are all DAPs which have a PDZ domain and are known to interact with and localize a number of membrane proteins

containing C-terminal PDZ ligands (73, 74). The observation that AQP4 is lost from astrocyte perivascular endfeet and sarcolemma of α-Syntrophin$^{-/-}$ mice but not from lung, kidney or the gastrointestinal tract, similar to what is seen in the MDX mice (75), indicates that α-Syntrophin might act as an adaptor protein localizing AQP4 to the dystrophin complex in musce fibers and perivascular endfeet. In transgenic mice expressing mutated α-Syntrophin lacking only the PDZ domain AQP4 is absent from the sarcolemma of muscle fibers (76) further supporting the idea that α-Syntrophin mediates localization of AQP4. However a direct interaction between AQP4 and α-Syntrophin has not been confirmed (77, 78). Experiments in cultured primary astrocytes and in MDCK cells show that the C-terminal PDZ binding motif is not required for the membrane localization of AQP4 in astrocytes nor for its basolateral targeting in MDCK cells (72, 78, 79). However experiments on HEK 293T cells expressing AQP4 indicate that the C-terminal PDZ binding motif influences the stability of the AQP4 protein (78). Also a study analyzing the diffusion of AQP4 square arrays in the cell membrane using quantum dot single particle tracking found that square arrays of AQP4 lacking the PDZ ligand are more mobile than normal square arrays which suggests that a PDZ interaction is required to localize AQP4 in the membrane (80). Studies on human muscular dystrophy patients have shown that AQP4 reduction in muscle fibers can take place without any loss of α-Syntrophin (34) and AQP4 can remain stable in the membrane despite strong reduction in α-Syntrophin (81). The specific localization of AQP4 in the membrane is almost certainly regulated by its association with the dystrophin complex, this association however is probably mediated by a thus far unknown mechanism or an indirect link to α-Syntrophin rather than a direct PDZ interaction with α-Syntrophin.

1.4 PDZ domain proteins

The PDZ domain which consists of around 90 amino acid residues was first recognized in several different signalling proteins as regions of sequence homology (82, 83). The first three proteins in which PDZ domains were identified and which the name derives from were PSD-95 (Post synaptic density protein 95), DLG (Disc large from *Drosophila melanogaster*) and ZO-1 (Zonula occludens 1 a tight junction protein). True PDZ domains are primarily found in metazoans and it has been suggested that they might have co-evolved with multicellularity (84). The human genome is estimated to contain 440 PDZ domains in 259 different proteins (85). Majority of all PDZ domains known to date interact with the C-terminal of transmembrane proteins such as receptors or channels. The role of PDZ proteins is commonly to provide scaffold for functional multiprotein complexes often at specific membrane domains. One of the best studied PDZ proteins is INAD which contains 5 PDZ domains and serves as a scaffold for proteins of the phototransduction cascade in the eye of *Drosophila melanogaster* interacting with PLC-β, PKC, TRP and rhodopsin. Collectively this complex with INAD is called the transducisome (84).

The structures of several PDZ domains individually and in a complex with a ligand have been solved showing that PDZ domains fold into a globular fold containing a peptide binding groove to interact with the C-terminal of partner proteins (84). At the end of the groove is the carboxylate binding loop which recognizes the terminal carboxylate of the ligand, this loop contains a well

conserved sequence motif R/K-X-X-X-G-L-G-F which binds the terminal carboxylate. Different PDZ domains recognize different C-terminal sequence motifs usually about 3-5 residues in length. According to the current nomenclature the C-terminal residue is referred to as P_0 and subsequent residues moving away from the C-terminal are called P_{-1}, P_{-2}, P_{-3} etc, the most critical residues for PDZ domain recognition are the P_0 and P_{-2}. Based on extensive library screens on PDZ protein specificities, PDZ ligands have been divided into three separate classes (Table 1). Some PDZ domains can interact with internal motifs in addition to C-terminal ligands, often other PDZ domains as in the interactions of α-Syntrophin and PSD95 with nNOS. The reason this interaction is possible is because the nNOS PDZ domain and other internal motifs form a loop capable of mimicking a C-terminal ligand (86, 87).

Table 1. Classification of PDZ ligands (adapted from 84)

PDZ Domain	**Consensus binding sequence***			
Position	**P_{-2}**	**P_{-1}**	**P_0**	**-COOH**
Class 1	S/T	X	Φ	-COOH
Class 2	Φ	X	Φ	-COOH
Class 3	X	X	C	-COOH

* P_0 is the C-terminal residue P-1 on residue closer to the N-terminal, etc.

X is any amino acid, Φ is a hydrophopic amino acid

2 Aims of the study

The aim of this project was to identify proteins that interact with the cytoplasmic tail of AQP4 at the astrocyte perivascular endfeet. The hypothesis was that PDZ domain proteins might bind the PDZ ligand Serine-Serine-Valine, the last three amino acids of the C-terminal end of AQP4. The project is in part based on previous results obtained at the University of Oslo by Pétur H. Petersen who identified four potential interaction partners of the AQP4 cytoplasmic tail using yeast two hybrid (Y2H) screen. The PDZ domain 10 of the protein Mupp1 (multiple PDZ domain protein 1) a large scaffolding protein containing 13 PDZ domains and known to interact with several transmembrane proteins such as the NMDA receptor (88) and protein tyrosine kinase (89). Sephs1 (Seleno phosphate synthethase 1) a protein without a PDZ domain that is known to play a role in the biosynthesis of selenocysteine (90), although relatively little else is known about it. Finally, two ubiquitins showed a positive interaction with the AQP4 cytoplasmic tail, notably however α-Syntrophin did not.

The first goal of this project was to use the Glutathione-S-Transferase (GST) pulldown protein interaction assay to confirm the findings of the Y2H screen. The second goal was to establish the cellular and subcellular location of those proteins shown to interact with AQP4 and determine whether they colocalize with AQP4 *in vivo* and *in vitro* using immunostaining of mouse tissues and cell transfections. To determine whether these proteins colocalize with AQP4 in astrocyte perivascular endfeet cocultures of primary astrocytes and HUVECs were used, in order for the astrocytes to polarize *in vitro* as they do *in vivo*. An additional goal was to use the BN-Page (Blue native page) gel electrophoresis technique in the laboratory of Dr. Torgeir Holen at the University of Oslo where it has been adapted to study AQP4 to further confirm interactions found using the Y2H screen and GST pulldown.

Specific aims:

1. Setting up and optimizing the GST pulldown technique.
2. Use GST pulldown to validate the Y2H screen results.
3. Determine if those proteins found using Y2H and GST pulldown colocalize with AQP4 in vivo and in vitro.
4. Establish a coculture model of the BBB using primary astrocytes and HUVECs and determine if colocalization takes place at the astrocyte perivascular endfeet.
5. Use BN-Page to confirm interaction between AQP4 and target proteins found using the Y2H and GST pulldown techniques.

3 Materials and Methods

3.1 Cell culture

3.1.1 HEK 293T cells

HEK (Human embryonic kidney) 293T cells (a gift from Dr. Alexander Schepsky, Department of Biochemistry and Molecular Biology at the University of Iceland) were cultured on 100 mm polystyrene plastic dishes (Becton Dickinson) using high glucose Dulbecco´s modified Eagle medium (DMEM) (HyClone) supplemented with 10% v/v Fetal bovine serum (FBS) (Hyclone) and 2 mM GLUTAMAX^{TM} I (Invitrogen). For maintenance the 293T cells were split every 2-3 days at 70-90% confluency by discarding the medium, washing 2x with 5 mL sterile PBS (Phosphate buffered saline) and incubating in 1 mL 0.25% w/v trypsin for 5 minutes. The cells were then plated on new dishes diluted 1:5 and cultured at 37°C in 90% humified 5% CO_2 atmosphere.

3.1.2 CRL-2006

The CRL-2006 cells (a gift from Dr. Torgeir Holen, Department of medicine at the University of Oslo) are immortalized type 1 astrocytes from rat cerebral cortex (91). The CRL-2006 cells were maintained in the same manner as HEK 293T (see 3.1.1).

3.1.3 Primary astrocytes

Primary astrocytes were isolated as described in (92). Briefly, for each culture two P1 or P2 pups of the wild type mouse strain (C57BL6/J-c/c) were decapitated, the head dipped in 70% ethanol and pinned down on sterile styrofoam covered with parafilm. Using sterilized instruments the brain was exposed, the meninges removed and discarded, the cortical and subcortical tissue dorsal and lateral to the lateral ventricles was collected and placed in a 60 mm cell culture dish containing 5 mL of DMEM supplemented with 20% v/v FBS, 0.1% v/v Pen/Strep (GIBCO) and 2 mM GLUTAMAX^{TM} I. The tissue was cut into approximately 1 mm^3 cubes and transferred along with the medium into a 15 mL falcon tube (Becton Dickinson) and vortexed for 1 minute. To further disintegrate the tissue into individual cells it was triturated using a sterile pasteur pipette until no clumps remained visible, the cells were then plated onto a polystyrene T25 cell culture bottle (Becton Dickinson).

The culture medium was replaced every three days and by the second medium replacement the FBS was lowered to 10% v/v. Once the culture became confluent, usually in about two weeks the cell culture flask was placed on a shaker (KS 4000 from IKA) and shaked at 100 rpm for 5 hrs to remove neurons, microglia and oligodendrocytes. The astrocytes were cultured at 37°C in 90% humified 5% CO_2 atmosphere, the cultures were split only when they were to be used for immunocytochemistry and were then split 1:2. They were not used for more than five passages, nor maintained longer than 8 weeks.

3.1.4 HUVECs

Primary human umbilical vein endothelial cells (HUVECs) (a kind gift from Brynhildur Thors, Department of Pharmacology and Toxicology at the University of Iceland) were cultured in T25 cell culture bottles in endothelial medium EGM-2 (Lonza) supplemented with 10% v/v FBS, hEGF (human recombinant Epidermal Growth Factor), hFGF-B (human Fibroblast Growth Factor-Basic), VEGF (Vascular Endothelial Growth Factor), R_3-IGF-1 (human recombinant Insulin-like Growth Factor), Hydrocortisone, Heparin, Ascorbic Acid, Gentamicin, Ampothericin-B and antibiotics; 50 UI/ml penicillin and 50 µg/ml streptomycin (Gibco).

For maintenance the HUVECs were split every 1-2 days at 70-90% confluency by discarding the medium, washing twice with 5 mL PBS (Phosphate buffered saline) and incubating in 1 mL of 2x trypsin for 5 minutes. The cells were then plated on new dishes 1:2 and cultured at 37°C in 90% humified 5% CO_2 atmosphere.

3.2 Transfection

Transfections were performed in accordance to the manufacturer´s instruction in the absence of serum using TransPass^{TM} D2 transfection reagent (New England BioLabs). In the case of HEK 293T the best transfection efficiency was achieved if the cells were 70-90% confluent at the time of transfection. When transfecting CRL-2006 best transfection efficiency was achieved when the the cells were 50-60% confluent at the time of transfection.

3.3 Coculture of primary astrocytes and HUVECs

Primary astrocytes were plated 1:2 on 6 well plates (Becton Dickinson) containing glass coverslips (prepared as described in 3.5) for immunocytochemistry and cultured until they reached 100% confluency usually in about 1-1.5 weeks. HUVECs were then plated in the wells 1:4 – 1:2, and the coculture was then maintained in EGM-2 medium with the medium being replaced every three days for one to two weeks at which point the coverslips were processed for immunocytochemistry.

3.4 Immunohistochemistry

Adult (C57BL6/J-c/c) mice were sacrificed by cervical dislocation, the brain removed and fast frozen for 10 seconds in 2-Methyl Butane (Sigma) (previously cooled down with liquid nitrogen) and placed in Tissue-Tek freezing medium (Sakura). The brain was then sectioned at 8-12 µm coronally using a cryostat (Microm HM 560). Tissue sections were allowed to adhere to a microscope slide (StarFrost) and stored at -20°C in a closed box.

Prior to use, the microscope slides were allowed to thaw at room temperature (RT). Chambers were defined by encircling the tissue sections using an ImmEdge Pen (Vector Laboratories). The tissue sections were then fixed using -20°C acetone for 5 minutes, -20°C MeOH for 5 minutes or RT 3.5% formaldehyde for 10 minutes. Type of fixation depended on the primary antibody being

used. After fixation the sections were washed three times in 1xPBS for 5 minutes and subsequently blocked in blocking solution (1xPBS containing 10% v/v NGS and 0.1% Triton X-100 v/v) for 45 minutes. The tissue sections were then incubated ON (Overnight) at 4°C in blocking solution (without Triton) with primary antibody/antibodies (Table 5. Appendix). Next day the sections were washed three times in 1xPBS for 5 minutes and incubated in blocking solution (without Triton) with secondary antibody/antibodies (Invitrogen) in the concentration 1/1000 for 30 minutes at RT in darkness. Finally the sections were washed three times in 1xPBS for 5 minutes and once in ddH_2O and allowed to dry. A small amount of Vectrashield mounting media (Vector Laboratories), was placed on the sections and a glass cover slip added, the cover slip was then fastened using nail polish.

3.5 Immunocytochemistry

For immunocytochemistry cells were grown on 15 mm circular cover slips previously acid washed and coated with poly-L-lysine as described in (93) in 9.5 cm^2 wells on 6 well cell culture plates (Becton Dickinson).

Immunostaining of cell culture cover slips was performed the same way as the immunostaining of fresh frozen tissue sections described in 3.4 with the following exceptions, the slides were blocked for 5 minutes, the slides were incubated in blocking solution with primary antibody/antibodies for 30 minutes at RT and the blocking solution contained no Triton. When fixing with 3.5% formaldehyde the slides were fixed for 5 minutes and the washed twice for seven minutes in 0.1% v/v before they were washed 3x in PBS and blocked.

3.6 Confocal microscopy

The slides were examined in a confocal microscope (Zeiss LSM 5 Pascal), equipped with one Argon (wavelengths 458, 488 and 514 nm), and two HeNe lasers (wavelengths 543 and 633 nm). The program used to collect images was Pascal LSM 510 release version 4.2 SPI. The software used to view and work with confocal images was Zeiss LSM Image Examiner.

3.7 Bacterial Transformation

Transformations were performed as described in (94). 50 µL competent *E.coli* were thawed on ice in an eppendorf tube, 1-5 µL of plasmid solution added and the cells kept on ice for 30 minutes. The cells were then heat-shocked by incubating them in a water bath at 42 °C for 35 seconds, subsequently 250 µL of LB medium (Bacto-Tryptone 1% w/v, Bacto-Yeast extract 0.5% w/v, NaCl 1% w/v) was added and the cells cultured on a shaker at 37°C for 1 hour. The cells were then plated on LB agar dish containing the appropriate antibiotic and cultured overnight at 37°C.

3.8 Preparing the GST, AQP4-GST and 3A-GST beads for GST pulldown

Beads for GST pulldown were prepared as described in (95). The *E.coli* BL21 strain was transformed (described in 3.7) using the the vectors pGEX6p1, pGEX6p1-AQP4-wt and pGEX6p1-AQP4-3A. After transformation a single colony was picked and grown in 10 mL LB medium with ampicillin (50 µg/mL) ON at 37°C, next day the ON cultures were diluted in 1 L LB medium with ampicillin and grown to A_{600} = 0.5-0.8. Expression of GST, AQP4-GST and AQP4-3A-GST was then activated by adding 1 mL of 100 mM IPTG (Isopropyl β-D-1-thiogalactopyranoside) to a final concentration of 0.1 mM to the medium the cultures were then grown for additional 4 hours. The cells were then spun down at 5000g for 20 minutes at 4°C in a Sorvall RC 5C centrifuge using the rotor SLA-3000. Each cell pellet was dissolved in 15 mL of cold lysis buffer A (50 mM Tris-HCl ph 7.5, 100 mM NaCl, 1 mM DTT, 0.2 mM PMSF, 1 µg/mL Aprotinin). The cells were lysed using sonication. Before sonication cells from each pellet were split between three 50 mL falcon tubes (5 mL per tube) and cells in each tube sonicated at 40% amplitude in one second pulses (sonication 1 sec : rest 1 sec) for 15 minutes using a Vibra-Cell VCX 750 sonicator from sonics. During sonication the sonicating rod was kept 0.5-1 cm below the surface and the tube arranged so the surface was still during sonication pulses, tubes were also kept in cold saltwater with ice in order to prevent heat denaturation of proteins.

After sonication the cell lysate was spun down at 30000 g for 20 minutes at 4°C in a Sorvall RC 5C centrifuge using the rotor SS-34. NaCl was added to the supernatant from each culture in a 15 mL falcon tube towards a 1 M concentration as well as 1 mL of 50% v/v glutathione sepharose beads (GE healthcare) in lysis buffer A prewashed 2x in lysis buffer A, this solution was then mixed overnight with rotation at 4°C. The following day the beads were spun down at 3000g for 30 minutes at 4°C in a Sorvall RT7 centrifuge, the supernatant discarded and the beads washed for 30 minutes in eppendorf on a rotator at 4°C, 2x in 1 mL lysis buffer A with 1 M NaCl and 2x in lysis buffer A only. Finally the beads were dissolved in lysis buffer A and glycerol (25% beads v/v, 25% lysis buffer A v/v, 50% glycerol v/v) and stored at -20°C until use.

3.9 GST pulldown

GST pulldown experiments were carried out as described in (96) with two modifications aimed at reducing unspecific binding of proteins to the sepharose beads. The beads were blocked in 5% BSA prior to their incubation in the cell lysate and when the beads were washed after incubation in the cell lysate the NaCl concentration of lysis buffer B was increased.

In order to prevent unspecific binding of proteins to the sepharose beads they were blocked using BSA (bovine serum albumin). 60-120 µL of 25% sepharose slurry (15-30 µL beads) described in 2.8 was spun down at 5000 g for 1 min and washed 3x in 500 µL lysis buffer B (20 mM Tris-HCl pH 7.5, 100 mM NaCl, 1% NP-40, 1 mM DTT, 0.2 mM PMSF and complete EDTA-free protease inhibitor cocktail tablet (Roche)) after each centrifugation a syringe with a needle

was used to remove the supernatant in order to avoid bead loss. 5% BSA solution was prepared and filtered using a 40 µm syringefilter and 1 mL was added to the beads in an eppendorf tube which was placed on a rotator at 4°C for at least 5 hours, subsequently the beads were washed 3x in lysis buffer B.

Confluent 293T cell cultures on 100 mm dishes were washed twice in PBS then 0.5-1mL lysis buffer B was added to each dish for lysis, the dishes were kept on ice for 10 minutes with gentle shaking and the cells were then scraped off and collected into an eppendorf tube. Subsequently the lysate was centrifuged at 15000 g and 4°C for 15 minutes. The supernatant was collected and added to the BSA blocked beads for at least 1 hour at 4°C on a rotator, a 50 µL sample of the supernatant was taken for positive control (input).

After incubation in lysate the beads were washed 3x in 500 µL lysis buffer B and for 1-5 hours in lysis buffer B with increased NaCl concentration usually lysis buffer B(0.3) (Lysis buffer B containing 0.3 M NaCl) or with higher NaCl depending on the prey protein. Finally, the beads were washed 3x in 500 µL lysis buffer B, dissolved in equal amounts of lysis buffer B and 2x sample buffer (125 mM Tris-HCl pH 6.8, 10% v/v glycerol, 2% w/v SDS, 5% v/v 2-Mercaptoethanol and 0,0025% bromophenol blue) and boiled for 5 minutes at 95°C. Results were then analyzed using acrylamide gel electrophoresis and western blot.

3.10 Western blotting

Acrylamide gels were made as described (94), different concentrations (6%-12.5%) of acrylamide were used in making the gels with higher concentration needed to resolve smaller proteins and vice versa for larger proteins. A recipe for 10 mL 6% and 12% gels can be seen in table 2.

Table 2. Preparation of acrylamide gels for protein electrophoresis.

Reagents.	**Stacking gel**	**Lower gel (12,5%)**	**Lower gel (10%)**	**Lower gel (6%)**
Water	3.4 mL	3.1 mL	4 mL	5.3 mL
30% Acrylamide	0.83 mL	4.2 mL	3.3 mL	2 mL
LTB/UTB*	0.68 mL	2.6 mL	2.6 mL	2.6 mL
10% APS	50 µL	100 µL	100 µL	100 µL
Temed	5 µL	5 µL	5 µL	5 µL

*LTB (1.5 M Tris, 0,4 % SDS, pH 8,8) stacking gel, UTB (0,5 M Tris, 0,4 % SDS, pH 6,8) lower gel.

Protein samples were loaded on the gel and electrophoresis was performed in running buffer (200 mM Glycine, 0.1% w/v SDS, 20 mM Tris) at a constant current of 40A for 1 hour. Proteins were then transferred to a polyvinylidene difluoride (PDVF) or nitrocellulose membrane (Invitrogen) at 400A for 1 hour in transfer buffer (25 mM Tris, 200 mM Glycine, 20% v/v MeOH). The membrane was then blocked for 30 minutes in milk solution (5% w/v non fat milk powder in PBST (137 mM NaCl, 2.7 mM KCl, 8 mM Na_2HPO_4, 2 mM KH_2PO_4, 0.1% v/v Tween)). The membrane was then incubated in milk solution containing primary antibody overnight at 4°C with

constant shaking, the concentration of different primary antibodies used in western blot can be seen in the Appendix (Table. 5).

After incubation in primary antibody the membrane was washed 3x in PBS-T, incubated with secondary antibody horseradish peroxidase-conjugated anti-mouse or rabbit (GE Healthcare) at dilution 1:10000 for 30 minutes and then washed again 3x in PBS-T. The protein bands were visualized using the enhanced chemiluminescence (ECL) system. The chemiluminescent signal was detected by using hyperfilm (Amersham).

3.11 Coomassie staining

After running protein sample on gels as described in 3.10 the gels were incubated in coomassie staining solution (0.2% w/v coomassie R250, 20% v/v MeOH and 10% v/v acetic acid) on a shaker for up to two hours in a closed container. The gels were then destained using destaining solution (50% v/v MeOH, 10% v/v acetic acid) for about two hours replacing the destaining solution 3-4 times until bands were clear and background staining minimal.

3.12 Cloning

For GST pulldown experiments the sequence coding for the last 70 amino acids of the AQP4 cytoplasmic tail was amplified and inserted into the vector pGEX6p1 (GE healthcare) which expresses the insert fused to a glutathione peptide in *E. coli*. Two constructs were made pGEX6p1-AQP4-wt which expresses the AQP4 cytoplasmic tail including the PDZ ligand SSV, and pGEX6p1-AQP4-3A in which the PDZ ligand has been replaced by three alanine residues.

As no known commercial antibody of sufficient quality against the Sephs1 protein exist it was decided to add a Myc tag on N-terminal of the protein so it could be determined using GST pulldown wether it interacts with AQP4.

Primers were designed according to instructions in (94), the primers and their charachteristics can be seen in table 3.

Vectors containing the mouse Sephs1 gene and the mouse AQP4 gene were used as templates for PCR of sephs1-myc and the AQP4 cytoplasmic tail respectively. For each PCR 0.01-0.1 ng of vector was mixed with 5 µL of 10x Pfu buffer (Fermentas), 1 µL of 10 mM dNTP Mix (Fermentas), 1 µL of Fw primer, 1 µL Rw primer, 2 µL of 25 mM $MgCl_2$ (Fermentas), 0.5 µL of Pfu polymerase (Fermentas) and 38.5 µL of water.

Table 3. Primers used to clone the AQP4 cytoplasmic tail and Sephs1.

Name	Sequence and description	Role
mSephs1FcMyc	1 2 3 4 5´gg|ggtacc|atg|gaacaaaaactttatttctgaagaagatctg| 5 6 ggc|tctactcgagagtcctttaacccgg|´3 1. Extension, required for cleavage close to the end of DNA fragments 2. Kpn1 restriction site 3. Start codon 4. Myc tag 5. glycine link 6. Sequence complementary to Sephs1 N-terminal	Fw primer used along with mSephs1RcMyc to amplify a Sephs1-Myc DNA fragment which fits into the pCMV-SPORT6 vector.
mSephs1RcMyc	1 2 3 4 5´g|gaattc|tca|ttaggaggtggcaccaggtgtg|´3 1. Extension, required for cleavage close to the end of DNA fragments 2. EcoRI restriction site 3. Stop codon 4. Sequence complementary to Sephs1 C-terminal	Rw primer used along with mSephs1FcMyc to amplify a Sephs1-Myc DNA fragment which fits into the pCMV-SPORT6 vector.
mAQP4F_cterm	1 2 3 5´|cg|ggatcc|gatgtggagctcaaacgtc|´3 1. Extension, required for cleavage close to the end of DNA fragments 2. BamHI restriction site 3. Sequence complementary to the N-end of AQ4 cytoplasmic tail	Fw primer used along with mAQP4R_cterm_wt and mAQP4R_3A_cterm to amplify the AQP4 cytoplasmic tail sequence and fit into the pGEX6p1 vector.
mAQP4R_cterm_wt	1 2 3 4 5´g|gaattc|tca|tacggaagacaatacctc|´3 1. Extension, required for cleavage close to the end of DNA fragments 2. EcoRI restriction site 3. Stop codon 4. Sequence complementary to AQP4 C-terminal	Rw primer used with mAQP4F_cterm to amplify the AQP4 cytoplasmic tail sequence and fit into the pGEX6p1 vector.
mAQP4R_3A_cterm	1 2 3 4 5´g|gaattc|tca|ggcggcggc|caatacctctcccgaag|´3 1. Extension, required for cleavage close to the end of DNA fragments 2. EcoRI restriction site 3. Stop codon 4. codes for 3x alanine residues 5. Sequence complementary to AQP4 C-terminal	Rw primer used with mAQP4F_cterm to amplify a mutated version of the AQP4 cytoplasmic tail sequence lacking the PDZ ligand SSV and fit into the pGEX6p1 vector.

The PCR reactions were then carried out as follows:

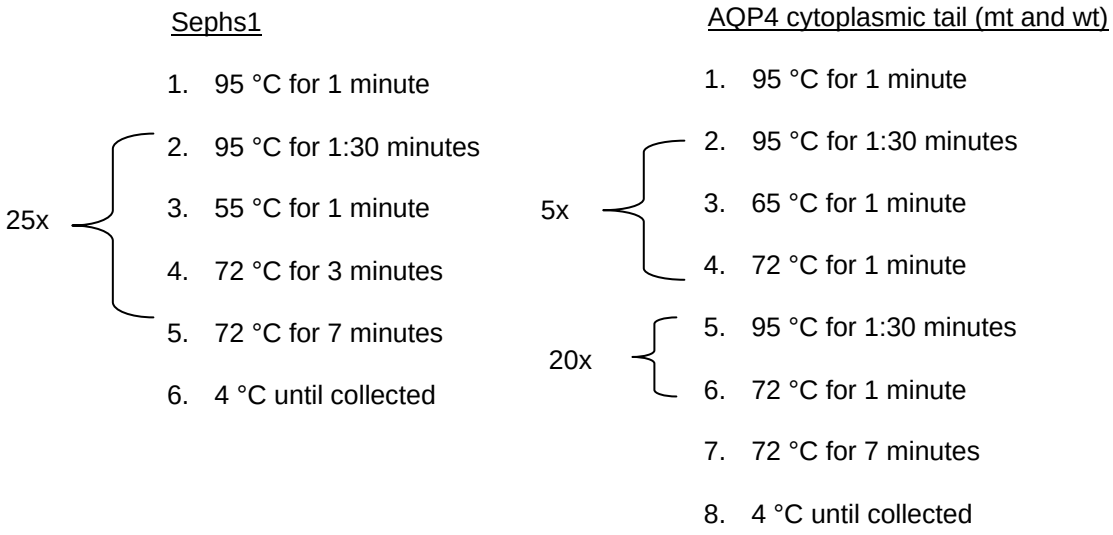

In order to avoid interference from the DNA polymerase during the restriction reaction the amplified PCR product was purified using the QIAquick PCR Purification Kit (Quiagen) according to the manufacturer´s instructions.

The purified Sephs1 PCR product was digested by mixing 2 µL of the restriction enzymes KpnI and EcoRI (Fermentas) with 2 µL of BamHI buffer and 14 µL of the PCR product, the AQP4 PCR product was digested in the same manner with the restriction enzymes EcoRI and BamHI and buffer R (Fermentas). At the same time the pCMV-SPORT6 and pGEX6p1 vectors were digested using the same restriction ezymes and buffers as their inserts, the restriction reactions were carried out ON at 37°C.

The digested plasmid DNA and PCR products were loaded along with 6x loading dye (Fermentas) on 2% agarose gel and electroporated for 1 hour at 100V, the gel was then incubated in TAE buffer (Tris Acetate-EDTA, 40 mM Tris acetate, pH 8.3, 1mM EDTA) containing 0.5 µg/mL EtBr (Sigma) for 30 minutes. The bands containing the digested plasmid and PCR product were visualized in UV light and cut out with a clean scalpel, the DNA was then isolated from the gel using the NucleoSpin kit (Macherey-Nagel) according to the manufacturer´s instructions.

The concentration of the isolated DNA was measured using NanoDrop (NanoDrop® ND-1000 Spectrophotometer). The ligation reaction was performed ON at 18°C in 50 µL volume mixing together 5 µL T4 ligase buffer (Fermentas), 1 µL T4 ligase (Fermentas), 10 ng of the digested vector and 2.5 ng of the digested PCR product, then nuclease free water was added to 50 µL.

Subsequently the ligase was inactivated by heating at 70°C for 5 minutes, 5 µL of the ligation reaction were then used to transform 50 µL of Top10 chemically competent *E. coli* (Invitrogen) as described in 3.7. After transformation one colony of cells was picked and grown in 5 mL LB medium with ampicillin (50 µg/mL) ON at 37°C, the vectors with the inserts were then isolated

using GeneJet plasmid miniprep kit (Fermentas) according to the manufacturer´s instructions. The pGEX6p1-AQP4-wt and pGEX6p1-AQP4-3A were sequenced to confirm that the sequence was correct (data not shown).

4 Results

4.1 Validation of the GST fusion proteins

After the GST fusion proteins AQP4-GST and 3A-GST as well as the unmodified GST protein were attached to beads, as described in section 3.8, the beads had to be validated before starting GST pulldown experiments. 10 µL of beads of each type were diluted in 50 µL buffer A and 60 µL 2x sample buffer and then boiled at 95°C for 3 minutes. 10 µL of each sample was loaded on two 12.5% PAGE gels one of which was used for coomassie staining and the other one for western blotting (Fig.4). On the coomassie stained gel a strong band of the correct size was observed for each of the GST proteins, 26 kD for the GST protein and 33 kD for the GST fusion proteins AQP4-GST and 3A-GST. Both AQP4-GST and 3A-GST could be detected on a western blot using the polyclonal AQP4 antibody AB2218 showing that the epitopes recognized by the antibody are unchanged in the 3A-GST construct (Fig. 4 B).

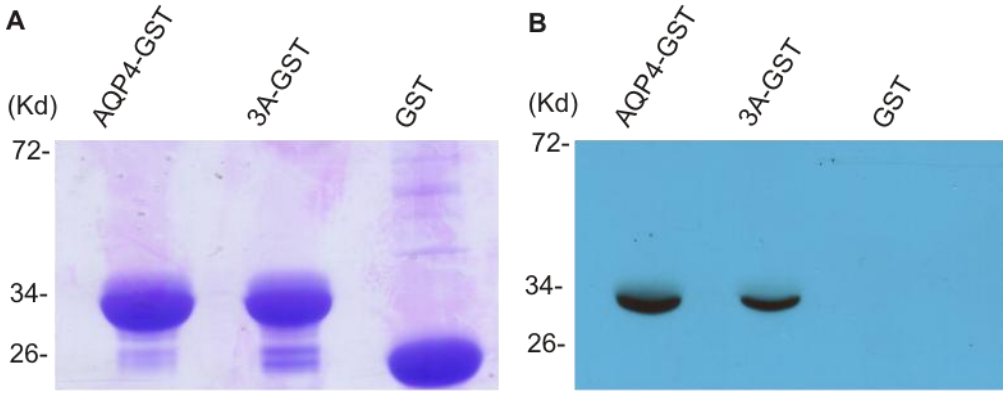

Figure 4. Validation of the GST beads.

The GST fusion proteins AQP4-GST and 3A-GST as well as the GST peptide were detached from the sepharose beads and analyzed using coomassie staining and western blot. **A.** Coomassie staining shows strong bands of the correct size for each of the GST proteins, 26 kD for the GST protein and 33 kD for AQP4-GST and A3-GST. **B.** Both GST fusion proteins AQP4-GST and 3A-GST can be detected on a western blot using the polyclonal AQP4 antibody AB2218.

4.2 GST pulldown of Mupp1

4.2.1 Optimization of Mupp1 GST pulldown and pulldown of endogenous Mupp1

The first GST pulldowns attempting to verify an interaction between AQP4 and Mupp1 endogenous to 293T cells using the GST pulldown protocol in (95) were not successful. Despite repeated experiments Mupp1 could always be detected on the 3A-GST and GST control beads

in additon to the AQP4-GST beads (Fig. 5 A), this suggests unspecific binding to the sepharose beads. However after adding two steps to the protocol Mupp1 was successfully pulled down specificially (Fig. 5 B).

These steps were;

1. Preincubation of the AQP4-GST, 3A-GST and GST beads in 5% BSA for at least 5 hours.
2. Washing the beads in buffer B with increased NaCl concentration for 1-5 hours after they had been removed from the cell lysate. The NaCl concentration of buffer B is 0.1 M, in the case of Mupp1 as well as Patj 7xMyc (section 4.4) and Syntrophin (section 4.8) it was sufficient to increase the concentration to 0.3 M.

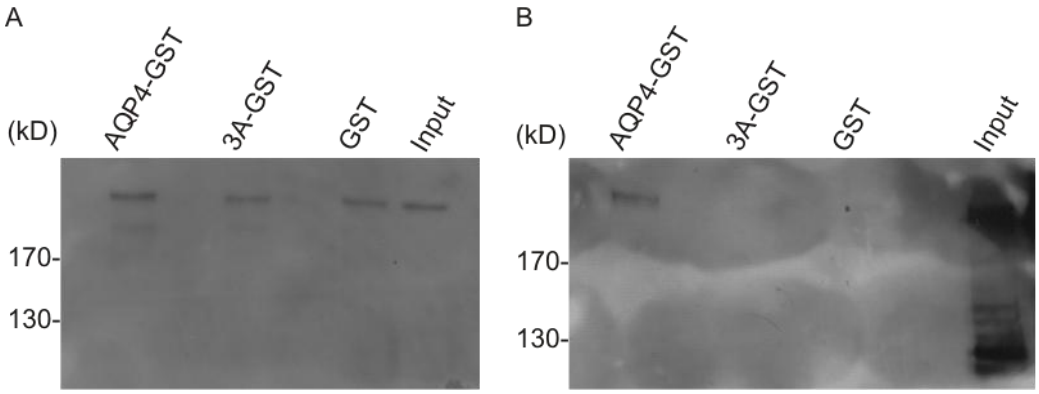

Figure 5. Mupp1 endogenous to 293T cells interacts with AQP4.

Results of pulldown from untransfected 293T cells visualized on a western blot using Mupp1 antibody. **A.** A ~220 kD band can be seen in input and on all beads showing that Mupp1 is binding unspecifically to the sepharose beads. **B.** After optimization of the GST pulldown protocol Mupp1 is only detected on the AQP4-GST beads and in the input showing that AQP4 interacts with Mupp1 endogenous to 293T cells in a PDZ specific manner. (The smaller bands seen in the input of figure B are likely the result of protein breakdown)

4.2.2 GST pulldown of Mupp1 7xMyc, Mupp1 9+10 and Mupp1 7+8

The Y2H screen showed an interaction between the AQP4 C-terminal tail and the 10th PDZ domain of Mupp1 (Fig. 6 “red circle“). To test if the interaction of AQP4 is specific for the 10th PDZ domain of Mupp1 three different Mupp1 constructs were used (Table 6, Appendix), Mupp1 7xMyc expresses a full length Mupp1 with seven Myc tags, Mupp1 9+10 and Mupp1 7+8 express Xpress tagged portions of Mupp1 containing PDZ domains 9 and 10 as well as 7 and 8 respectively (Fig. 6). GST pulldown from 293T cells transfected with the three constructs shows that Mupp1 7xMyc and Mupp1 9+10 but not Mupp1 7+8 interact with the PDZ ligand of AQP4 (Fig. 7).

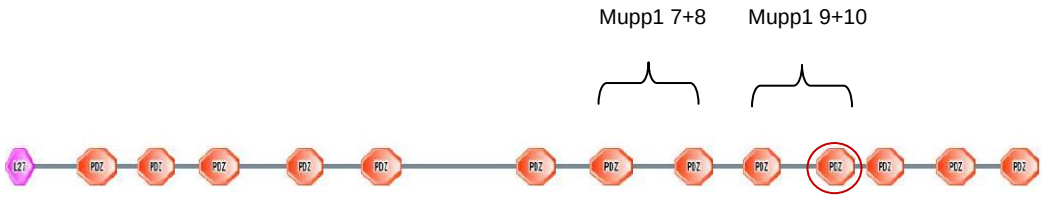

Figure 6. Schematic picture of Mupp1.

Mupp1 contains 14 protein interaction domains, 13 PDZ domains (orange) and one L27 domain, the 10th PDZ domain is highlighted with a circle. The PDZ domains 7-10 are expressed by the constructs Mupp1 7+8 and Mupp1 9+10. (Downloaded from http://smart.embl-heidelberg.de/smart/change_mode.pl on 03.12.2009)

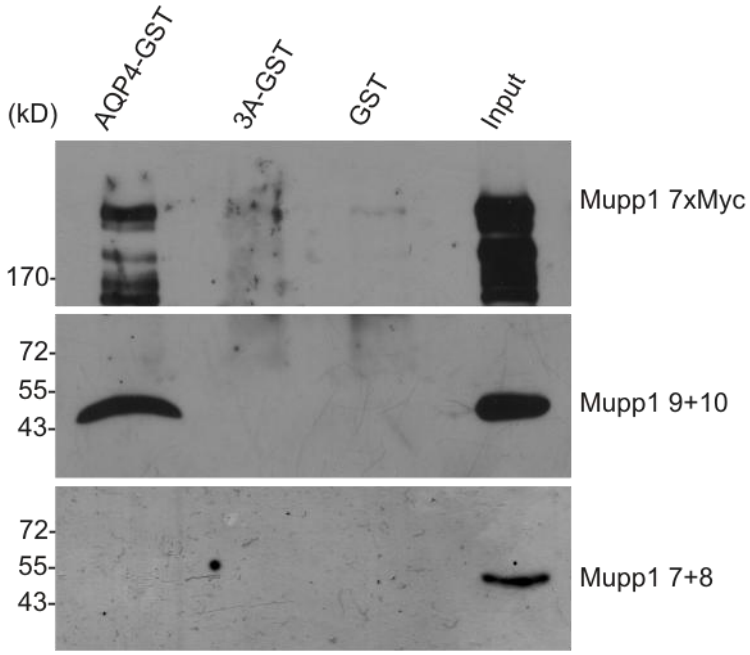

Figure 7. The 10th PDZ domain of Mupp1 interacts with AQP4.

Results of pulldown from 293T cells transfected with Mupp1 7xMyc, Mupp1 9+10 and Mupp1 7+8 visualized on western blot using Myc and Xpress antibodies. Strong bands can be seen in input and AQP4-GST for Mupp1 7xMyc (~228 kD) and Mupp1 9+10 (~50 kD) conversely for Mupp1 7+8 the only detectable band is in the input. (The small extra bands seen in the Mupp1 7x Myc are the result of protein breakdown) input 5%.

4.3 Coimmunostaining of tissue sections for AQP4 and Mupp1

To determine if the interaction between Mupp1 and AQP4 takes place *in vivo* in astrocyte endfeet, mouse brain sections were coimmunostained for AQP4 and Mupp1. This experiment showed that AQP4 and Mupp1 do not colocalize in the brain (Fig. 8 B-C). AQP4 staining is strongest around brain capillaries presumably in astrocyte endfeet (Fig. 8 A-C). Mupp1 is absent from astrocyte endfeet but is clearly in brain capillary endothelial cells (Fig. 8 B-C) as it shows the same localization as the endothelial marker CD31 (Fig. 8 A). AQP4 and Mupp1 are both expressed in ependymal cells but do not colocalize, AQP4 is localized basolaterally but Mupp1 apically (Fig. 9).

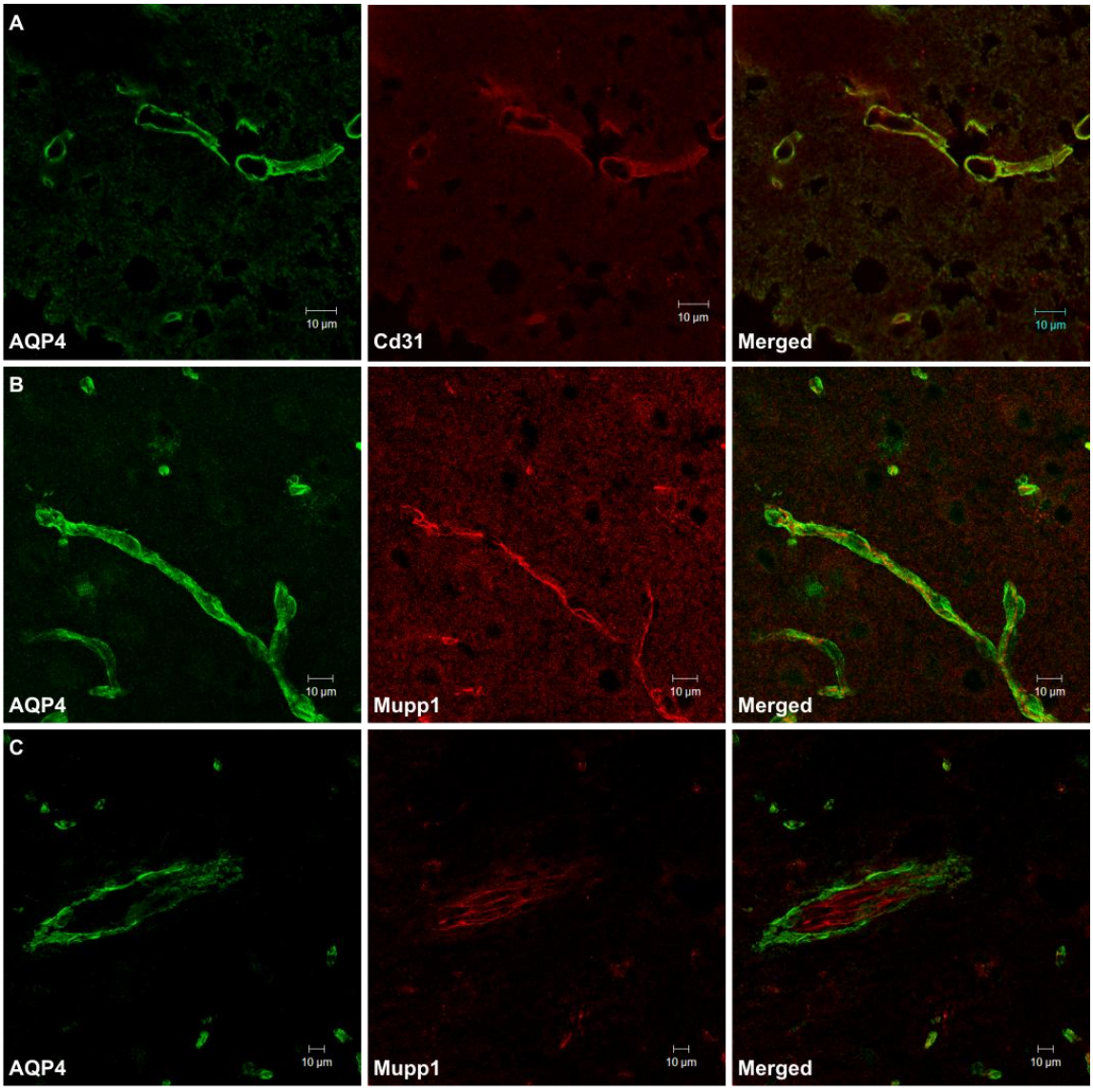

Figure 8. AQP4 and Mupp1 do not colocalize around brain capillaries.

IF staining of MeOH fixed mouse brain sections with **A.** AQP4 (green) and CD31 (red) antibodies (60x magnification) **B-C.** AQP4 (green) and Mupp1 (red) antibodies (40x magnification). AQP4 immunoreactivity is in astrocyte endfeet enveloping brain capillaries, in contrast Mupp1 is localized to the endothelial cells of brain capillaries as is CD31.

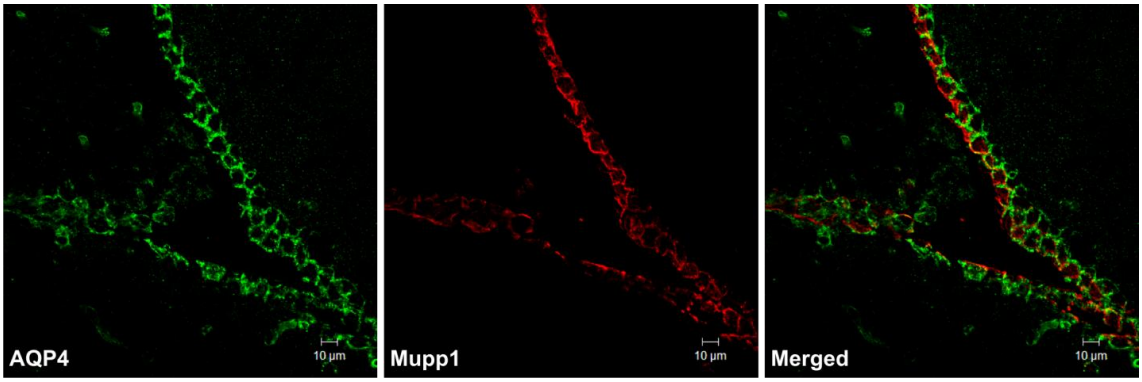

Figure 9. AQP4 and Mupp1 do not colocalize in ependymal cells.

IF staining of MeOH fixed mouse brain sections with AQP4 (green) and Mupp1 (red) antibodies (40x magnification). Both AQP4 and Mupp1 immunoreactivity is seen in ependymal cells lining the ventricles, however the two proteins do not colocalize AQP4 is localized basolaterally and Mupp1 apically.

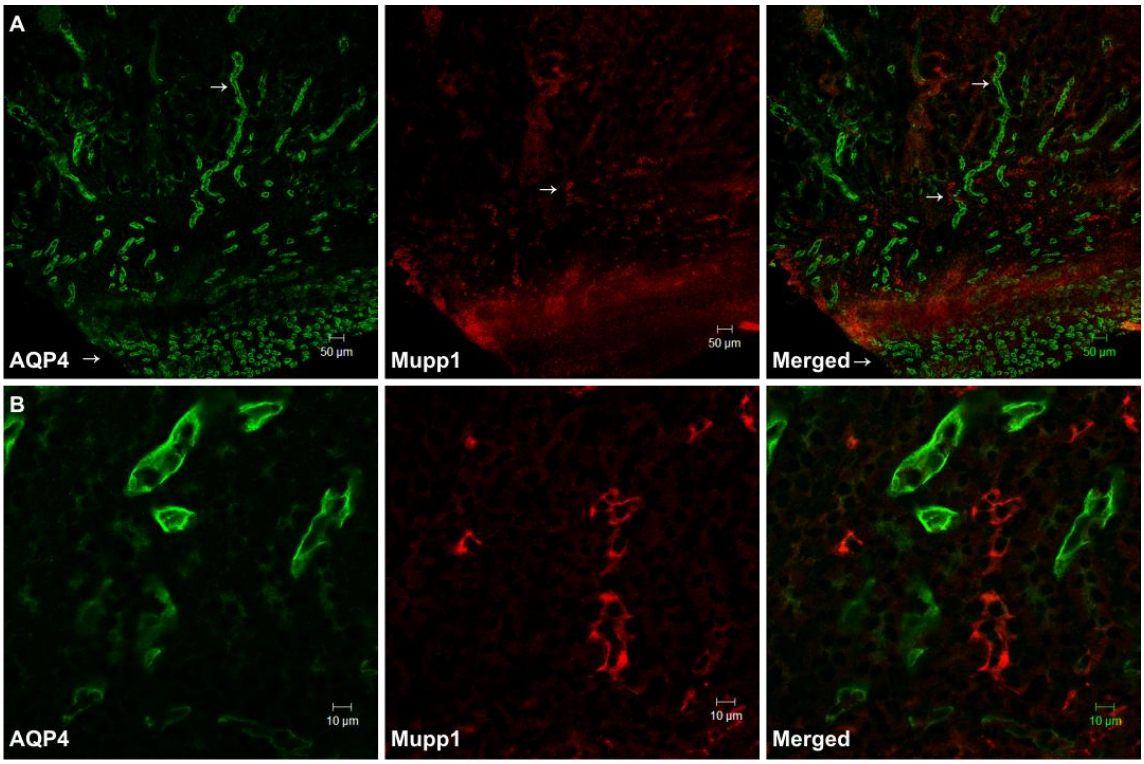

Figure 10. AQP4 and Mupp1 do not colocalize in the kidney.

IF staining of MeOH fixed mouse kidney sections with AQP4 (green) and Mupp1 (red) antibodies **A.** AQP4 immunoreactivity is widespread at the tip of the medulla in what appears to be collecting duct cross sections (lower arrow), AQP4 positive collecting duct longitudinal sections can be seen reaching from the medulla to the edge of the cortex (upper arrow). Mupp1 immunoreactive cells of unknown type are only seen in a limited area within the medulla (middle arrow). (10x magnification) **B.** Close up pictures of areas in figure A containing AQP4 and Mupp1 positive cells. (60x magnification).

It is well established that Mupp1 is found in the kidney (96) like AQP4 but coimmunostaining of kidney

sections for AQP4 and Mupp1 revealed that AQP4 and Mupp1 do not colocalize in the kidney. In the kidney AQP4 immunoreactivity is widespread in the medulla but is strongest at the tip of the medulla (Fig. 10 A “lower arrow“) which represents cross sections of collecting ducts but AQP4 is localized to the principal cells of the collecting duct. AQP4 positive collecting duct longitudinal sections can also been seen reaching from the medulla to the edge of the cortex (Fig. 10 A “upper arrow“). Mupp1 immunoreactivity however is not as widespread and only seen in cells of unknown type residing rather deep within the medulla (Fig. 10 A “middle arrow“). In figure 10 B an area deep within the medulla containing both AQP4 and Mupp1 positive cells can be seen showing clearly that AQP4 and Mupp1 are not localized to the same cells within the kidney.

AQP4 and Mupp1 also do not colocalize in 293T cells transfected with mAQP4 and Mupp 7xMyc (data not shown).

4.4 GST pulldown of Patj and in vitro coimmunosaining of Patj and AQP4

As the 10th PDZ domain of Mupp1 showed specific binding with the AQP4 C-terminal, which however does not seem to occur *in vivo* this suggested the possibility that proteins similar to Mupp1 could possibly be the actual *in vivo* binding partner. The protein most similar to Mupp1 is Patj (Pals1 Associated Tight Junction protein) a PDZ scaffolding protein which is closely related to Mupp1 and shares several binding partners with it (97).

Patj is a structural paralogue of Mupp1 and contains an L27 domain and 10 PDZ domains (Fig.11) while Mupp1 contains an L27 domain and 13 PDZ domains (Fig. 6). Comparison of the amino acid sequence of individual Patj and Mupp1 PDZ domains using the clustalw2 software shows that all of the PDZ domains of Mupp1 except PDZ 4, 6, 9 and 13 share more than 50% sequence identity with PDZ domains of Patj, and PDZ domain 10 of Mupp1 and PDZ domain 8 of Patj share the highest sequence identity or 77% (Table 4).

Figure 11. Schematic picture of Patj.

A schematic picture of Patj, the 8th PDZ domain of Patj is highlighted with a red circle. (Downloaded from http://smart.embl-heidelberg.de/smart/change_mode.pl on 03.12.2009)

Because the 8th PDZ domain of Patj shows such high homology with the 10th PDZ domain of Mupp1 which interacts with the AQP4 PDZ ligand according to Y2H and GST pulldown results it was decided to examine whether Patj as well interacts with the AQP4 PDZ ligand. GST pulldown from 293T cells transfected with the construct Patj 7xMyc which expresses full length Patj with 7 myc tags showed that Patj interacts with AQP4 in a PDZ dependent manner (Fig. 12). Cotransfection of the Patj 7xMyc and mAQP4 constructs in 293T cells and subsequent

coimmunostaining with Myc and AQP4 antibodies showed clearly that the two proteins colocalize at the plasma membrane (Fig. 13).

Table 4. Comparison of PDZ domains amino acid sequence.

Comparison of the amino acid sequence of individual PDZ domains of mouse Mupp1 and Patj. Highest sequence identities are shown in bold and the comparison of Mupp1 PDZ 10 and Patj PDZ 8 is highlighted in yellow.

Mupp1/Patj	PDZ 1	PDZ 2	PDZ 3	PDZ 4	PDZ 5	PDZ 6	PDZ 7	PDZ 8	PDZ 9	PDZ 10
PDZ 1	**56**	35	29	14	22	30	35	35	38	32
PDZ 2	33	**66**	33	16	24	24	34	37	37	25
PDZ 3	25	40	**54**	19	27	20	29	34	31	24
PDZ 4	15	25	21	41	24	23	34	30	23	26
PDZ 5	25	30	21	28	**60**	20	30	36	27	17
PDZ 6	12	30	18	9	26	9	23	28	25	21
PDZ 7	27	25	32	17	20	**65**	20	36	25	35
PDZ 8	23	32	20	28	28	25	**72**	41	30	29
PDZ 9	25	32	18	15	28	19	28	31	30	20
PDZ 10	29	33	28	22	34	34	36	**77**	38	32
PDZ 11	32	41	30	19	22	27	26	36	**67**	28
PDZ 12	29	28	27	11	18	31	21	26	22	**66**
PDZ 13	34	34	28	20	32	32	33	45	34	42

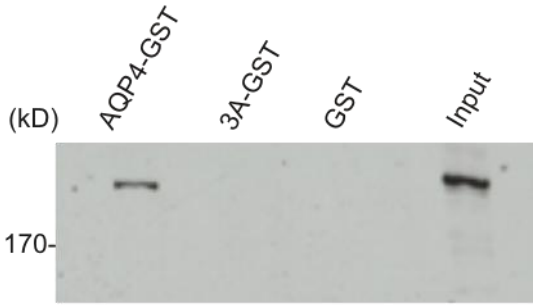

Figure 12. Patj interacts with AQP4.

Results of a GST pulldown from a lysate of 293T cells transfected with Patj 7xMyc visualized on a western blot using a Myc antibody. Clear ~207 kD bands can be seen in input and AQP4-GST indicating a PDZ specific interaction between Patj 7xMyc and AQP4.

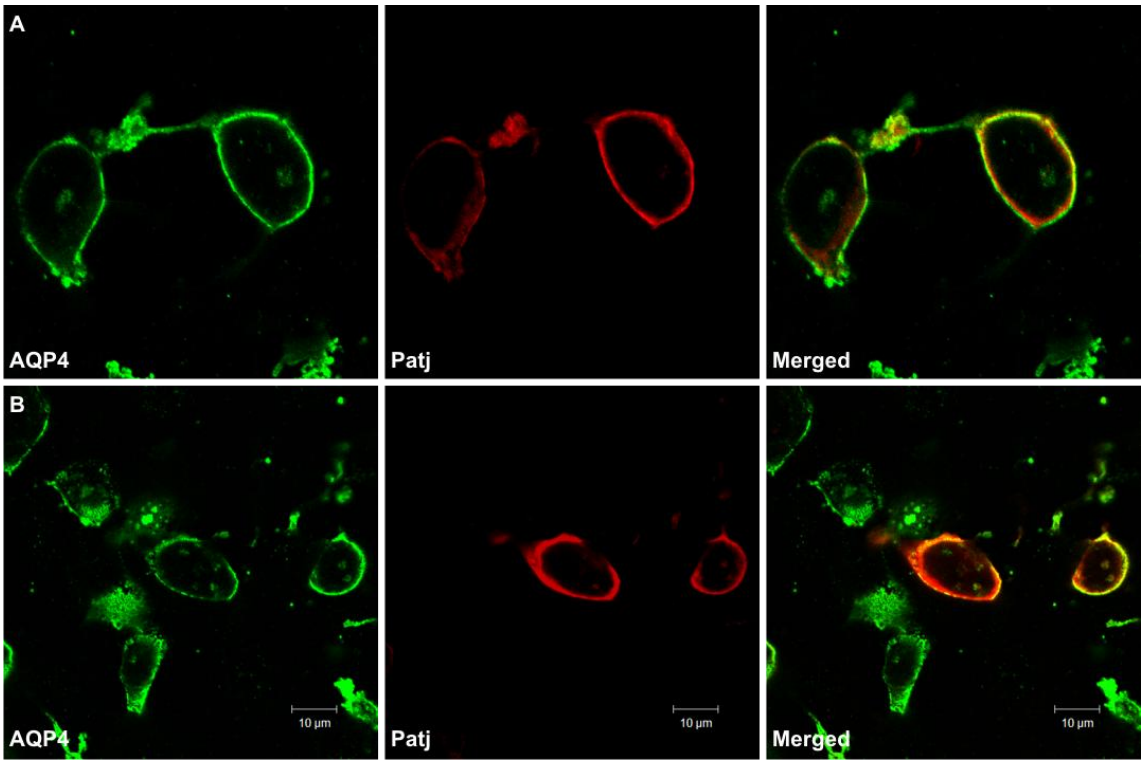

Figure 13. Patj colocalizes with AQP4 *in vitro*.

A-B. IF staining of MeOH fixed 293T cells transfected with mAQP4 and Patj 7xMyc using AQP4 (green) and Myc (red) antibodies (60x magnification). AQP4 and Patj 7xMyc show clear colocalization at the cell membrane.

In order to complement the results of the GST pulldown assay it was also attempted to show whether AQP4 and Patj interact using BN-Page. This however, was not successful possibly due to the fact that BN-Page is optimized to analyze protein interaction between membrane proteins. Prior to BN-Page electrophoresis the use of detergents is neccessary to solubilize membrane protein complexes which, in the case of this study were AQP4 tetramers and square arrays. PDZ interactions are of variable strength and conceivably the interaction between AQP4 and Patj was dissociated by the detergent which was used.

Although the it could not be determined using BN-Page whether AQP4 and Patj interact it was successfully used to show how different AQP4 isoforms are arranged in the cell membrane (53).

4.5 Coimmunostaining of tissue sections for AQP4 and Patj

Patj is able to bind AQP4 *in vitro*, as Mupp1, the next step was to determine whether Patj was an *in vivo* binding partner of AQP4. Two different antibodies were used to assess whether Patj and AQP4 colocalize *in vivo,* Patj (Bivic) a polyclonal rabbit antibody and Patj (abnova) a mouse monoclonal antibody. The Patj (Bivic) antibody was used in combination with the Syntrophin antibody AB 11425 a monoclonal mouse antibody for coimmunostaining of brain sections but

AQP4 and Syntrophin show clear colocalization around brain capillaries (Fig. 14 A). Patj (Abnova) was used in combination with the AQP4 antibody AB 2218 a polyclonal rabbit antibody for coimmunostaining of brain and kidney sections.

Both Syntrophin and AQP4 colocalized with Patj around brain capillaries in coimmunostainings on brain sections (Fig. 14 B and Fig. 15 A-B). Coimmunostaining of kidney sections with the AQP4 and Patj (abnova) antibodies showed that similar to Mupp1 Patj is exclusively found in the medulla in a different cell type than AQP4 (Fig. 16).

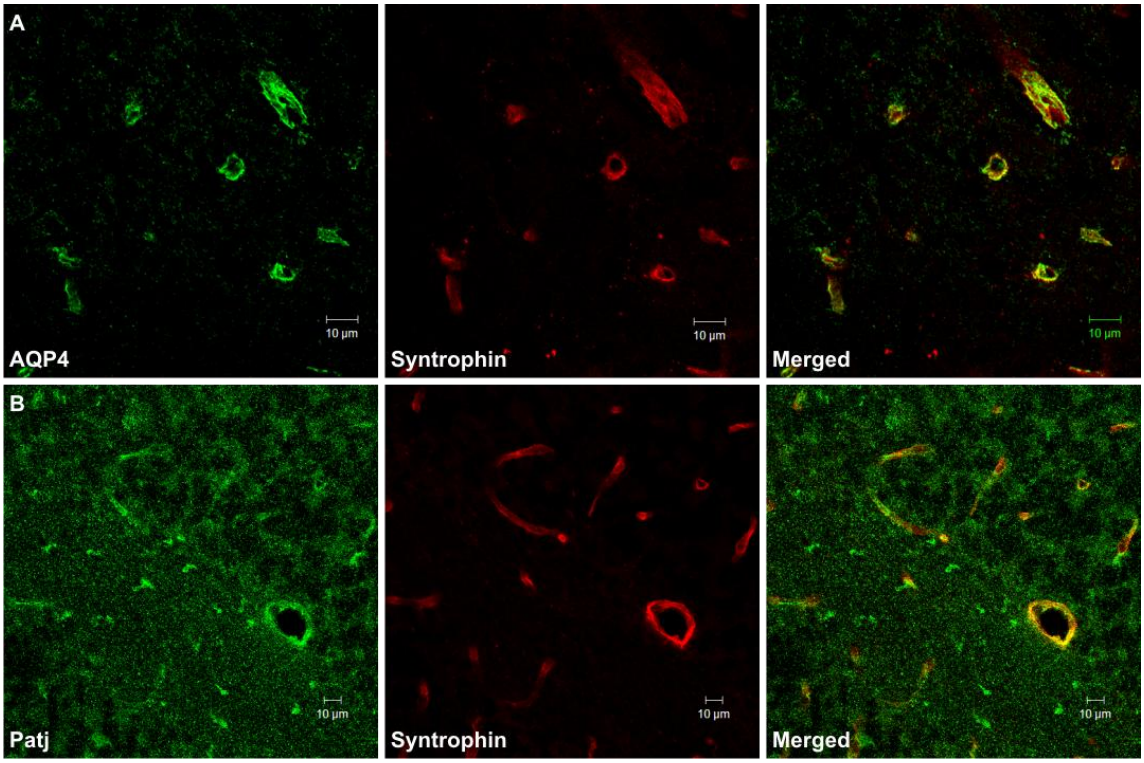

Figure 14. Patj and AQP4 colocalize with Syntrophin around brain capillaries.

IF staining of mouse brain sections with **A.** AQP4 (green) and Syntrophin (red) antibodies, AQP4 and Syntrophin show a clear coloclization around brain capillaries. (60x magnification)(MeOH fixation) **B.** Patj (Bivic) (green) and Syntrophin (red) antibodies, (60x magnification)(Aceton fixation)

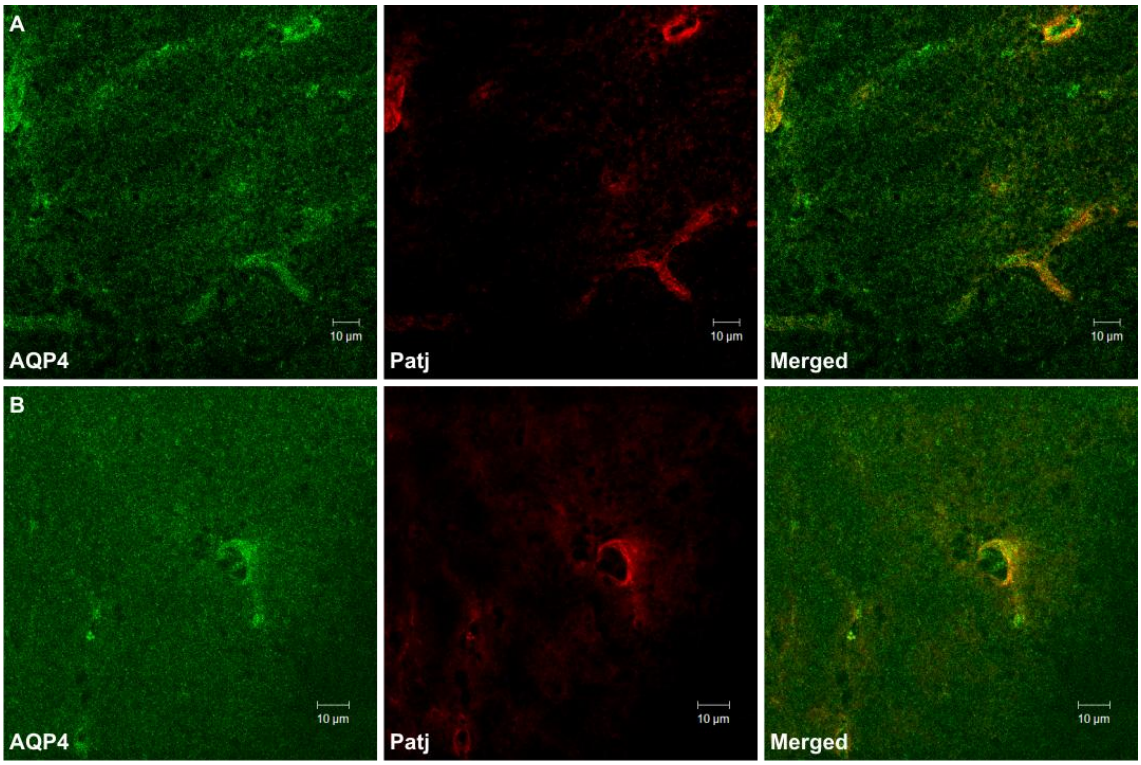

Figure 15. Patj and AQP4 colocalize around brain capillaries.

IF staining of acetone fixed mouse brain sections with **A-B.** Patj (abnova) (green) and AQP4 (red) antibodies (60x magnification).

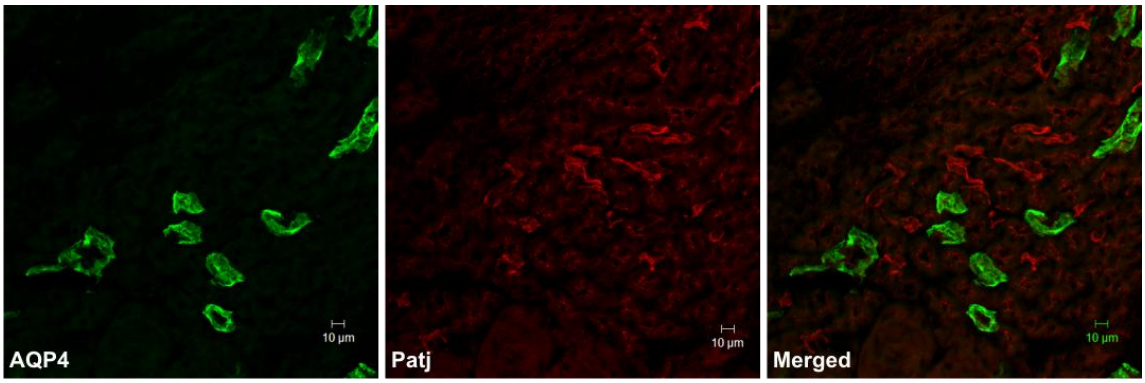

Figure 16. Patj and AQP4 do not colocalize in the kidney.

Patj is only found in the medulla and is not found in the same cell type as AQP4.

IF staining of MeOH fixed mouse kidney sections with AQP4 (green) and Patj (abnova) (red) antibodies (20x magnification).

4.6 Establishing primary astrocyte-HUVEC cocultures

It is possible to model the formation of astrocyte endfeet and the BBB by coculturing astrocytes and endothelial cells. Once in coculture with endothelial cells, astrocytes show a polarized distribution of AQP4 towards the astrocyte-endothelial interface similar to what is seen *in vivo* in perivascular endfeet. In order to determine if Patj and Syntrophin also display this polarized distribution and whether they colocalize with AQP4 in astrocyte endfeet it was decided to establish astrocyte-endothelial cocultures using primary mouse astrocytes and HUVECs.

About one or two weeks after HUVECs were added to a confluent layer of astrocytes as described in 3.3, the HUVECs form colonies which are completely surrounded by astrocytes (Fig. 17 A). The colonies are of variable sizes some just 5-10 cells (Fig. 17 B) but others much larger (Fig. 17 C). Around the colonies the astrocytes seem to be a bit more dense than elsewhere (Fig. 17 B-C arrows)

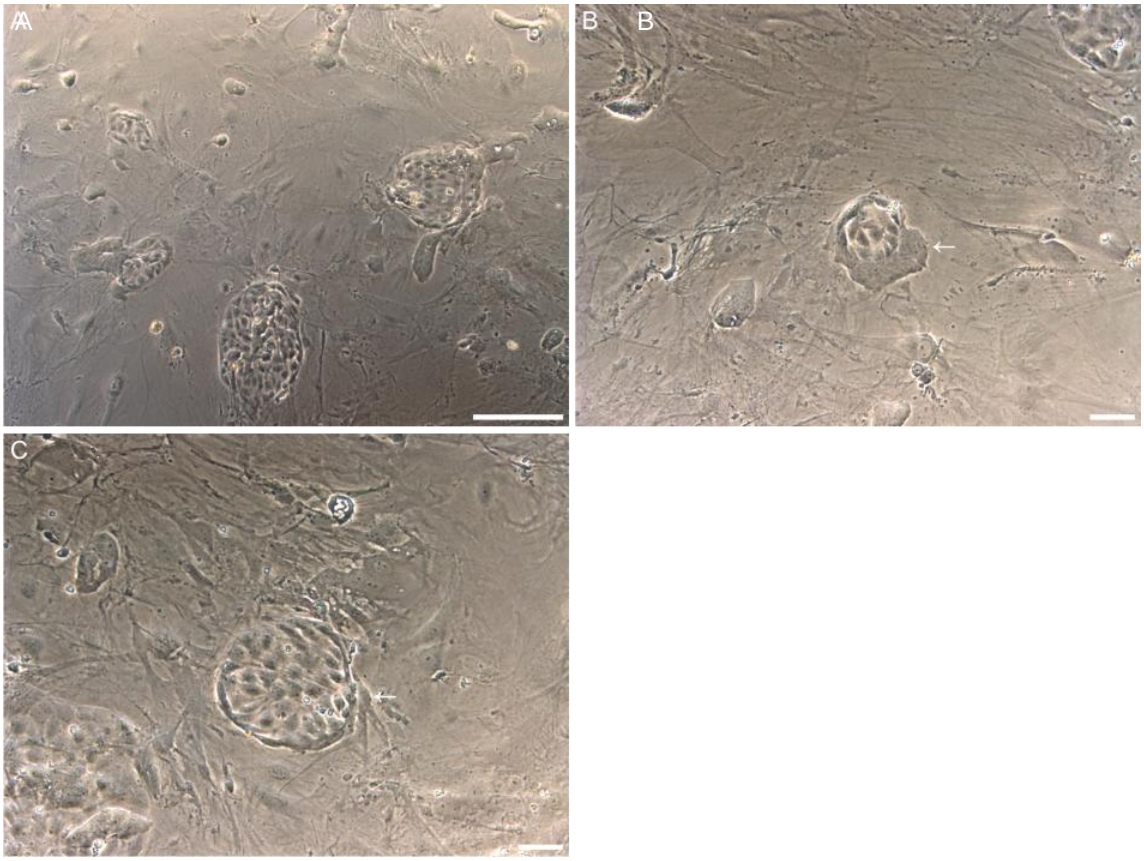

Figure 17. Cocultures of primary astrocytes and HUVEC´s.

Phase contrast light microscopy photographs of primary astrocyte-HUVEC cocultures. HUVEC´s form colonies of variable sizes completely surrounded by astrocytes. **A.** 10x magnification. **B-C.** 20x magnification.(Bar 100 µm)

Coimmunostaining of cocultures with antibodies against CD31 an endothelial marker and GFAP an astrocyte marker shows clearly how colonies are surrounded by astrocytes (Fig. 18). In figure 17 the HUVEC colonies seem completely surrounded by astrocytes yet in figure 18 B it is clear

that the GFAP staining does not completely surround the colony which probably stems from the fact that not all astrocytes are GFAP positive (16).

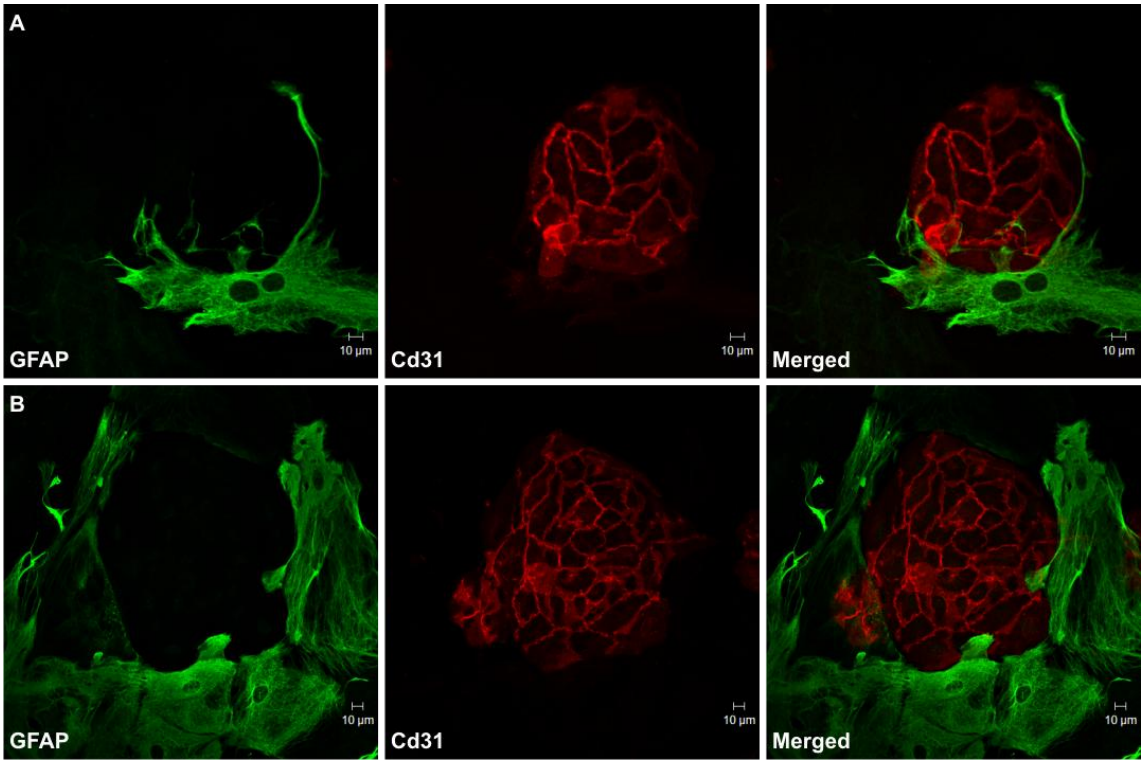

Figure 18. GFAP and GD31 coimmunostaining of cocultures.

GFAP positive astrocytes envelop colonies of CD31 positive HUVEC´s.

A-B. IF staining of cocultures fixed with formaldehyde using the GFAP (green) and CD31 (red) antibodies (20x magnification).

In primary astrocyte cultures AQP4 is evenly distributed across the astrocyte cell membrane showing no polarized location of any kind (Fig. 19 A). When astrocytes are cocultured with HUVECs AQP4 immunoreactivity is stronger in the parts of the astrocytes which are in close contact to HUVEC colonies while the rest of the astrocyte body shows similar staining as is seen in figure 19 A (Fig. 19 B-D).

Notably in AQP4 immunostaining of cocultures there is clearly immunoreactivity intracellulary in HUVECs which could be an artifact or possibly real AQP4 staining (Fig. 19 B-D) but as is mentioned in section 1.3.1 it has been claimed that AQP4 is expressed in endothelial cells.

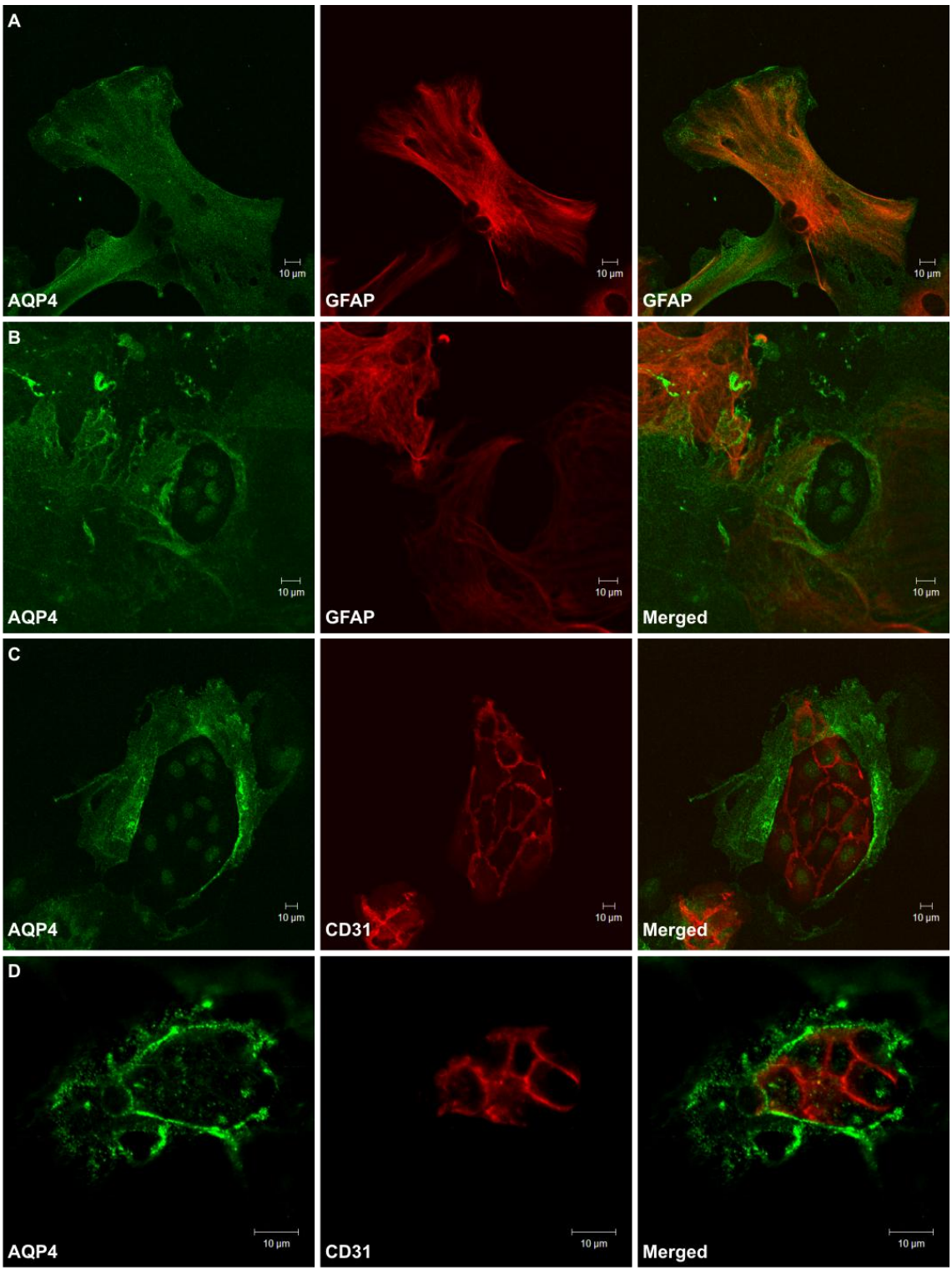

Figure 19. AQP4 is polarized around HUVEC colonies.

Astrocytes in coculture clearly show a polarized location of AQP4 compared with astrocytes grown alone. IF staining of formaldehyde fixed cocultures with **A-B.** AQ4 (green) and GFAP (red) antibodies (60x and 20x magnification respectively) **C-D.** AQP4 (green) and CD31 (red) antibodies (20x and 60x magnification respectively).

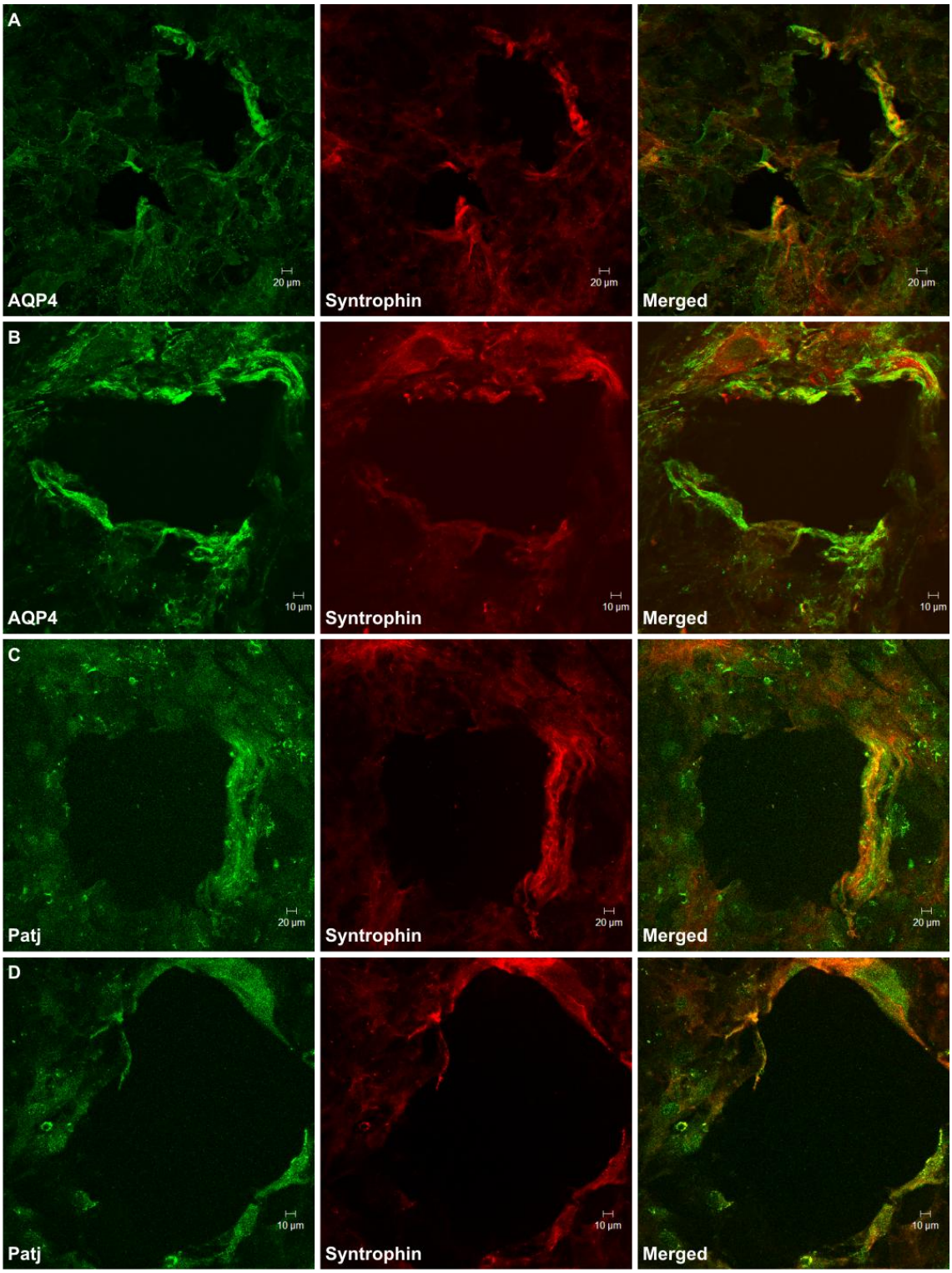

Figure 20. Syntrophin colocalizes with AQP4 and Patj in astrocytes.

IF staining of acetone fixed cocultures with **A-B.** AQP4 (green) and Syntrophin (red) and **C-D.** Patj (green) and Syntrophin (red). (A.C. and B.D. 20x and 40x magnification respectively).

4.7 Patj in primary astrocyte-HUVEC cocultures

Immunostainings of cocultures for Patj only worked well with the Patj (Bivic) antibody and only by using acetone fixation. Seemingly during the staining process the HUVECs fall off possibly because of the acetone and what is left are empty areas. Coimmunostainings using the Syntrophin antibody with the Patj (Bivic) and AQP4 antibodies show that Syntrophin seems to colocalize with both AQP4 (Fig. 20 A-B) and Patj (Fig. 20 C-B) around these empty areas.

Because of the problems resulting from acetone fixation of the cocultures it was also attempted to cotransfect the CRL-2006 astrocyte cell line with mAQP4 and Patj 7xMyc with the goal or coculturing them with HUVECs as an alternative approach to determine if AQP4 and Patj colocalize in endfeet. However the CRL-2006 astrocytes who normally do not express AQP4 did not survive when transfected with the mAQP4 vector presumably because of excessive water influx.

4.8 GST pulldown of Syntrophin

The Syntrophin family contains five members; α, β1, β2, γ1, and γ2 Syntrophins which are all known to be a part of the dystrophin complex and all contain PDZ domains (65). Even though the Y2H screen did not detect an interaction between α-Syntrophin and the cytoplasmic tail of AQP4 and previous attempts of others to do the same have not been successful (78) it is possible that the association of AQP4 with the dystrophin complex is mediated by a Syntrophin other than α-Syntrophin. Therefore it was decided to carry out a GST pulldown on a lysate from untransfected 293T cells and use the Syntrophin antibody AB 11425 to visualize the results on a western blot but this antibody recognizes β1, β2 and α-Syntrophin (Fig. 21). As can be seen on figure 21 a Syntrophin endogenous to 293T cells interacts with AQP4 in a PDZ specific manner.

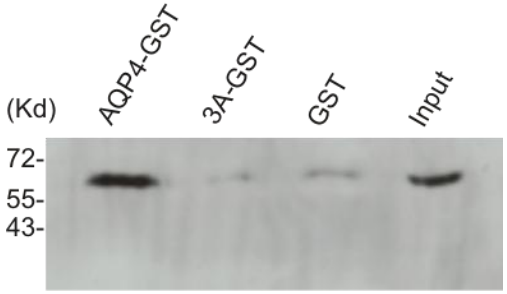

Figure 21. Syntrophin endogenous to 293T cells interacts with AQP4.

Results of a GST pulldown from a lysate of untransfected 293T cells visualized on a western blot using the Syntrophin antibody AB 11425 which recognizes α, β1 and β2 Syntrophins. Strong 60 kD bands can be seen in the input and AQP4-GST indicating a PDZ specific interaction between AQP4 and a Syntrophin endogenous to 293T cells (input 5%).

4.9 GST pulldown of Sephs1-Myc and Ubiquitin

Three proteins who do not contain a PDZ domain were identified in the Y2H screen, Sephs1 and two Ubiquitins. They were also tested for interaction with AQP4 using GST pulldown

As good antibodies against Sephs1 were not available mSephs1 was myc tagged (3.12) and introduced into 293T cells by transfection in order to perform GST pulldown. The Sephs1-Myc protein expressed from the mSephs1-Myc plasmid was of the correct size ~50 kD (Fig. 22 "input"). However it could not be determined using GST pulldown whether Sephs1 interacts with AQP4, as the Sephs1-Myc protein seems prone to attach unspecifically to the sepharose beads and could therefore always be detected on all three types of beads AQP4-GST, 3A-GST and GST. Even though the beads were washed for 5 hours in buffer B(0.5) equally strong bands could still be seen on each bead (Fig. 22)

The results of the Y2H screen indicated that the AQP4 C-terminal interacts with two Ubiquitins, in order to test this, GST pulldown was carried out on untransfected 293T cells and the results analyzed on western blot using the mouse monoclonal Ubiquitin antibody P4D1-A11. The results of the GST pulldown suggest that Ubiquitin does not interact with AQP4. However, this experiment was only performed twice, once with three hour wash in buffer B (contains 0.1 M NaCl) and once with three hour wash in buffer B(0.3). When the beads were only washed in buffer B faint but equally strong ~8 kD bands can be seen on all beads (Fig. 23 A) but when buffer B(0.3) was used no Ubiquitin could be detected on the beads (Fig. 23 B).

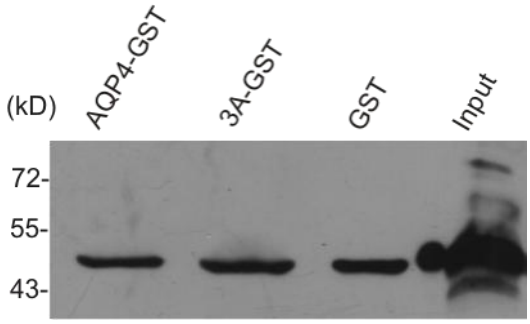

Figure 22. GST pulldown of Sephs1-Myc.

Results of a GST pulldown from a lysate of 293T cells transfected with mSephs1-Myc visualized on a western blot using the Myc antibody. Equally strong ~50 kD bands could be detected on each bead indicating that Sephs1-Myc is binding unspecifically to the sepharose beads. (input 5%)

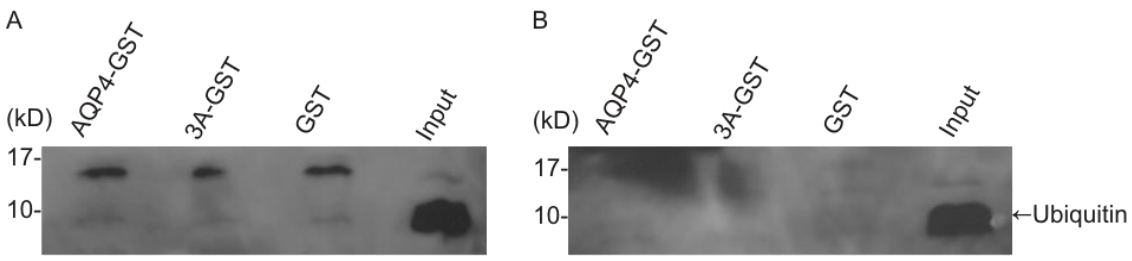

Figure 23. GST pulldown of Ubiquitin endogenous to 293T cells

Results of a GST pulldown from a lysate of untransfected 293T cells visualized on a western blot using the Ubiquitin antibody P4D1-A11. **A.** When the beads were washed only in buffer B very faint ~8 kD bands can be seen from all beads but a strong band in the input. The other bands ~15 kD likely represent ubiquitinated proteins. **B.** When the beads are washed in buffer B(0.3) bands can only be seen in input but not on the beads.

5 Discussion

The aim of this project was to identify and analyze proteins interacting with the AQP4 cytoplasmic C-terminal tail, specifically proteins containing PDZ domains as AQP4 contains the C-terminal sequence motif SSV which is known to interact with PDZ domains.

Strong evidence suggest that AQP4 is anchored at the astrocyte perivascular endfeet by the dystrophin complex (68, 69). While it has been hypothesized that the association of AQP4 with the dystrophin complex takes place via a PDZ mediated interaction with α-Syntrophin, to date AQP4 has however not been shown to interact directly with α-Syntrophin (78) or any other PDZ domain containing protein. Whether AQP4 is at all localized by a PDZ mediated interaction is unclear as there exist evidence both in favor (80) and against (72, 79) PDZ mediated AQP4 localization, the identification of PDZ proteins interacting with the C-terminal of AQP4 could therefore be of great significance and shed new light on the function of AQP4.

The interaction of AQP4 with four candidate proteins previously identified by a Y2H screen, the PDZ scaffolding protein Mupp1, Sephs1 and two Ubiquitins were analyzed using the *in vitro* protein interaction assay GST pulldown as well as coimmunostaining of tissue sections and cell cultures. In addition, the possibility of AQP4 interacting with the Syntrophins was re-examined.

5.1 The interaction of AQP4 with Mupp1

The results of this study argue strongly for an interaction of the 10th PDZ domain of Mupp1 with the AQP4 C-terminal PDZ ligand *in vitro*. In addition to show an interaction with AQP4 in the Y2H screen, Mupp1 endogenous to 293T cells as well as full length Myc tagged Mupp1 were pulled down by AQP4-GST but not 3A-GST showing that the interaction is PDZ specific (Fig. 5 and 7). The fact that Mupp1 9+10 was pulled down only by AQP4-GST while Mupp1 7+8 was not pulled down at all, is pivotal because it shows that the AQP4 PDZ ligand does not interact unspecifically to any PDZ domains when they are overexpressed (Fig. 7). However Mupp1 and AQP4 did not show any colocalization neither *in vitro* in transfected 293T cells nor *in vivo* in brain and kidney sections (Fig. 8 and 10). Although there is a possibility that AQP4 and Mupp1 colocalize and interact in other tissues which were not examined in this study it is unlikely, specifically considering that both proteins are expressed in ependymal cells but still do not colocalize (Fig. 9).

5.2 The interaction of AQP4 with Patj

5.2.1 Colocalization and interaction of Patj and AQP4 in vitro

Because the 10th PDZ domain of Mupp1 interacted so specifically with AQP4 it was decided to examine Patj, a paralogue of Mupp1. Comparison of individual Mupp1 PDZ domains with those of Patj revealed that the 10th PDZ domain of Mupp1 and the 8th of Patj share 77% amino acid sequence identity (Table 4). Like Mupp1 Patj was pulled down only by AQP4-GST showing that it

interacts with AQP4 in a PDZ specific manner (Fig. 12) but unlike Mupp1 it showed a clear colocalization with AQP4 *in vitro* at the cell membrane of 293T cells cotransfected with mAQP4 and Patj 7xMyc (Fig. 13).

5.2.2 Immunostaining of tissue sections for Patj

Two antibodies were used for Patj immunostaining of tissue sections and primary astrocyte-HUVEC cocultures, Patj (Abnova) a mouse monoclonal antibody and Patj (Bivic) a rabbit polyclonal antibody. For immunohisto- and immunocytochemistry with these antibodies the best results were obtained when the samples were fixed using acetone, the problem with acetone fixation is however that the morphology is not as well maintained as when other fixation methods are employed.

Coimmunostaining of brain sections using the Patj (Bivic) and Syntrophin antibodies showed a clear colocalization of Patj and Syntrophin around brain capillaries which indirectly shows colocalization of AQP4 and Patj because AQP4 and Syntrophin colocalize clearly around brain capillaries as well (Fig. 14).

Coimmunostaining of brain and kidney sections using the AQP4 and Patj (Abnova) antibodies revealed that AQP4 and Patj colocalize around brain capillaries, in the kidney however AQP4 and Patj are localized to different cell types in the medulla and do not colocalize (Fig. 15 and 16). These *in vivo* coimmunostaining experiments strongly suggest that Patj is localized to the astrocyte perivascular endfeet.

5.2.3 Establishing primary astrocyte-HUVEC cocultures and Patj immunostaining of cocultures

A primary astrocyte-HUVEC coculture model was successfully established in this study. The main goals of this model was to use HUVECs to induce endfeet formation in astrocytes as well as to polarize AQP4 towards the HUVEC-astrocyte interface. Next step was then to confirm if Patj and Syntrophin colocalize with AQP4 in astrocytes at the HUVEC-astrocyte interface.

In coculture HUVECs formed small colonies completely surrounded by astrocytes (Fig. 17 and 18), in the astrocytes surrounding the HUVEC colonies AQP4 immunoreactivity was very strong adjacent to the astrocyte-HUVEC interface. The parts of the astrocyte cell body which were not in contact with HUVEC colonies displayed even distribution of AQP4 similar to what is seen in primary astrocytes cultured alone (Fig. 19).

Immunostaining of primary astrocyte-HUVEC coculture for Patj were hindered by the fact that high quality antibodies were not available. The HUVECs also tended to fall off the slides leaving empty areas behind and the astrocytes did not retain their morphology very well, presumably due to the acetone fixation. Only the Patj (Bivic) antibody was suitable for Patj immunostaining in primary astrocyte-HUVEC cocultures, the Patj (abnova) antibody did not work. Despite these

hurdles Syntrophin showed a colocalization with both AQP4 and Patj in astrocytes surrounding empty areas possibly left behind when the HUVECs fell off (Fig. 20).

5.2.4 Possible roles of the AQP4-Patj interaction

What the functional significance of the interaction of AQP4 with Patj is, remains an open question. However, considering that Patj is a PDZ scaffolding protein containing ten PDZ domains and most interaction partners of PDZ scaffolding proteins are membrane proteins, it is likely that Patj localizes AQP4 with other membrane proteins. A possible candidate for such a protein would be the potassium channel Kir4.1 which harbours a class I PDZ ligand on its C-terminal. Kir4.1 is localized in astrocyte perivascular endfeet (98) and clears excess K^+ generated during neuronal activity from the extracellular space. AQP4 and Kir4.1 show a strict colocalization in Müller glia (99) and Kir4.1, like AQP4, is associated with the dystrophin complex in Müller glia (100). It has been proposed that AQP4 and Kir4.1 are functionally coupled (30), although this hypothesis has been challenged (101). Kir4.1 has been shown to interact with the PDZ scaffolding protein Cipp (Channel Interacting PDZ domain Protein) (102, 103). Cipp which is primarily expressed in brain and kidney is a short isoform of Patj and contains four PDZ domains which match PDZ domains 7-10 of full length Patj (102). So it is possible that Patj brings together AQP4 and Kir4.1 in endfeet.

Another possibility is that AQP4 is localized to the leading edge of migrating astrocytes by Patj. In migrating epithelial cells Patj is found at the leading edge in a complex with the polarity proteins Par (Partition defective protein) and aPKC (atypical protein kinase C) (104). The Par proteins along with aPKC can also be found at the leading edge of migrating astrocytes (105) and it is well established that AQP4 as well is localized at the leading edge of migrating astrocytes (58, 60).

5.3 The interaction of AQP4 with a Syntrophin endogenous to 293T cells

The Y2H screen was unable to detect an interaction between the AQP4 C-terminal tail and α-Syntrophin. However in this study it was shown using GST pulldown that AQP4 interacts in a PDZ specific manner with a Syntrophin endogenous to 293T cells. The antibody used to visualize the results of the GST pulldown on a western blot recognizes three isoforms of Syntrophin α, β1 and β2 so the Syntrophin which was shown to interact with AQP4 could be any one of those isoforms.

It is however possible in the case of Syntrophin that the Y2H result is a false negative and/or that the GST pulldown result does not represent what happens *in vivo* as both these techniques have limitations. The fact that Y2H is performed in yeast can lead to false negative or false positive results when interaction between mammalian proteins are being studied, as mammalian proteins are not neccessarily correctly modified postranslationally when expressed in yeast. Furthermore, potential interaction partners are overexpressed during Y2H which can lead to unspecific interactions. A factor which can lead to a false postive result from GST pulldown is the fact that

the interaction takes place *in vitro* after the cell has been lysed and all cellular organization has been abolished. Under these circumstances a prey protein which would never interact with the GST bait protein *in vivo* due to its subcellular location is floating free and can interact with the bait protein, an obvious example of this would be the interaction of AQP4 with Mupp1. One additional factor which can affect the results of both Y2H and GST pulldown is that both techniques rely on fusion proteins, removing a portion of a protein as is done in GST pulldown or fusing it with another protein which is done both in GST pulldown and Y2H can lead to a false positive or false negative result.

Assuming that the interaction of Syntrophin with AQP4-GST is not an artifact, other possibilities remain. First, AQP4 might simply interact directly with α-Syntrophin and the result of the Y2H screen is false possibly due to incorrect or lack of post translational modifications. This possibility is supported by the fact that the association of AQP4 with the dystrophin complex is lost in the α-Syntrophin$^{-/-}$ mouse and as a result AQP4 diffuses unspecifically in the plasma membrane. The second possibility is that AQP4 might be interacting with either β1 or β2 Syntrophin instead of α-Syntrophin which would explain the Y2H result. In support of this β2 syntrophin has been shown to be a part of a dystrophin complex in HeLa cells containing the dystrophin isoform DP71 (106) which is the primary dystrophin isoform in the brain and is found in astrocyte endfeet (107). The mislocalization of AQP4 in α-Syntrophin$^{-/-}$ mice could then be a result of loss of β-Syntrophin due to instability of the dystrophin complex once α-Syntrophin is missing. The third possibility is that AQP4 interacts with α-Syntrophin indirectly through an intermediate protein and both proteins, α-Syntrophin and the intermediate are pulled down during GST pulldown experiments.

5.4 The interaction of AQP4 with Sephs1 and Ubiquitin

In addition to Mupp1, the Y2H screen identified two Ubiquitins and Sephs1 as potential interaction partners of the AQP4 C-terminal tail. As none of these proteins contain a PDZ domain they would be expected to interact with both the AQP4-GST and 3A-GST.

Using GST pulldown it was determined that Ubiquitin neither interacts with AQP4-GST nor 3A-GST, in contrast to the Y2H result. As is discussed in 5.3 possible reasons for this could be that the Y2H results were false positives due to incorrect or lack of post translational modifications of the Ubiquitins or AQP4 C-terminal or protein overexpression.

Because no commercial antibodies of sufficient quality exist against Sephs1 the vector mSephs1-Myc was created to use in GST pulldown experiments. Once transfected with mSephs1-Myc 293T cells expressed a protein of the correct size as detected by a western blot using a Myc antibody. However, it could not be determined using GST pulldown whether Sephs1-Myc interacts with AQP4, as it interacted unspecifically to the sepharose beads and could therefore always be detected on all beads even though they were washed in buffer B(0.5).

In order to evaluate whether Sephs1-Myc interacts with AQP4-GST it may be possible to increase the NaCl concentration of the wash buffer during pulldown experiment until Sephs1-Myc

unspecifically bound to the beads falls off which would work assuming that Sephs1-Myc has more affinity for AQP4 than for the sepharose beads. Alternatively the GST proteins could have been eluted off the beads using reduced glutathione which would work if Sephs1-Myc is interacting unspecifically with the sepharose beads but not the GST peptide.

5.5 Future perspectives

5.5.1 Patj

The logical next step in studying the interaction of Patj with AQP4-GST is to carry out GST pulldown experiments on 293T cells transfected with smaller fragments or even individual PDZ domains of Patj, as was done with Mupp1. In this way it would be possible to identify the PDZ domain or domains of Patj which AQP4-GST interacts with, presumably the 8th PDZ domain. In addition showing that AQP4-GST does not interact unspecifically with all overexpressed Patj PDZ domains is an important negative control.

To further confirm the interaction of AQP4 and Patj *in vitro,* an interesting approach would be to create the vector mAQP4-3A, which would be analogous to the mAQP4 vector except that the SSV sequence motif would be replaced by three alanine residues. The mAQP4 and mAQP4-3A vectors could then be used along with Patj 7xMyc to cotransfect MDCK cells, as it is well established that AQP4 is localized basolaterally in these cells. Only the full length AQP4 would be expected to colocalize with Patj or its individual PDZ domains.

Due to the fact that high quality antibodies for Patj are not available, Patj could not be shown to localize in astrocyte endfeet surrounding HUVEC colonies in the primary astrocyte-HUVEC cocultures. An attempt to overcome this problem by cotransfecting CRL-2006 with mAQP4 and Patj 7xMyc was not successful because transfection of CRL-2006 with mAQP4 results in cell death presumably because of excessive water influx (section 4.7).

A potential solution to this problem could be to mutate the NPA motif of mAQP4 so it is unable to transport water. CRL-2006 cells cotransfected with NPA mutated mAQP4 and Patj 7xMyc could then also be used to determine if AQP4 and Patj colocalize during astrocyte migration. To establish whether Patj localizes AQP4 to the astrocyte endfeet and to the leading edge of migrating astrocytes the PDZ domain of Patj which interacts with AQP4 could be mutated or the SSV sequence motif of the NPA mutated mAQP4 replaced by three alanine residues.

5.5.2 Syntrophin

To establish whether AQP4-GST interacts with α, β1 or β2 Syntrophin or interacts indirectly with α-Syntrophin through an intermediate protein, a suitable approach would be to add an epitope tag to all three Syntrophin isoforms, express them and use GST pulldown to find which one is interacting with AQP4. If AQP4 then shows an interaction with α but not β1 or β2-Syntrophins it would be possible to purify the epitope tagged α-Syntrophin using a column lined with the antibody which recognizes the epitope tag. The epitope tagged α-Syntrophin could then be

released from the column into a solution and because it is then the only protein present in this solution GST pulldown could be used to determine whether α-Syntrophin interacts with AQP4 through an intermediate protein or not.

6 Concluding remarks

It has long been postulated that the C-terminal PDZ ligand of AQP4 interacts with a PDZ domain protein that might serve to localize AQP4 specificially to the astrocyte perivascular endfeet or be important for its function. However, it was unknown which protein this might be. In this study a novel PDZ dependent interaction of AQP4 with the scaffolding protein Patj was identified using GST pulldown. This study also shows that AQP4 and Patj colocalize at the cell membrane in cell culture and around brain capillaries in mouse brain sections. Taken together these results show that AQP4 and Patj most likely interact in astrocyte perivascular endfeet.

Additionally in this study a primary astrocyte-HUVEC coculture model was developed, which models the formation of astrocyte endfeet as judged by the polarized distribution of AQP4. This model will without doubt be useful for future studies of AQP4 in the laboratory.

In this project it was also revealed that AQP4 interacts with a Syntrophin endogenous to HEK 293T cells in a PDZ dependent manner. In combination with the results of the Y2H screen, this indicates that AQP4 interacts with α-Syntrophin, possibly through an unknown intermediate protein or interacts with β1 or β2 Syntrophin.

Appendix

Table 5. List of antibodies used in this study.

Antibody	Clone	Species	Isotype	Dilution (IF)	Dilution (WB)	Origin Cat nr./ Ref.
AQP4	Polyclonal	Rabbit	IgG	1/200	1/2500	Millipore AB2218
Synthropin	1351	Mouse	IgG1	1/200	1/2500	Abcam AB11425
Mupp1	43	Mouse	IgG1	1/200	1/500	BD Biosc. 611559
Patj	Polyclonal	Rabbit	IgG	1/200	-	Bivic. A.L (108)
Patj	603199	Mouse	IgG1	1/200	-	Abnova H-A01
GFAP	GA5	Mouse	IgG1	1/200	-	Chemicon MAB360
GFAP	Polyclonal	Rabbit	IgG	1/100	-	Dako Z0334
CD31	JC70A	Mouse	IgG1	1/50	-	Dako M0823
Myc	4A6	Mouse	IgG1	1/200	1/500	Upstate 05-724
Xpress	-	Mouse	IgG1	-	1/10000	Invitrogen R910-25
Ubiquitin	P4D1-A11	Mouse	IgG1	-	1/1000	Upstate 05-944

Table 6. List of plasmids used in this study.

Name	Vector	Insert	Species	Origin
Mupp1 7xMyc	pME18S	Mupp1 + 7xMyc	Mouse	Adachi M (97)
Mupp1 7+8	pCDNA4	Mupp1 PDZ 7+8 (Xpress)	Rat	Baraban J (109)
Mupp1 9+10	pCDNA5	Mupp1 PDZ 9+10 (Xpress)	Rat	Baraban J (109)
Patj 7xMyc	pCAGGS	Patj + 7xMyc	Mouse	Adachi M (97)
pGEX-6p1	pGEX-6p1	-	-	GE Healthcare
pGEX-6p1-AQP4-wt	pGEX-6p1	AQP4 C-term (70 aa)	Mouse	See 3.12
pGEX-6p1-AQP4-3A	pGEX-6p1	AQP4 C-term (70 aa) (SSV→AAA)	Mouse	See 3.12
mAQP4	pCMV-SPORT6	AQP4	Mouse	GE Healthcare
mSephs1-Myc	pCMV-SPORT6	Sephs1 (Myc tag)	Mouse	See 3.12

References

1. Agre P, Kozono D. Aquaporin water channels: molecular mechanisms for human diseases. FEBS Lett. 2003 Nov;555(1):72-8.

2. Macey RI, Farmer REL. INHIBITION OF WATER AND SOLUTE PERMEABILITY IN HUMAN RED CELLS. Biochimica Et Biophysica Acta. 1970;211(1):104-&.

3. Knepper MA. THE AQUAPORIN FAMILY OF MOLECULAR WATER CHANNELS. Proc Natl Acad Sci U S A. 1994 Jul;91(14):6255-8.

4. Preston GM, Agre P. ISOLATION OF THE CDNA FOR ERYTHROCYTE INTEGRAL MEMBRANE-PROTEIN OF 28-KILODALTONS - MEMBER OF AN ANCIENT CHANNEL FAMILY. Proc Natl Acad Sci U S A. 1991 Dec;88(24):11110-4.

5. Preston GM, Carroll TP, Guggino WB, Agre P. APPEARANCE OF WATER CHANNELS IN XENOPUS OOCYTES EXPRESSING RED-CELL CHIP28 PROTEIN. Science. 1992 Apr;256(5055):385-7.

6. Kruse E, Uehlein N, Kaldenhoff R. The aquaporins. Genome Biol. 2006;7(2):6.

7. King LS, Kozono D, Agre P. From structure to disease: The evolving tale of aquaporin biology. Nat Rev Mol Cell Biol. 2004 Sep;5(9):687-98.

8. Ishibashi K, Hara S, Kondo S. Aquaporin water channels in mammals. Clin Exp Nephrol. 2009 Apr;13(2):107-17.

9. Smith BL, Agre P. ERYTHROCYTE MR-28,000 TRANSMEMBRANE PROTEIN EXISTS AS A MULTISUBUNIT OLIGOMER SIMILAR TO CHANNEL PROTEINS. J Biol Chem. 1991 Apr;266(10):6407-15.

10. Jung JS, Preston GM, Smith BL, Guggino WB, Agre P. MOLECULAR-STRUCTURE OF THE WATER CHANNEL THROUGH AQUAPORIN CHIP - THE HOURGLASS MODEL. J Biol Chem. 1994 May;269(20):14648-54.

11. Walz T, Hirai T, Murata K, Heymann JB, Mitsuoka K, Fujiyoshi Y, et al. The three-dimensional structure of aquaporin-1. Nature. 1997 Jun;387(6633):624-7.

12. Cheng AC, vanHoek AN, Yeager M, Verkman AS, Mitra AK. Three-dimensional organization of a human water channel. Nature. 1997 Jun;387(6633):627-30.

13. Sui HX, Han BG, Lee JK, Walian P, Jap BK. Structural basis of water-specific transport through the AQP1 water channel. Nature. 2001 Dec;414(6866):872-8.

14. Fu D, Libson A, Stroud R, Nfs. The structure of GlpF, a glycerol conducting channel. Ion Channels: From Atomic Resolution Physiology to Functional Genomics. Chichester: John Wiley & Sons Ltd; 2002. p. 51-65.

15. Gonen T, Walz T. The structure of aquaporins. Q Rev Biophys. 2006 Nov;39(4):361-96.

16. Nedergaard M, Ransom B, Goldman SA. New roles for astrocytes: Redefining the functional architecture of the brain. Trends Neurosci. 2003 Oct;26(10):523-30.

17. Bushong EA, Martone ME, Jones YZ, Ellisman MH. Protoplasmic astrocytes in CA1 stratum radiatum occupy separate anatomical domains. J Neurosci. 2002 Jan;22(1):183-92.

18. Iadecola C, Nedergaard M. Glial regulation of the cerebral microvasculature. Nat Neurosci. 2007 Nov;10(11):1369-76.

19. Mathiisen TM, Lehre KP, Danbolt NC, Ottersen OP. The perivascular astroglial sheath provides a complete covering of the brain microvessels: an electron microscopic 3D reconstruction. Glia. 2010 Jul;58(9):1094-103.

20. Abbott NJ, Ronnback L, Hansson E. Astrocyte-endothelial interactions at the blood-brain barrier. Nat Rev Neurosci. 2006 Jan;7(1):41-53.

21. Abbott NJ. Astrocyte-endothelial interactions and blood-brain barrier permeability. J Anat. 2002 Jun;200(6):629-38.

22. Hawkins BT, Davis TP. The blood-brain barrier/neurovascular unit in health and disease. Pharmacol Rev. 2005 Jun;57(2):173-85.

23. Janzer RC, Raff MC. ASTROCYTES INDUCE BLOOD-BRAIN-BARRIER PROPERTIES IN ENDOTHELIAL-CELLS. Nature. 1987 Jan;325(6101):253-7.

24. Rossi DJ. Another BOLD role for astrocytes: coupling blood flow to neural activity. Nat Neurosci. 2006 Feb;9(2):159-61.

25. Anderson CM, Nedergaard M. Astrocyte-mediated control of cerebral microcirculation. Trends Neurosci. 2003 Jul;26(7):340-4.

26. Zonta M, Angulo MC, Gobbo S, Rosengarten B, Hossmann KA, Pozzan T, et al. Neuron-to-astrocyte signaling is central to the dynamic control of brain microcirculation. Nat Neurosci. 2003 Jan;6(1):43-50.

27. Takano T, Tian GF, Peng WG, Lou NH, Libionka W, Han XN, et al. Astrocyte-mediated control of cerebral blood flow. Nat Neurosci. 2006 Feb;9(2):260-7.

28. Simard M, Nedergaard M. The neurobiology of glia in the context of water and ion homeostasis. Neuroscience. 2004;129(4):877-96.

29. Pellerin L. How astrocytes feed hungry neurons. Mol Neurobiol. 2005 Aug;32(1):59-72.

30. Amiry-Moghaddam M, Ottersen OP. The molecular basis of water transport in the brain. Nat Rev Neurosci. 2003 Dec;4(12):991-1001.

31. Hasegawa H, Ma TH, Skach W, Matthay MA, Verkman AS. MOLECULAR-CLONING OF A MERCURIAL-INSENSITIVE WATER CHANNEL EXPRESSED IN SELECTED WATER-TRANSPORTING TISSUES. J Biol Chem. 1994 Feb;269(8):5497-500.

32. Jung JS, Bhat RV, Preston GM, Guggino WB, Baraban JM, Agre P. MOLECULAR CHARACTERIZATION OF AN AQUAPORIN CDNA FROM BRAIN - CANDIDATE OSMORECEPTOR AND REGULATOR OF WATER-BALANCE. Proc Natl Acad Sci U S A. 1994 Dec;91(26):13052-6.

33. Frigeri A, Nicchia GP, Verbavatz JM, Valenti G, Svelto M. Expression of aquaporin-4 in fast-twitch fibers of mammalian skeletal muscle. J Clin Invest. 1998 Aug;102(4):695-703.

34. Au CG, Butler TL, Egan JR, Cooper ST, Lo HP, Compton AG, et al. Changes in skeletal muscle expression of AQP1 and AQP4 in dystrophinopathy and dysferlinopathy patients. Acta Neuropathol. 2008 Sep;116(3):235-46.

35. Chou CL, Ma TH, Yang BX, Knepper MA, Verkman S. Fourfold reduction of water permeability in inner medullary collecting duct of aquaporin-4 knockout mice. Am J Physiol-Cell Physiol. 1998 Feb;274(2):C549-C54.

36. Ma TH, Yang BX, Gillespie A, Carlson EJ, Epstein CJ, Verkman AS. Generation and phenotype of a transgenic knockout mouse lacking the mercurial-insensitive water channel aquaporin-4. J Clin Invest. 1997 Sep;100(5):957-62.

37. Zhang D, Vetrivel L, Verkman AS. Aquaporin deletion in mice reduces Intraocular pressure and aqueous fluid production. J Gen Physiol. 2002 Jun;119(6):561-9.

38. Verkman AS, Ruiz-Ederra J, Levin MH. Functions of aquaporins in the eye. Prog Retin Eye Res. 2008 Jul;27(4):420-33.

39. Elkjaer ML, Vajda Z, Nejsum LN, Kwon TH, Jensen UB, Amiry-Moghaddam M, et al. Immunolocalization of AQP9 in liver, epididymis, testis, spleen, and brain. Biochem Biophys Res Commun. 2000 Oct;276(3):1118-28.

40. Gorelick DA, Praetorius J, Tsunenari T, Nielsen S, Agre P. Aquaporin-11: a channel protein lacking apparent transport function expressed in brain. BMC Biochem. 2006;7:14.

41. Tait MJ, Saadoun S, Bell BA, Papadopoulos MC. Water movements in the brain: role of aquaporins. Trends Neurosci. 2008 Jan;31(1):37-43.

42. Takata K, Matsuzaki T, Tajika Y, Ablimit A, Hasegawa T. Localization and trafficking of aquaporin 2 in the kidney. Histochem Cell Biol. 2008 Aug;130(2):197-209.

43. Wells T. Vesicular osmometers, vasopression secretion and aquaporin-4: a new mechanism for osmoreception? Mol Cell Endocrinol. 1998 Jan 15;136(2):103-7.

44. Nielsen S, Nagelhus EA, AmiryMoghaddam M, Bourque C, Agre P, Ottersen OP. Specialized membrane domains for water transport in glial cells: High-resolution immunogold cytochemistry of aquaporin-4 in rat brain. J Neurosci. 1997 Jan;17(1):171-80.

45. Kobayashi H, Minami S, Itoh S, Shiraishi S, Yokoo H, Yanagita T, et al. Aquaporin subtypes in rat cerebral microvessels. Neurosci Lett. 2001 Jan;297(3):163-6.

46. Dolman D, Drndarski S, Abbott NJ, Rattray M. Induction of aquaporin 1 but not aquaporin 4 messenger RNA in rat primary brain microvessel endothelial cells in culture. J Neurochem. 2005 May;93(4):825-33.

47. Dermietzel R. Visualization by freeze-fracturing of regular structures in glial cell membranes. Naturwissenschaften. 1973 Apr;60(4):208.

48. Rash JE, Staehelin LA, Ellisman MH. Rectangular arrays of particles on freeze-cleaved plasma membranes are not gap junctions. Exp Cell Res. 1974 May;86(1):187-90.

49. Yang B, Brown D, Verkman AS. The mercurial insensitive water channel (AQP-4) forms orthogonal arrays in stably transfected Chinese hamster ovary cells. J Biol Chem. 1996 Mar 1;271(9):4577-80.

50. Verbavatz JM, Ma T, Gobin R, Verkman AS. Absence of orthogonal arrays in kidney, brain and muscle from transgenic knockout mice lacking water channel aquaporin-4. J Cell Sci. 1997 Nov;110 (Pt 22):2855-60.

51. Sorbo JG, Moe SE, Ottersen OP, Holen T. The molecular composition of square arrays. Biochemistry. 2008 Feb 26;47(8):2631-7.

52. Strand L, Moe SE, Solbu TT, Vaadal M, Holen T. Roles of aquaporin-4 isoforms and amino acids in square array assembly. Biochemistry. 2009 Jun 30;48(25):5785-93.

53. Fenton RA, Moeller HB, Zelenina M, Snaebjornsson MT, Holen T, MacAulay N. Differential water permeability and regulation of three aquaporin 4 isoforms. Cell Mol Life Sci. 2010 Mar;67(5):829-40.

54. Verkman AS, Binder DK, Bloch O, Auguste K, Papadopoulos MC. Three distinct roles of aquaporin-4 in brain function revealed by knockout mice. Biochim Biophys Acta-Biomembr. 2006 Aug;1758(8):1085-93.

55. Manley GT, Fujimura M, Ma TH, Noshita N, Filiz F, Bollen AW, et al. Aquaporin-4 deletion in mice reduces brain edema after acute water intoxication and ischemic stroke. Nat Med. 2000 Feb;6(2):159-63.

56. Papadopoulos MC, Verkman AS. Aquaporin-4 gene disruption in mice reduces brain swelling and mortality in pneumococcal meningitis. J Biol Chem. 2005 Apr;280(14):13906-12.

57. Papadopoulos MC, Manley GT, Krishna S, Verkman AS. Aquaporin-4 facilitates reabsorption of excess fluid in vasogenic brain edema. Faseb J. 2004 Jun;18(9):1291-+.

58. Saadoun S, Papadopoulos MC, Watanabe H, Yan DH, Manley GT, Verkman AS. Involvement of aquaporin-4 in astroglial cell migration and glial scar formation. J Cell Sci. 2005 Dec;118(24):5691-8.

59. Auguste KI, Jin SW, Uchida K, Yan DH, Manley GT, Papadopoulos MC, et al. Greatly impaired migration of implanted aquaporin-4-deficient astroglial cells in mouse brain toward a site of injury. Faseb J. 2007 Jan;21(1):108-16.

60. Papadopoulos MC, Saadoun S, Verkman AS. Aquaporins and cell migration. Pflugers Arch. 2008 Jul;456(4):693-700.

61. Puwarawuttipanit W, Bragg AD, Frydenlund DS, Mylonakou MN, Nagelhus EA, Peters MF, et al. Differential effect of alpha-syntrophin knockout on aquaporin-4 and kir4.1 expression in retinal macroglial cells in mice. J Neurochem. 2006 Jul;98:103-.

62. Binder DK, Yao XM, Zador Z, Sick TJ, Verkman AS, Manley GT. Increased seizure duration and slowed potassium kinetics in mice lacking aquaporin-4 water channels. Glia. 2006 Apr;53(6):631-6.

63. Binder DK, Oshio K, Ma TH, Verkman AS, Manley GT. Increased seizure threshold in mice lacking aquaporin-4 water channels. Neuroreport. 2004 Feb;15(2):259-62.

64. Eid T, Lee TSW, Thomas MJ, Amiry-Moghaddam M, Bjornsen LP, Spencer DD, et al. Loss of perivascular aquaporin 4 may underlie deficient water and K+ homeostasis in the human epileptogenic hippocampus. Proc Natl Acad Sci U S A. 2005 Jan;102(4):1193-8.

65. Worton R. MUSCULAR-DYSTROPHIES - DISEASES OF THE DYSTROPHIN-GLYCOPROTEIN COMPLEX. Science. 1995 Nov;270(5237):755-6.

66. Campbell KP. 3 MUSCULAR-DYSTROPHIES - LOSS OF CYTOSKELETON EXTRACELLULAR-MATRIX LINKAGE. Cell. 1995 Mar;80(5):675-9.

67. Bulfield G, Siller WG, Wight PAL, Moore KJ. X-CHROMOSOME-LINKED MUSCULAR-DYSTROPHY (MDX) IN THE MOUSE. Proceedings of the National Academy of Sciences of the United States of America-Biological Sciences. 1984;81(4):1189-92.

68. Wakayama Y, Jimi T, Misugi N, Kumagai T, Miyake S, Shibuya S, et al. DYSTROPHIN IMMUNOSTAINING AND FREEZE-FRACTURE STUDIES OF MUSCLES OF PATIENTS WITH EARLY STAGE AMYOTROPHIC LATERAL SCLEROSIS AND DUCHENNE MUSCULAR-DYSTROPHY. J Neurol Sci. 1989 Jun;91(1-2):191-205.

69. Shibuya S, Wakayama Y. CHANGES IN MUSCLE PLASMA-MEMBRANES IN YOUNG MICE WITH X-CHROMOSOME-LINKED MUSCULAR-DYSTROPHY - A FREEZE-FRACTURE STUDY. Neuropathol Appl Neurobiol. 1991 Aug;17(4):335-44.

70. Frigeri A, Nicchia GP, Nico B, Quondamatteo F, Herken R, Roncali L, et al. Aquaporin-4 deficiency in skeletal muscle and brain of dystrophic mdx mice. Faseb J. 2001 Jan;15(1):90-8.

71. Zelenina M, Zelenin S, Bondar AA, Brismar H, Aperia A. Water permeability of aquaporin-4 is decreased by protein kinase C and dopamine. Am J Physiol Renal Physiol. 2002 Aug;283(2):F309-18.

72. Madrid R, Le Maout S, Barrault MB, Janvier K, Benichou S, Merot J. Polarized trafficking and surface expression of the AQP4 water channel are coordinated by serial and regulated interactions with different clathrin-adaptor complexes. EMBO J. 2001 Dec 17;20(24):7008-21.

73. Ahn AH, Freener CA, Gussoni E, Yoshida M, Ozawa E, Kunkel LM. The three human syntrophin genes are expressed in diverse tissues, have distinct chromosomal locations, and each bind to dystrophin and its relatives. J Biol Chem. 1996 Feb 2;271(5):2724-30.

74. Alessi A, Bragg AD, Percival JM, Yoo J, Albrecht DE, Froehner SC, et al. gamma-Syntrophin scaffolding is spatially and functionally distinct from that of the alpha/beta syntrophins. Exp Cell Res. 2006 Oct 1;312(16):3084-95.

75. Yokota T, Miyagoe Y, Hosaka Y, Tsukita K, Kameya S, Shibuya S, et al. Aquaporin-4 is absent at the sarcolemma and at perivascular astrocyte endfeet in alpha 1-syntrophin knockout mice. Proc Jpn Acad Ser B-Phys Biol Sci. 2000 Feb;76(2):22-7.

76. Adams ME, Mueller HA, Froehner SC. In vivo requirement of the alpha-syntrophin PDZ domain for the sarcolemmal localization of nNOS and aquaporin-4. J Cell Biol. 2001 Oct 1;155(1):113-22.

77. Inoue M, Wakayama Y, Jimi T, Shibuya S, Hara H, Unaki A, et al. Skeletal muscle syntrophin interactors revealed by yeast two-hybrid assay. Nagoya J Med Sci. 2008 Aug;70(3-4):117-26.

78. Neely JD, Amiry-Moghaddam M, Ottersen OP, Froehner SC, Agre P, Adams ME. Syntrophin-dependent expression and localization of Aquaporin-4 water channel protein. Proc Natl Acad Sci U S A. 2001 Nov 20;98(24):14108-13.

79. Nakahama K, Fujioka A, Nagano M, Satoh S, Furukawa K, Sasaki H, et al. A role of the C-terminus of aquaporin 4 in its membrane expression in cultured astrocytes. Genes Cells. 2002 Jul;7(7):731-41.

80. Crane JM, Van Hoek AN, Skach WR, Verkman AS. Aquaporin-4 dynamics in orthogonal arrays in live cells visualized by quantum dot single particle tracking. Mol Biol Cell. 2008 Aug;19(8):3369-78.

81. Frigeri A, Nicchia GP, Repetto S, Bado M, Minetti C, Svelto M. Altered aquaporin-4 expression in human muscular dystrophies: a common feature? Faseb J. 2002 May;16(7):1120-+.

82. Cho KO, Hunt CA, Kennedy MB. THE RAT-BRAIN POSTSYNAPTIC DENSITY FRACTION CONTAINS A HOMOLOG OF THE DROSOPHILA DISKS-LARGE TUMOR SUPPRESSOR PROTEIN. Neuron. 1992 Nov;9(5):929-42.

83. Kim E, Niethammer M, Rothschild A, Jan YN, Sheng M. CLUSTERING OF SHAKER-TYPE K+ CHANNELS BY INTERACTION WITH A FAMILY OF MEMBRANE-ASSOCIATED GUANYLATE KINASES. Nature. 1995 Nov;378(6552):85-8.

84. Harris BZ, Lim WA. Mechanism and role of PDZ domains in signaling complex assembly. J Cell Sci. 2001 Sep;114(18):3219-31.

85. Hung AY, Sheng M. PDZ domains: Structural modules for protein complex assembly. J Biol Chem. 2002 Feb;277(8):5699-702.

86. Christopherson KS, Hillier BJ, Lim WA, Bredt DS. PSD-95 assembles a ternary complex with the N-methyl-D-aspartic acid receptor and a bivalent neuronal NO synthase PDZ domain. J Biol Chem. 1999 Sep;274(39):27467-73.

87. Gee SH, Sekely SA, Lombardo C, Kurakin A, Froehner SC, Kay BK. Cyclic peptides as non-carboxyl-terminal ligands of syntrophin PDZ domains. J Biol Chem. 1998 Aug;273(34):21980-7.

88. Krapivinsky G, Medina I, Krapivinsky L, Gapon S, Clapham DE. SynGAP-MUPP1-CaMKII synaptic complexes regulate p38 MAP kinase activity and NMDA receptor dependent synaptic AMPA receptor potentiation. Neuron. 2004 Aug;43(4):563-74.

89. Mancini A, Koch A, Stefan M, Niemann H, Tamura T. The direct association of the multiple PDZ domain containing proteins (MUPP-1) with the human c-Kit C-terminus is regulated by tyrosine kinase activity. FEBS Lett. 2000 Sep;482(1-2):54-8.

90. Lobanov AV, Hatfield DL, Gladyshev VN. Selenoproteinless animals: Selenophosphate synthetase SPS1 functions in a pathway unrelated to selenocysteine biosynthesis. Protein Sci. 2008 Jan;17(1):176-82.

91. Radany EH, Brenner M, Besnard F, Bigornia V, Bishop JM, Deschepper CF. DIRECTED ESTABLISHMENT OF RAT-BRAIN CELL-LINES WITH THE PHENOTYPIC CHARACTERISTICS OF TYPE-1 ASTROCYTES. Proc Natl Acad Sci U S A. 1992 Jul;89(14):6467-71.

92. Hertz L, Peng L, Lai JCK. Functional studies in cultured astrocytes. Methods. 1998 Nov;16(3):293-+.

93. Fischer AH, Jacobson KA, Rose J, Zeller R. Preparation of Cells and Tissues for Fluorescence Microscopy. In: Spector DL, Goldman RD, editors. Basic methods in microscopy. New York: Cold Spring Harbor Laboratory Press; 2006. p. 107-9.

94. Sambrook J, Russell DW. Molecular Cloning: a laboratory manual. third ed. Argentine J, editor. New York: Cold Spring Harbor Laboratory Press; 2001.

95. Vikis H, G., Kun-Liang G. Glutathione-S-Transferase-Fusion Based Assays for Studying Protein-Protein interactions. In: Fu H, editor. Protein-Protein Interactions: Methods and applications. New Jersey: Humana Press; 2004. p. 175-86.

96. Lanaspa MA, Almeida NE, Andres-Hernando A, Rivard CJ, Capasso JM, Berl T. The tight junction protein, MUPP1, is up-regulated by hypertonicity and is important in the osmotic stress response in kidney cells. Proc Natl Acad Sci U S A. 2007 Aug 21;104(34):13672-7.

97. Adachi M, Hamazaki Y, Kobayashi Y, Itoh M, Tsukita S, Furuse M. Similar and distinct properties of MUPP1 and Patj, two homologous PDZ domain-containing tight-junction proteins. Mol Cell Biol. 2009 May;29(9):2372-89.

98. Higashi K, Fujita A, Inanobe A, Tanemoto M, Doi K, Kubo T, et al. An inwardly rectifying K+ channel, Kir4.1, expressed in astrocytes surrounds synapses and blood vessels in brain. Am J Physiol-Cell Physiol. 2001 Sep;281(3):C922-C31.

99. Nagelhus EA, Horio Y, Inanobe A, Fujita A, Haug FM, Nielsen S, et al. Immunogold evidence suggests that coupling of K+ siphoning and water transport in rat retinal Muller cells is mediated by a coenrichment of Kir4.1 and AQP4 in specific membrane domains. Glia. 1999 Mar;26(1):47-54.

100. Fort PE, Sene A, Pannicke T, Roux MJ, Forster V, Mornet D, et al. Kir4.1 and AQP4 associate with Dp71- and utrophin-DAPs complexes in specific and defined microdomains of Muller retinal glial cell membrane. Glia. 2008 Apr 15;56(6):597-610.

101. Ruiz-Ederra J, Zhang H, Verkman AS. Evidence against functional interaction between aquaporin-4 water channels and Kir4.1 potassium channels in retinal muller cells. J Biol Chem. 2007 Jul;282(30):21866-72.

102. Kurschner C, Mermelstein PG, Holden WT, Surmeier DJ. CIPP, a novel multivalent PDZ domain protein, selectively interacts with Kir4.0 family members, NMDA receptor subunits, neurexins, and neuroligins. Mol Cell Neurosci. 1998 Jun;11(3):161-72.

103. Joo SH, Pei D. Synthesis and screening of support-bound combinatorial peptide libraries with free C-termini: determination of the sequence specificity of PDZ domains. Biochemistry. 2008 Mar 4;47(9):3061-72.

104. Shin K, Wang Q, Margolis B. PATJ regulates directional migration of mammalian epithelial cells. EMBO Rep. 2007 Feb;8(2):158-64.

105. Etienne-Manneville S, Manneville JB, Nicholls S, Ferenczi MA, Hall A. Cdc42 and Par6-PKCzeta regulate the spatially localized association of Dlg1 and APC to control cell polarization. J Cell Biol. 2005 Sep 12;170(6):895-901.

106. Fuentes-Mera L, Rodriguez-Munoz R, Gonzalez-Ramirez R, Garcia-Sierra F, Gonzalez E, Mornet D, et al. Characterization of a novel Dp71 dystrophin-associated protein complex (DAPC) present in the nucleus of HeLa cells: members of the nuclear DAPC associate with the nuclear matrix. Exp Cell Res. 2006 Oct 1;312(16):3023-35.

107. Nicchia GP, Nico B, Camassa LM, Mola MG, Loh N, Dermietzel R, et al. The role of aquaporin-4 in the blood-brain barrier development and integrity: studies in animal and cell culture models. Neuroscience. 2004;129(4):935-45.

108. Lemmers C, Medina E, Delgrossi MH, Michel D, Arsanto JP, Le Bivic A. hINADl/PATJ, a homolog of discs lost, interacts with crumbs and localizes to tight junctions in human epithelial cells. J Biol Chem. 2002 Jul 12;277(28):25408-15.

109. Estevez MA, Henderson JA, Ahn D, Zhu XR, Poschmann G, Lubbert H, et al. The neuronal RhoA GEF, Tech, interacts with the synaptic multi-PDZ-domain-containing protein, MUPP1. J Neurochem. 2008 Aug;106(3):1287-97.

Published paper

Cell. Mol. Life Sci. (2010) 67:829–840
DOI 10.1007/s00018-009-0218-9

Cellular and Molecular Life Sciences

RESEARCH ARTICLE

Differential water permeability and regulation of three aquaporin 4 isoforms

Robert A. Fenton · Hanne B. Moeller · Marina Zelenina · Marteinn T. Snaebjornsson · Torgeir Holen · Nanna MacAulay

Received: 29 September 2009 / Revised: 3 November 2009 / Accepted: 16 November 2009 / Published online: 15 December 2009

Abstract Aquaporin 4 (AQP4) is expressed in the perivascular glial endfeet and is an important pathway for water during formation and resolution of brain edema. In this study, we examined the functional properties and relative unit water permeability of three functional isoforms of AQP4 expressed in the brain (M1, M23, Mz). The M23 isoform gave rise to square arrays when expressed in *Xenopus laevis* oocytes. The relative unit water permeability differed significantly between the isoforms in the order of M1 > Mz > M23. None of the three isoforms were permeable to small osmolytes nor were they affected by changes in external K^+ concentration. Upon protein kinase C (PKC) activation, oocytes expressing the three isoforms demonstrated rapid reduction of water permeability, which correlated with AQP4 internalization. The M23 isoform was more sensitive to PKC regulation than the longer isoforms and was internalized significantly faster. Our results suggest a specific role for square array formation.

Keywords Aquaporin · Glial cells · Water permeability · Regulation · Protein kinase C · Isoforms

All authors belong to Nordic Center of Excellence for Water Imbalance Related Disorders.

Electronic supplementary material The online version of this article (doi:10.1007/s00018-009-0218-9) contains supplementary material, which is available to authorized users.

R. A. Fenton · H. B. Moeller
The Water and Salt Research Center, Department of Anatomy, University of Aarhus, 8000 Aarhus, Denmark

M. Zelenina
Department of Women's and Children's Health, Karolinska Institutet, 171-77 Stockholm, Sweden

M. Zelenina
Department of Applied Physics, Royal Institute of Technology, Stockholm, Sweden

M. T. Snaebjornsson
Department of Anatomy, University of Iceland, Reykjavik, Iceland

M. T. Snaebjornsson · T. Holen
Department of Anatomy, University of Oslo, PO Box 1105, Blindern, 0317 Oslo, Norway

N. MacAulay (✉)
Department of Cellular and Molecular Medicine, The Panum Institute, University of Copenhagen, Blegdamsvej 3, 12.6, 2200 Copenhagen, Denmark
e-mail: macaulay@sund.ku.dk

Introduction

Aquaporin 4 (AQP4) is the principal water channel in the central nervous system. It is predominantly expressed in areas with close contact to the blood vessels or to the cerebrospinal fluid, such as the pericapillary glial endfeet and the ventricular ependymal cell lining, in which fluid exchange takes place between the brain and the blood/cerebrospinal fluid [1, 2]. The distinct polarized expression of AQP4 appears to be promoted by the basal lamina-associated extracellular matrix component, agrin [3]. During pathophysiological conditions leading to brain edema, AQP4 plays a role in the underlying brain water accumulation, either by permitting water entry into the brain parenchyma or by allowing accumulated water to exit, depending on whether the edema is of cytotoxic or vasogenic origin (reviewed in [4]).

AQP4 in brain tissue, cultured primary astrocytes, or expressed in various heterologous expression systems is

reported to be regulated by numerous protein kinases, such as protein kinase C (PKC), protein kinase A (PKA), Ca^{2+}/calmodulin-dependent kinase II (CamKII), casein kinase II (CKII), and protein kinase G (PKG) [5–11]. Phosphorylation-dependent regulation of AQP4 might thus encompass several processes, including gating, protein internalization, lysosomal targeting, and Golgi transition.

Three of the AQP4 isoforms have been demonstrated to transport water: M1 (AQP4a) consisting of 323 amino acids, the shorter M23 (AQP4c) consisting of 301 amino acids, and Mz (AQP4e) consisting of 364 amino acids [12–14]. M23 is the prevalent isoform in the mammalian brain [15] and gives rise to the square arrays detected in the astrocytic endfeet [16–18]. The isoform composition of these square arrays is currently debated [19–21]. Co-transfection of the M1 and M23 isoforms modulate the size of square arrays [16], possibly due to palmitoylation of two cysteines at positions 13 and 17, which are lacking in the shorter M23 isoform [21, 22]. The importance of these two residues for square array formation was recently challenged and new molecular determinants put forth [23].

The rationale for endogenous expression of distinct isoforms of AQP4 in the brain and the function of square arrays have remained elusive, although the adhesive properties of AQP4 between adjoining membranes expressing the M23 isoform may provide a possible explanation [24]. Previously, two conflicting reports have estimated the unit water permeability of M1 and M23 to be either identical [15] or eightfold higher in M23 compared to M1 [25]. In this study, we aimed to resolve this discrepancy, in addition to investigating possible differences in the permeability profile and phosphorylation-dependent regulation of all three AQP4 isoforms.

Materials and methods

Oocyte preparation and expression of AQP4 isoforms

Xenopus laevis frogs were obtained from Nasco (USA) or National Center for Scientific Research (France). After surgical removal of the oocytes from anesthetized frogs, the follicular membrane was removed by incubation in Kulori medium (90 mM NaCl, 1 mM KCl, 1 mM $CaCl_2$, 1 mM $MgCl_2$, 5 mM HEPES, pH 7.4, 182 mOsm) containing 10 mg/ml collagenase (type 1; Worthington, NJ, USA) and trypsin inhibitor (1 mg/ml; Sigma, Denmark) for 1 h. Subsequently, the oocytes were washed five times in Kulori medium containing 0.1% bovine serum albumin (Sigma) and incubated in 100 mM K_2HPO_4 with 0.1% BSA for 1 h. After the final oocyte collection, the frogs were anesthetized and killed by decapitation. The protocol complies with the European Community guidelines for the use of experimental animals, and the experiments were approved by The Danish National Committee for Animal Studies. The three isoforms of rat AQP4 (AQP4a, AQP4c, and AQP4e) will in the remainder of the paper be referred to as M1, M23, and Mz, respectively. Note that it is not fully resolved whether the AQP4e cDNA encodes the Mz band detected in brain lysate [14]. The cDNAs encoding the isoforms in the oocyte expression vector pXOOM were linearized downstream from the poly-A segment, and in vitro transcribed using mMessage Machine according to manufacturer's instruction (Ambion). cRNA was extracted with MEGAclear (Ambion) and microinjected into defolliculated *Xenopus* oocytes (25 ng RNA/oocyte).

Freeze fracture electron microscopy

AQP4-expressing oocytes were fixed in 0.1 M sodium cacodylate (NaCac), 2.5% glutaraldehyde, pH 7.4 for 80 min with slow shaking and subsequently stored in 0.12 M NaCac, 34% glycerol, 0.12% gluteraldehyde at 4°C. Freeze fracture was performed essentially as previously described [26]. In brief, fixed oocytes were equilibrated overnight in 25% glycerol at 4°C, attached to gold holders, and snap frozen in Freon 22 cooled in liquid nitrogen. Oocytes were fractured in a Balzer's freeze fracture apparatus (BAF 300; Balzers) at −100°C. Samples were immediately rotary shadowed at an angle of 25° with platinum and carbon replicated. The replicas were cleaned overnight in 40% chrome oxide, rinsed with water, and analyzed with a CM100 TEM microscope (FEI).

Blue native gel electrophoresis (BN-PAGE) of AQP4 isoforms expressed in HeLa cells and *Xenopus* oocytes

HeLa cells were grown in 75-cm^2 culture flasks using Dulbecco's modified Eagle medium (DMEM; Invitrogen) supplemented with 10% fetal bovine serum (FBS; Gibco) and 1% L-glutamine (Lonza). At 24 h prior to transfection, cells were seeded at a density of 20,000 cells/cm^2. FuGENE6 transfection reagent (Roche) was used at the ratio of 3:1 (FuGENE6:DNA) in accordance with the manufacturer's instructions. Then, 24 h post-transfection cells were trypsinized and suspended in 9 ml of medium before centrifugation at 1,000*g* for 10 min. Subsequently, cells were washed in 10 ml of phosphate buffered saline (PBS) and centrifuged again at 1,000*g* for 10 min. Cells from one 75-cm^2 culture flask were homogenized in 200 µl of HEPES buffer (10 mM HEPES, pH 7.4, 2 mM EDTA, 333 mM sucrose, and complete protease inhibitor cocktail; Roche) using cold mortar and pestle. The lysate was centrifuged at 1,000*g* for 10 min and the supernatant used for BN-PAGE electrophoresis. *Xenopus* oocytes and cerebellum from rat were homogenized in the HEPES buffer in the

ratio 1:10 (mg tissue: µl buffer) and the lysate was then treated as described above for the cell lysate. Next, 2–10 µg of total protein sample was mixed with 4× native PAGE sample buffer (Invitrogen) and 5% dodecyl β-D-maltoside (DDM) to a final concentration of 1× sample buffer and 1% DDM in a volume of 20 µl. Samples were incubated at RT for 10 min and then centrifuged for 10 min at 10,000*g*. After centrifugation, the supernatant was mixed with Coomassie G-250 1:4 (Coomassie G-250:DDM). Samples were loaded on a 4–16% BN-PAGE Bis–Tris gradient gel. NativeMark unstained protein standard (Invitrogen) was used as a molecular weight marker. Electrophoresis was carried out at 150 V, with the dark cathode buffer (5% 20× running buffer and 5% cathode additive; both Invitrogen) for the first 20 min, and with the light cathode buffer (5% 20× running buffer, 0.5% cathode additive) for the next 140 min. The anode buffer was the same as the cathode buffer but contained no cathode additive. Gels were then blotted to PVDF membranes and probed with AQP4 antibodies, as described previously [20].

Osmotic water permeability measurements on *Xenopus* oocytes

The osmotic water permeability measurements were performed as previously described [27]. During the measurements, the membrane potential of the oocytes was measured by two-electrode voltage clamp with a Dagan Clampator interfaced to an IBM-compatible PC using a Digidata 1322 A/D converter and pClamp 9.2 (Axon Instruments). The oocyte was placed in a small chamber with a glass bottom, through which the oocyte could be viewed via a long distance objective (×4) and a CCD camera. To quantify the oocyte volume changes, oocyte images were captured and processed as previously described in detail [27]. The experimental chamber was perfused by a control solution (100 mM NaCl, 2 mM KCl, 1 mM $CaCl_2$, 1 mM $MgCl_2$, 10 mM HEPES, pH 7.4) and hypertonic test solution which was obtained by adding 20 mOsm of mannitol to the control solution. For measurements of the reflection coefficients, the mannitol was replaced with equiosmolar urea, glycerol, or formamide. Osmolarities of the test solutions were determined with an accuracy of 1 mOsm by a cryoscopic osmometer (Gonotec, Berlin, Germany). For the experiments with 8 mM K^+, the control 2 mM K^+ solution contained an additional 6 mM choline chloride to keep the two control solutions equiosmolar. Phorbol 12-myristate 13-acetate (PMA) was obtained from Sigma–Aldrich. The osmotic water permeability is given in units of (cm/s) and was calculated as $L_p = -J_v/A \times \Delta\pi \times V_w$, where J_v is the water flux during the osmotic challenge, A is the true membrane surface area (about nine times the apparent area due to membrane foldings [28]), $\Delta\pi$ is the osmotic challenge, and V_w is the partial molal volume of water, 18 cm^3/mol.

Immunoblotting on *Xenopus* oocytes

The preparation of oocyte plasma membranes was modified from [29] and has been recently described in detail [30]. In brief, total oocyte membranes were obtained by homogenization (with a p200 pipette) of two oocytes in 1 ml HbA+ buffer: 5 mM $MgCl_2$, 5 mM NaH_2PO_4, 1 mM EDTA, 80 mM sucrose, 20 mM Tris, pH 7.48, containing the protease inhibitors leupeptin (8 µM) and pefabloc (0.4 mM). The supernatant was recovered following 10 min centrifugation at 250*g* and subsequently centrifuged at 14,000*g* for 20 min to obtain the total membrane fraction. The pellets were resuspended in 20 µl HbA+ followed by addition of 5 µl of 5× sample buffer (7.5% SDS, 250 mM Tris (pH 6.8), 30% glycerol, bromphenol blue, and 60 mg/ml DTT) and heated at 65°C for 15 min. Plasma membranes were obtained from a minimum of 15 oocytes for each construct/condition. The oocytes were treated as previously described [29] prior to homogenization and consecutive centrifugation steps [30]. Total oocyte membranes and purified plasma membranes were subjected to immunoblotting using rabbit polyclonal anti-AQP4 antibody (Alamone Labs, Israel), 1:1,000. Sites of antibody–antigen reaction were visualized using an enhanced chemiluminescence substrate (GE Healthcare, Denmark) before exposure to light-sensitive film. Numerous film exposures were performed to be certain that the linearity of the film was not exceeded. The band densities were quantified by densitometry.

Immunocytochemistry and confocal laser scanning microscopy on *Xenopus* oocytes

The oocytes were fixed for 1 h in 3% paraformaldehyde in Kulori medium, rinsed in Kulori medium, dehydrated in a series of ethanol concentrations (40 min in 70, 96, and 99% ethanol) and incubated in xylene for 1 h. Oocytes were infiltrated with paraffin for 1 h at 50°C before embedding. Next, 2-µm sections were cut on a Leica RM 2126 microtome and immunostained as described previously [31] using rabbit polyclonal anti-AQP4 antibody. An Alexa 488-conjugated secondary antibody was used for visualization (DAR; Invitrogen). A Leica TCS SL confocal microscope and Leica confocal software were used for imaging of the oocytes. Control AQP4-expressing oocytes were used to set laser intensity and capture settings on the microscope such that saturation of images for each condition was avoided. The microscope and laser settings were kept constant within each experiment. Images were taken

using an HCX PL APO ×63 oil objective lens. A minimum of two images per oocyte, with 3–5 oocytes per experiment, were used for statistical analysis. Image semi-quantification and validation has recently been described in detail [30]. To facilitate comparisons between experiments and between individual oocytes, plasma membrane fluorescence was normalized to total oocyte fluorescence.

Water permeability measurements in mammalian cells

A human bronchial epithelial cell line BEAS-2b (European Collection of Cell Cultures, Center for Applied Microbiology and Research, Salisbury, Wiltshire, UK; subpassages 8–16) was cultured on coverslips (Bioptechs, Butler, PA) coated with collagen type I and fibronectin (Sigma–Aldrich Sweden) in Dulbecco's MEM/NUT MIX F-12 (1:1) medium (Gibco, Paisley, Scotland, UK) containing 0.5 U/ml penicillin, 50 μg/ml streptomycin, and supplemented with 10% heat-inactivated FBS and 2 mM L-glutamine. On the second day of culture, the cells were transiently transfected using CLONfectin (Clontech) according to the manufacturer's protocol. cDNA constructs used for the transfection were described previously [32]. cDNA fragments encoding human AQP4 M1 and AQP4 M23 were subcloned into the pIRES2-EGFP vector (Clontech). The resulting constructs expressed AQP4 and GFP as separate proteins in the same cell. Experiments were performed on the fourth day of culture. Cells positive for AQP4 M1 and M23 were identified by GFP fluorescence. The GFP signal was distributed evenly in the cytoplasm of the cells. The cells positive for AQP4 M1 and M23 were not different in morphology compared to each other or to the untransfected cells.

Water permeability of the cells was measured as previously described [7, 11, 33]. Briefly, the cells were mounted in a closed chamber on the stage of an inverted confocal laser scanning microscope in isoosmotic, 300 mOsm PBS. The cells were loaded with 20 μM calcein-AM (Molecular Probes; Invitrogen) for 5 min at RT. Loading with calcein was similar in transfected and untransfected cells. The cells were perfused with isosmotic PBS and scanned every 1.8 s with excitation at 488 nm. The fluorescent signal was collected at 515–525 nm from an optical slice within the cell body. The cells were then subjected to an osmotic shock by switching the perfusate to a hypoosmotic, 200 mOsm, PBS, obtained by omission of 50 mM NaCl from the isosmotic solution. The swelling of the cells was monitored as a decrease of calcein fluorescence, which occurred due to the dilution of the fluorophore and a reduction in self-quenching. The initial slope of the fluorescence intensity curve was used to calculate water permeability (P_f) of each cell as described in detail previously [7, 11, 32, 33]. The P_f of all cells in each experiment was expressed relative to the mean maximal P_f in cells transfected with M1.

Osmolyte uptake measurements in *Xenopus* oocytes

The uptake of osmolytes was measured using radioactively labeled compounds. The experiments were performed in 24-well plates (five oocytes/condition) containing 500 μl test solution (100 mM NaCl, 2 mM KCl, 1 mM $CaCl_2$, 1 mM $MgCl_2$, 10 mM HEPES, pH 7.4) containing 20 mOsm of the unlabeled osmolyte and trace amounts of [^{14}C]mannitol, [^{14}C]urea, [^{14}C]glycerol, or [^{14}C]formamide (Amersham, UK). The oocytes were pre-incubated in control solution containing 20 mOsm of non-permeable sucrose in order to avoid imposing an osmotic challenge at the initiation of the uptake experiment. The oocytes were incubated in the test solution for 5 min at RT with gentle shaking, washed four times in ice-cold test solution without the radioactive osmolytes, and dissolved individually in 200 μl 10% SDS. Finally, 2 ml scintillation fluid (Opti-fluor; Packard, Netherlands) was added and the samples counted in a scintillation counter (Packard Tri-Carb).

Data are presented as mean ± SE for n = number of cells. Student's t test has been used for the statistical analysis.

Results

Three isoforms of AQP4 (M1, M23, and Mz) were individually expressed in *Xenopus* oocytes to investigate possible differences in their functional properties. This expression system is widely used to assess relative unit water permeability and solute permeability of different aquaporins (see, e.g., [30, 34]). Expression of the AQP4 isoforms increased the water permeability of the oocytes from (in $\times 10^{-3}$ cm/s) 0.10 ± 0.01 ($n = 19$) for the non-injected oocytes to 1.47 ± 0.05 ($n = 37$) for M1, 1.60 ± 0.11 ($n = 37$) for M23, and 1.31 ± 0.06 ($n = 37$) for Mz.

Formation of square arrays

To validate the use of *Xenopus* oocytes as an expression system for this comparative study, we explored the ability of AQP4 isoforms to form square arrays in oocytes by performing freeze fracture electron microscopy. As shown in Fig. 1a, b, and c, highly ordered structures characteristic of square arrays were visible in M23-expressing oocytes (P-face as well as E-face). These arrays were only apparent at the oocyte plasma membrane (electronic

supplementary material, Fig. 1). Due to the extensive invaginations of the *Xenopus* oocyte membrane [28], only sporadic patches of plasma membrane were in the plane of the fracture, which excluded quantitative studies of the array formation. No ordered structures were observed in oocytes expressing M1 and Mz (Fig. 1d, e). In addition, we analyzed M1-, M23-, and Mz-expressing oocytes using blue native poly-acryl gel electrophoresis (BN-PAGE) that was recently established as a biochemical assay to visualize AQP4 higher order structures [20]. As shown in Fig. 1f, the M23 isoform, whether heterologously expressed in HeLa cells or *Xenopus* oocytes, gave rise to the higher order structures that are the hallmark of the square arrays and also apparent in rat cerebellum. The M1 and Mz isoforms did not form higher order structures when expressed in HeLa cells or in *Xenopus* oocytes. Thus, in *Xenopus* oocytes, AQP4 assembles similarly to native tissue, making oocytes a suitable model for functional studies.

Relative unit water permeability of AQP4 isoforms expressed in *Xenopus* oocytes

The relative unit water permeability of M1 and M23 is debated [15, 25] and we therefore set out to resolve this issue. We have recently established sensitive methods to estimate the relative unit water permeability of different aquaporins [30] in which the water permeability of the AQP-expressing oocyte is normalized to the abundance of the AQP in the oocyte plasma membrane. We determined the water permeability of oocytes expressing M1, M23, or Mz by exposing the oocytes to an osmotic challenge of 20 mOsm mannitol (added to the control solution) (Fig. 2a). The water permeability of the native oocyte membrane (<10% of the total L_p) was deducted in order to obtain the contribution from each AQP4 (in $\times 10^{-3}$ cm/s): 1.15 ± 0.04 for M1 ($n = 25$), 1.17 ± 0.09 for M23 ($n = 25$), and 1.07 ± 0.05 for Mz ($n = 20$) for a total of 4–5 batches, which were not significantly different from

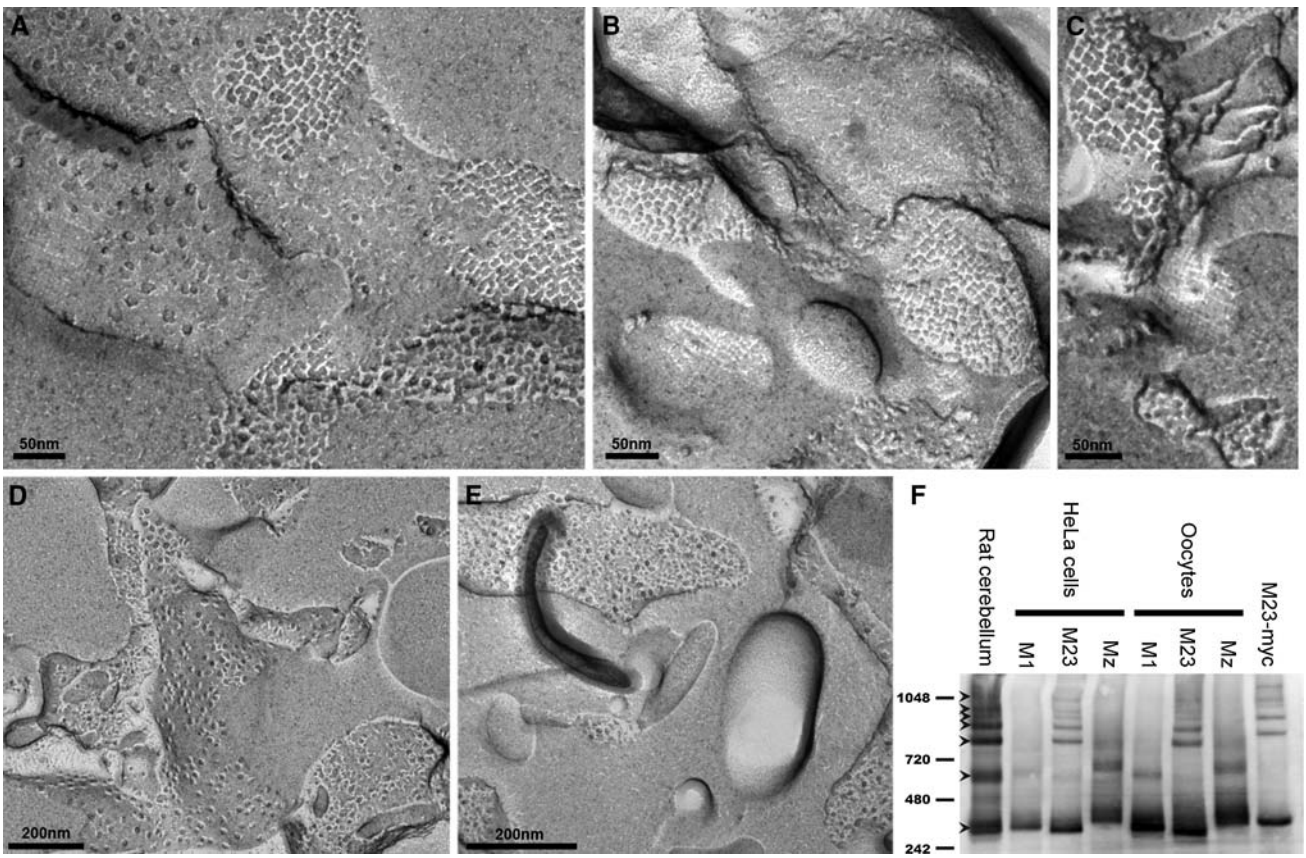

Fig. 1 The M23 isoform forms square arrays in *Xenopus laevis* oocytes. **a–c** At the plasma membrane, highly ordered structures characteristic of square arrays are observed for the M23 isoform. In contrast, neither the M1 isoform (**d**) nor the Mz isoform (**e**) show similar ordered structures. **f** BN-PAGE analysis of AQP4. In contrast to the M1 and Mz isoforms, the M23 isoform forms higher molecular weight moieties in both HeLa cells and *Xenopus* oocytes. *Lane 1* brain lysate (rat cerebellum), *lanes 2–4* M1, M23, and Mz expressed in HeLa cells, *lanes 5–7* M1, M23, and Mz expressed in *Xenopus* oocytes. Control M23-myc expressed in HeLa cells also exhibited higher order bands (*lane 8*). Molecular weight markers are indicated to the *left*, in kDa. The lower tetramer band and six higher order bands are indicated by *arrowheads*

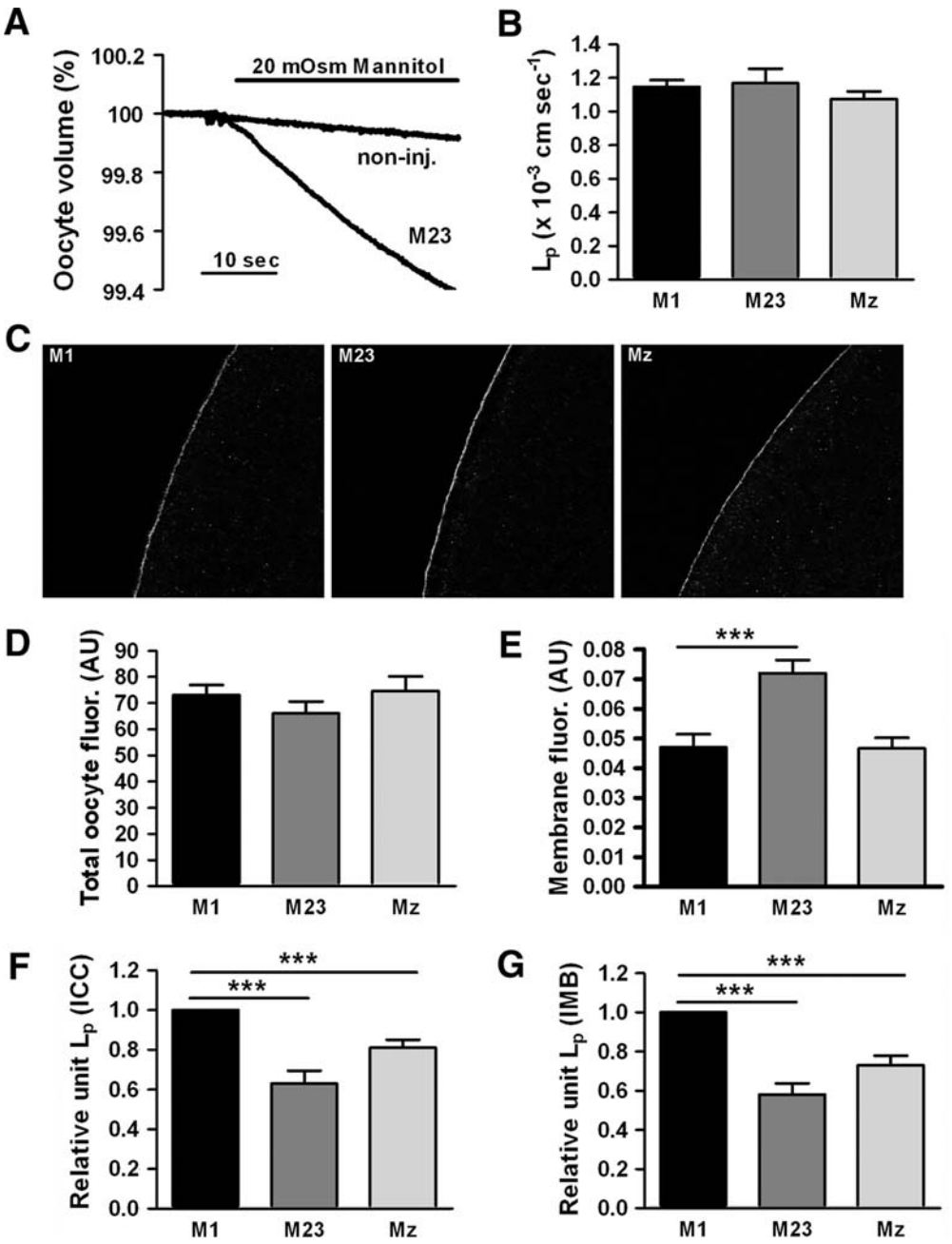

Fig. 2 The relative unit water permeability of M1, M23, and Mz expressed in oocytes. **a** An oocyte expressing the M23 isoform and a non-injected oocyte (with L_ps of 1.14 and 0.11×10^{-3} cm/s, respectively) were challenged with an osmotic gradient of 20 mOsm mannitol for 30 s. **b** The average water permeability of oocytes expressing M1, M23, or Mz with the contribution of the native oocyte membrane deducted ($n = 20$–25 of each). **c** Representative confocal laser scanning microscopy of oocytes expressing M1, M23 and Mz immunolabeled for AQP4. **d** Oocyte total fluorescent counts (in arbitrary units) were used to asses the abundance of AQP4 in oocytes expressing the three isoforms ($n = 15$–20 of each). **e** Oocyte plasma membrane fluorescent counts (in arbitrary units) were used to asses the AQP4 abundance in the plasma membrane of oocytes expressing the three isoforms ($n = 15$–20 of each). **f** Normalized relative unit water permeability of the three isoforms based on quantification by immunocytochemistry ($n = 4$–5 experiments based on 3–5 oocytes of each). **g** Normalized relative unit water permeability of the three isoforms based on quantification by immunoblotting of purified plasma membranes ($n = 3$ experiments, each based on $n = 5$ oocytes of each isoform for the L_p determination and $n = 20$ oocytes of each isoform for the plasma membrane purification). ***$P < 0.001$ (compared to M1)

each other (Fig. 2b). Subsequently, we determined the relative abundance of AQP4 protein in each oocyte (total abundance and plasma membrane abundance) by immunolabeling of the same oocytes employed for the L_p measurements using an anti-AQP4 antibody that recognizes the C-terminal part of the protein. Representative confocal images of the immunostained oocytes are shown in Fig. 2c. Semi-quantification of the images for each isoform revealed a similar amount of total fluorescent counts corresponding to total AQP4 protein in the oocytes (Fig. 2d), whereas the plasma membrane abundance differed between the isoforms, with M23 demonstrating a significantly larger fraction of the total protein in the plasma membrane ($P < 0.001$): (in arbitrary units, average of all oocytes used in the 4–5 batches of oocytes used in the dataset): 0.047 ± 0.004 for M1 ($n = 20$), 0.072 ± 0.004 for M23 ($n = 18$), and 0.047 ± 0.004 for Mz ($n = 18$) (Fig. 2e).

To compare the unit water permeability of the three isoforms, the water permeability relative to the plasma membrane abundance was calculated for *each* experiment (batch of oocytes) after which it was normalized to M1 and

then averaged. As shown in Fig. 2f, the relative unit water permeability of M23 was significantly lower than M1 ($P < 0.001$). The relative unit water permeability of Mz was intermediate and significantly lower than M1 ($P < 0.001$): 1.00 ± 0.00 for M1, 0.63 ± 0.07 for M23, and 0.81 ± 0.04 for Mz ($n = 4$–5 experiments with 3–5 oocytes expressing each isoform). To verify these results, we performed immunoblotting of total oocyte membranes and purified plasma membranes from M1-, M23-, and Mz-expressing oocytes day-matched with water permeability measurements on the same batch of oocytes. The total expression of AQP4 was similar for M1-, M23-, and Mz-expressing oocytes (data not shown) but in accordance with the immunostaining data, the M23 abundance was increased in the plasma membrane (data not shown). The relative unit water permeability of the different isoforms was calculated based on the densitometry of the immunoblotting of the purified plasma membranes (Fig. 2g): 1.00 ± 0.00 for M1, 0.58 ± 0.06 for M23, and 0.73 ± 0.05 for Mz ($n = 3$ experiments, each based on $n = 5$ oocytes for L_p measurement and $n = 20$ oocytes for membrane preparation for each isoform), thus confirming the reduced relative unit water permeability of the M23 isoform.

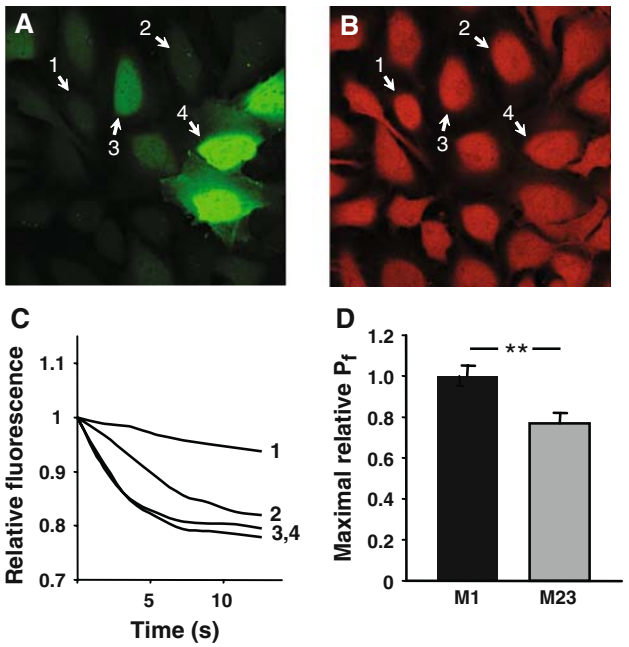

Fig. 3 The relative unit water permeability of M1 and M23 in transfected human bronchial epithelial cell line. **a** The level of GFP fluorescence within the cells. **b** Loading with calcein, which was used for water permeability measurements, was similar in AQP4-positive and AQP4-negative cells. *Numbers* indicate the same cells before (**a**) and after (**b**) calcein loading. **c** Single cell traces showing the dilution of calcein due to the cell swelling after an osmotic challenge. In cells with low GFP (and hence AQP4) expression (cells 1–3 in **a**), the swelling rate was increasing (*line 1* through *line 3* in **c**) with the increase in GFP (AQP4) level. The swelling of the cells 3 and 4 occurred at practically identical speed, probably due to saturation of the plasma membrane with AQP4. **d** Maximal relative water permeability in cells expressing M1 ($n = 22$) and M23 ($n = 13$), $^{**}P < 0.01$

Water permeability of AQP4 isoforms expressed in mammalian cells

To exclude the possibility that the reduced water permeability of M23 compared to M1 was specific to *Xenopus* oocytes as an expression system, we compared the relative water permeability of M1 and M23 in a bronchial epithelial cell line. The cells were transiently transfected with cDNA constructs that in each transfected cell produced two separate proteins, AQP4 and green fluorescent protein (GFP). GFP, which is a compact water soluble protein, was distributed throughout the cytoplasm and the nucleus of transfected cells (Fig. 3a). The cells with a weaker GFP signal demonstrated low water permeability, as judged from a low rate of swelling after hypoosmotic challenge (Fig. 3a, cell 1, and Fig. 3c, line 1). The cells with a stronger GFP signal had a higher water permeability (Fig. 3a, cells 2, 3, and Fig. 3c, lines 2, 3). With further increase in GFP expression, the rate of the swelling did not increase any further and the swelling of the cells 3 and 4 (Fig. 3a) occurred at practically identical speed (Fig. 3c), probably due to a saturation of the capacity of the plasma membrane to accommodate the water channels. The relative maximal P_f values that could be achieved in cells transfected with the M1 isoform were significantly higher than those in cells transfected with M23: 1.00 ± 0.05 for M1 ($n = 22$ cells) and 0.77 ± 0.05 for M23 ($n = 13$ cells), $P < 0.01$ (Fig. 3d).

Sensitivity to external K^+-concentration

To investigate a possible effect of K^+ on the water permeability of M1-, M23-, and Mz-expressing oocytes, we compared the water permeability in test solutions containing 8 mM KCl to the water permeability obtained in the presence of 2 mM KCl. In this experiment, oocytes had L_ps of (in $\times 10^{-3}$ cm/s) 1.63 ± 0.19 for M1, 2.38 ± 0.19 for M23, 1.37 ± 0.25 for Mz ($n = 5$ of each), and 0.10 ± 0.01 for non-injected oocytes ($n = 4$). The L_p of each oocyte was assessed at both K^+ concentrations and thereby served as its own control. The data are therefore presented as the ratio between the L_p obtained at 8 mM KCl and the L_p obtained at 2 mM KCl (Fig. 4). The water permeability of the three isoforms and the non-injected oocytes showed no significant degree of K^+-dependence; $L_{p(8K)}/L_{p(2K)}$: 0.98 ± 0.02 for M1, 1.01 ± 0.01 for M23, 1.05 ± 0.02 for Mz ($n = 5$ of each), and 1.02 ± 0.02 for non-injected oocytes ($n = 4$).

Solute permeability profile

To explore if M1-, M23-, or Mz-expressing oocytes were permeable to urea, glycerol, or formamide, we determined the L_p with 20 mOsm of each of these osmolytes and related them to the L_p obtained with the larger osmolyte, mannitol, to obtain the reflection coefficient, σ. These oocytes had L_ps of (in $\times 10^{-3}$ cm/s) 1.93 ± 0.12 for M1, 2.10 ± 0.41 for M23, 1.78 ± 0.33 for Mz ($n = 4$ of each), and 0.09 ± 0.02 for non-injected oocytes ($n = 3$). The reflection coefficients were identical for the three isoforms and the non-injected oocytes, which indicated that AQP4, independent of the isoform, was not permeable to these small molecules (Fig. 5a). The reflection coefficient was reduced for formamide, both for AQP4-expressing oocytes and for the non-injected oocytes, indicating that the native oocyte plasma membrane is slightly permeable to formamide. As a very low permeability to the osmolyte would not be detectable by this method, we performed uptake experiments using radio-labeled ^{14}C-mannitol, ^{14}C-urea, ^{14}C-glycerol, and ^{14}C-formamide (Fig. 5b). The pattern of the solute uptake by oocytes expressing M1, M23, Mz, and non-injected oocytes was identical to that observed for the reflection coefficients; expression of any of the three isoforms did not confer an increased permeability of the oocyte to any of these solutes ($n = 4$ experiments, 5 oocytes per condition).

PKC-dependent regulation

AQP4 is downregulated by PKC [8, 11, 35, 36] which we have found to be due to internalization of the protein [35].

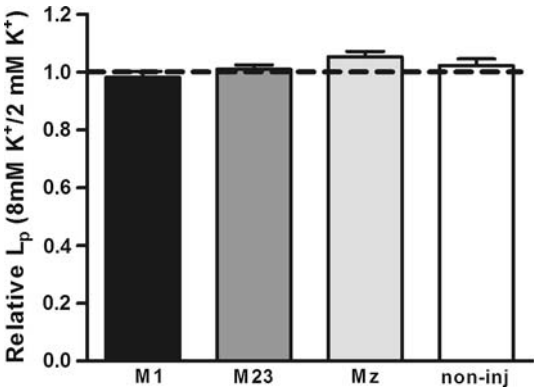

Fig. 4 Lack of K^+-dependent water permeability in M1, M23, and Mz-expressing oocytes. Oocytes expressing the three different isoforms were voltage-clamped to −50 mV to avoid K^+-dependent changes in membrane potential and exposed to test solution containing the standard 2 mM K^+ (+6 mM Ch^+) in which the L_p was determined. Subsequently the same oocyte was exposed to a test solution containing 8 mM K^+ in which the L_p was determined. The data are presented as the L_p obtained in 8 mM K^+ relative to that obtained in 2 mM K^+ ($n = 4$ of each)

Here, we investigated the rate of PKC-dependent downregulation of the three different isoforms. For each oocyte, the membrane-permeable PKC-activator, PMA (1 nM), was added to the test solution after determination of the oocyte basal water permeability. In this way, each oocyte was its own control and variations in the expression level did not affect the data. The L_p of the oocytes employed in this set of experiments was (in $\times 10^{-3}$ cm/s): 1.36 ± 0.07

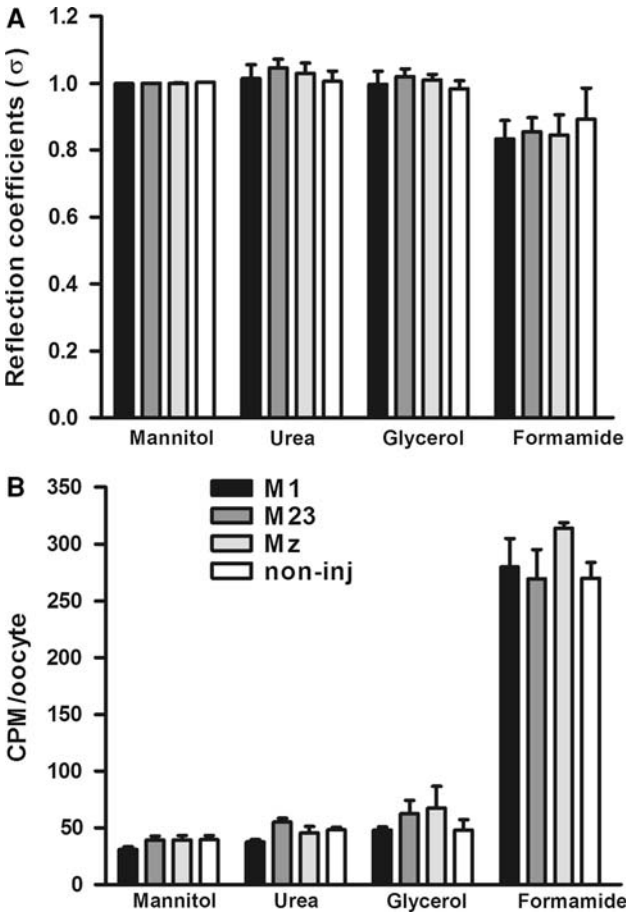

Fig. 5 Lack of permeability to small osmolytes in M1, M23, and Mz-expressing oocytes. **a** The L_p of oocytes expressing M1, M23, and Mz as well as non-injected oocytes was determined with different osmolytes; mannitol, urea, glycerol, and formamide (20 mOsm of each). The L_p obtained with urea, glycerol, and formamide was plotted relative to that obtained with mannitol for each oocyte (reflection coefficient, σ). The reflection coefficients for oocytes expressing M1, M23, or Mz were not significantly different from that of the non-injected oocytes ($n = 4$ of each isoform and $n = 3$ for the non-injected oocytes). **b** Oocytes expressing M1, M23, and Mz as well as non-injected oocytes were exposed to test solution containing different osmolytes; mannitol, urea, glycerol, and formamide (20 mOsm of each) in addition to trace amounts of the [^{14}C]-labeled osmolyte. The data are presented as the average uptake of four experiments performed in pentaplicate, with no significant difference between oocytes expressing the three isoforms and the non-injected oocytes

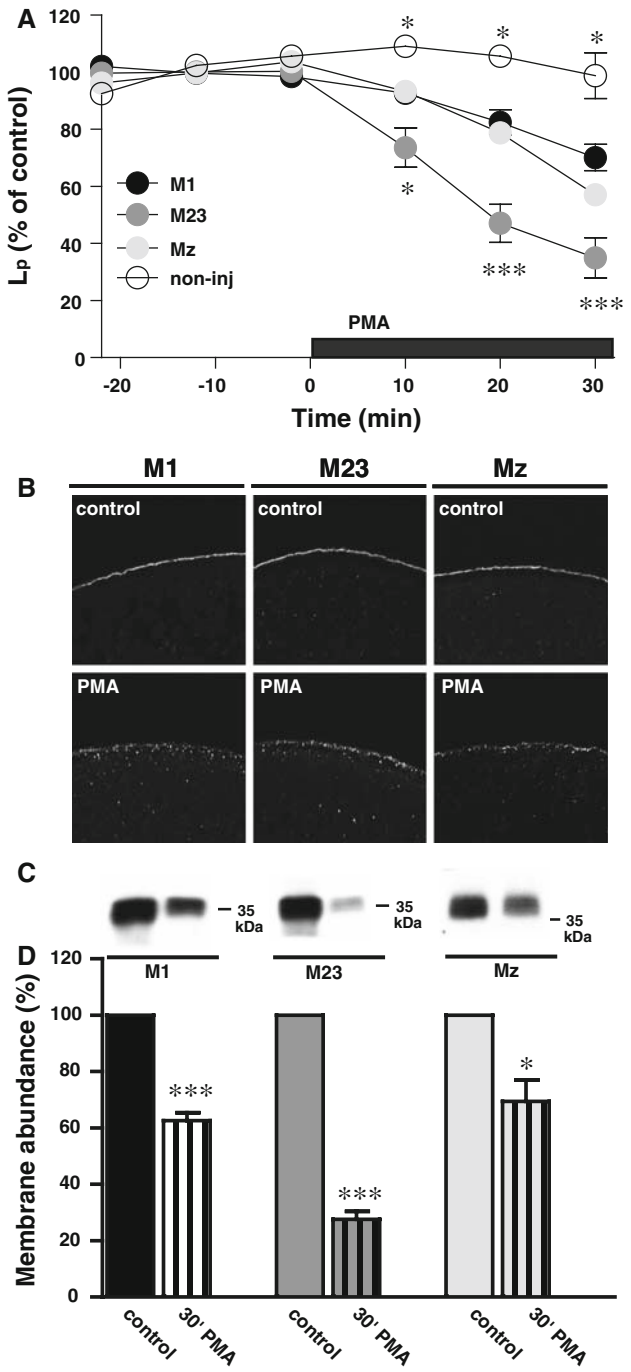

◀ **Fig. 6** PKC-dependent down-regulation of AQP4. **a** The relative water permeability of oocytes expressing M1, M23, or Mz or non-injected oocytes as a function of time. 1 nM PMA was included in the external solution as marked by the *black bar*. After 30 min of PMA treatment, the L_p was reduced to (in % of control) for M1; 70 ± 5 ($n = 8$), M23; 35 ± 7 ($n = 7$), Mz; 57 ± 4, error bar within the symbol ($n = 9$), and non-injected; 99 ± 8 ($n = 3$). The significance levels on the graph refer to M1, $^*P < 0.05$, $^{***}P < 0.001$. **b** Representative confocal laser scanning microscopy of oocytes expressing M1, M23, and Mz immunolabeled for AQP4 without (*upper panels*) or with (*lower panels*) 30 min PMA treatment (1 nM). **c** Representative immunoblot of plasma membrane purification of oocytes expressing M1, M23, or Mz in control condition and after 30 min of PMA treatment (1 nM), minimum 15 oocytes for each condition. **d** Relative membrane abundance of M1, M23, and Mz was assessed by densitometry of the immunoblots as presented in panel (**c**) of oocytes with control treatment or 30 min PMA treatment (1 nM). 15–20 oocytes were used for each condition ($n = 3$ experiments), $^*P < 0.05$, $^{***}P < 0.001$. The M23-expressing oocytes had a significantly lower AQP4 abundance in the plasma membrane after PMA treatment compared to M1 and Mz, $P < 0.01$

for M1 ($n = 8$), 1.40 ± 0.15 for M23 ($n = 8$), 1.19 ± 0.08 for Mz ($n = 9$), and 0.05 ± 0.01 for non-injected oocytes ($n = 3$). Figure 6a shows the PMA-dependent reduction of the L_p for the various isoforms of AQP4. The water permeability of oocytes expressing the three isoforms were down-regulated in response to PMA, but M23-expressing oocytes showed a faster and more pronounced down-regulation than M1- and Mz-expressing oocytes, with the non-injected oocytes being insensitive to PMA treatment. The significance levels on the graph refer to the M1 isoform. After 30 min of PMA treatment, the L_p was (in % of control); 70 ± 5 ($n = 8$) for M1, 35 ± 7 ($n = 7$) for M23, 57 ± 4 ($n = 9$) for Mz, and 99 ± 8 ($n = 3$) for the non-injected oocytes. To visualize the predicted PMA-dependent internalization of AQP4, immunocytochemistry was performed with the C-terminal anti-AQP4 antibody on oocytes expressing M1, M23, or Mz incubated for 30 min in control solution with or without 1 nM PMA ($n = 11$–14 of each). Representative confocal images clearly demonstrate appearance of AQP4 in intracellular vesicles, indicating PMA-dependent internalization of all three isoforms (Fig. 6b). In order to quantify the level of internalization, we prepared purified plasma membranes of M1-, M23-, and Mz-expressing oocytes after 30 min incubation in control solution with or without 1 nM PMA. The purified plasma membranes were immunoblotted with the anti-AQP4 antibody, representatives of which are shown in Fig. 6c. A summary of the densitometry is shown in Fig. 6d. After 30 min of PMA treatment, the amount of AQP4 left in the plasma membrane (in % of control) was 63 ± 3 for M1, 28 ± 3 for M23, and 69 ± 8 for Mz ($n = 3$ experiments with 15–20 oocytes for each condition per experiment). For all isoforms, PMA-dependent reduction in plasma membrane abundance was significantly different from control ($P < 0.001$ for M1 and M23 and $P < 0.05$ for Mz) and the PMA-dependent internalization of M23 was in addition significantly more pronounced than that of M1 and Mz ($P < 0.01$). PMA reduced the water permeability (Fig. 6a) and the membrane abundance of AQP4 (Fig. 6d) to the same extent for all three isoforms, suggesting that the effect of PKC on AQP4 may be due to the level of AQP4 internalization and not to a direct effect on channel function.

Discussion

In the present study, we investigated functional parameters of three isoforms of AQP4. All three isoforms were strictly permeable to water and did not allow permeation of smaller osmolytes, which is in agreement with previous studies performed on M1 and/or M23 [13, 34, 37], but has not previously been shown for Mz. The water permeability did not alter with the membrane potential and electrophysiological experiments were unable to detect any ionic conductance through either of the three isoforms (data not shown).

The large square arrays observed in freeze fracture replicas of perivascular glial endfeet [17] can be reconstituted in cell-line models by transfection of the M23 isoform of AQP4 [16, 18]. To validate the *Xenopus* expression system used here for functional comparison of AQP4 isoforms, it was necessary to investigate the formation of square arrays in this cell type. To this end, we performed freeze fracture studies of oocytes expressing the three isoforms. Expression of the M23 isoform in oocytes gave rise to square arrays, while the M1 or Mz failed to induce the formation of these higher order structures. To exclude the possibility that putative square arrays could have been overlooked in the M1- and Mz-expressing oocytes due to the membrane invaginations [28], we employed a newly developed biochemical assay for studying higher order AQP4 structures, BN-PAGE [20]. This method confirmed that M23, but not M1 and Mz, was organized in the high-molecular weight complexes when expressed in either *Xenopus* oocytes or HeLa cells. Taken together, our freeze fracture and BN-PAGE experiments validated our use of *Xenopus* oocytes for functional analysis of the three AQP4 isoforms.

The relative unit water permeability of the M1 and M23 isoforms has been debated in several studies. Experiments using heterologous expression of M1 and M23 in *Xenopus* oocytes have demonstrated identical water permeability of oocytes expressing M1 or M23 [13, 15], although the membrane abundance of AQP4 was not quantified in these studies. A conflicting study has reported an eightfold higher water permeability of the M23 isoform compared to the M1 isoform LLC-PK1 cells [25]. Comparative determination of the water permeability in the latter study may have been complicated by the large variability in size of the LLC-PK1 cells, which was dependent on the AQP4 isoform expressed, and the fact that the calculation of the water permeability was based on an assumption of the LLC-PK1 cells being spherical. In the present study, the overall water permeability of oocytes expressing the different AQP4 isoforms was similar, which is in agreement with the previous studies performed on *Xenopus* oocytes [13, 15]. In addition, the *total* abundance of AQP4 was similar for the three isoforms, although the M23 isoform had a significantly higher *plasma membrane* abundance compared to the other isoforms. The plasma membrane abundance was assessed with immunocytochemistry as well as with immunoblotting of purified plasma membranes to rule out possible isoform-specific differences in antibody binding, i.e., steric hindrance upon square array formation. Relating the water permeability of M1-, M23-, and Mz-expressing oocytes to the amount of AQP4 in the plasma membrane revealed that the relative unit water permeability of the M23 isoform was $\sim$40% lower than that of M1 while Mz was intermediate in its water permeability ($\sim$20% lower than M1).

To exclude the possibility that the lower relative water permeability of M23 was specific to the oocyte expression system, the difference between the water permeability of M1 and M23 was investigated in a mammalian expression system. In these experiments, the maximal water permeability of M23-expressing cells was also lower than that of M1-expressing cells, which is in agreement with our oocyte data. However, the membrane abundance of the two isoforms was not quantified in this set of data nor in a previous study on COS-7 cells transfected with c-myc-tagged M1 or M23 [19] in which a similar result was obtained. Taken together, in contrast to [25], but in agreement with [19], our results suggest that the unit water permeability of M23 is lower than the other isoforms.

In astrocytes and retinal Müller cells, AQP4 is extensively co-localized with the inwardly rectifying K^+ channel Kir4.1 [38, 39]. The co-localization of a K^+ channel with an aquaporin has warranted suggestions that AQP4 might facilite K^+ clearance from the perisynaptic space [38, 39]. To that effect, it has indeed been shown that mice lacking either AQP4 itself [40] or the endfoot-specific localization of AQP4 [41] had a slower K^+ clearance and therefore more intense and longer lasting experimentally induced seizures. However, the functional characteristics of Kir4.1 in freshly isolated glial cells were not altered by genetic deletion of AQP4, which suggests that Kir4.1 is not directly affected by its co-localization with AQP4 [42, 43]. Our recent studies showed that Kir4.1 was activated by cell swelling, and that AQP4 thereby may pose an indirect effect on the activity of Kir4.1 [44]. The question then arose if the water permeability of AQP4 could be affected by the increase in external K^+ concentration that inevitably leads to glial cell swelling [45, 46]. Increasing the K^+ concentration in the test solution from 2 to 8 mM did not alter the water permeability of M1-, M23-, or Mz-expressing oocytes, which bears evidence of AQP4 being insensitive to increase in external K^+ concentration (at least in the range tested).

AQP4 is regulated by several protein kinases with various effects on the protein, such as gating, internalization,

trafficking to the plasma membrane, and lysosomal targeting [5–11]. PKC has been shown to phosphorylate AQP4 directly in rat brain homogenate [8] and in AQP4-expressing glioma cells [36], although this was not apparent in mouse primary cultured astrocytes [9]. PKC activation down-regulates the water permeability of AQP4 expressed in a mammalian cell line, glioma cells, or in *Xenopus* oocytes [8, 11, 35, 36]. We recently showed that the PKC-dependent reduction of the water permeability of AQP4-expressing *Xenopus* oocytes was due to internalization of AQP4 [35]. In the present study, it was evident that the water permeability of the M23-expressing oocytes was significantly more sensitive to PKC activation than oocytes expressing the longer isoforms. Importantly, PKC-dependent AQP4 internalization was also more prominent with the M23 isoform. There was no significant difference between the PMA-dependent reduction in water permeability and the PMA-dependent level of internalization for any of the three isoforms, suggesting that the effect of PKC on AQP4 is primarily due to the level of AQP4 internalization and not to a direct effect on channel function. The increased PKC sensitivity of the M23 isoform suggests a function for the organization of AQP4 isoforms into large square arrays. One may speculate that, after phosphorylation of AQP4, the internalization machinery will be able to retrieve more units of AQP4 per unit of adaptor proteins if AQP4 is organized into square arrays. The more efficient internalization of large amounts of AQP4 with square arrays would thus increase dynamic regulation of AQP4 in vivo, and therefore we may have revealed the first functional rationale for maintaining the elaborate square arrays. Disruption of square arrays in the glial endfeet within minutes after the onset of cerebral ischemia has indeed been demonstrated [47–49], although a conflicting study identifies square arrays present in the astrocytic endfeet 60 min after the onset of hypoxia [50]. One may speculate whether the putative hypoxia-induced disruption of square arrays may be indicative of phosphorylation-dependent internalization of AQP4, i.e., via the G-protein coupled vasopressin receptor, $V1_aR$ [35].

Acknowledgments Technical assistance was provided by Charlotte G. Iversen, Mikkel Olsen, and Inger Merete Paulsen. The authors wish to give special thanks to Karen Thomsen for expert freeze fracture studies. The study was supported by the Nordic Centre of Excellence in Water-Imbalance Related Disorders, the Lundbeck Foundation (to N.M.), the Danish Medical Research Council (FSS) (to N.M., R.A.F.), E. Danielsen's Foundation (to N.M.), the Augustinus Foundation (to N.M.), the Michaelsen's Foundation (to N.M.), the Novo Nordisk Foundation (to R.A.F.), the Carlsberg Foundation (to R.A.F.) and the L'Oreal/UNESCO/Royal Danish Academy of Sciences Scholarship to Young Women in Science (to N.M.), Heart–Lung Foundation (to M.Z.), and the Functional genomics program of the Norwegian Research Council, FUGE (to T.H.). Additional funding to R.A.F was provided by a Marie Curie Intra-European Fellowship. The Water and Salt Research Center at the University of Aarhus is established and supported by the Danish National Research Foundation (Danmarks Grundforskningsfond).

References

1. Amiry-Moghaddam M, Ottersen OP (2003) The molecular basis of water transport in the brain. Nat Rev Neurosci 4:991–1001
2. Nielsen S, Nagelhus EA, Amiry-Moghaddam M, Bourque C, Agre P, Ottersen OP (1997) Specialized membrane domains for water transport in glial cells: high-resolution immunogold cytochemistry of aquaporin-4 in rat brain. J Neurosci 17:171–180
3. Noell S, Fallier-Becker P, Beyer C, Kroger S, Mack AF, Wolburg H (2007) Effects of agrin on the expression and distribution of the water channel protein aquaporin-4 and volume regulation in cultured astrocytes. Eur J Neurosci 26:2109–2118
4. Zador Z, Stiver S, Wang V, Manley GT (2009) Role of aquaporin-4 in cerebral edema and stroke. Handb Exp Pharmacol 190:159–170
5. Carmosino M, Procino G, Tamma G, Mannucci R, Svelto M, Valenti G (2007) Trafficking and phosphorylation dynamics of AQP4 in histamine-treated human gastric cells. Biol Cell 99:25–36
6. Gunnarson E, Axehult G, Baturina G, Zelenin S, Zelenina M, Aperia A (2005) Lead induces increased water permeability in astrocytes expressing aquaporin 4. Neuroscience 136:105–114
7. Gunnarson E, Zelenina M, Axehult G, Song Y, Bondar A, Krieger P, Brismar H, Zelenin S, Aperia A (2008) Identification of a molecular target for glutamate regulation of astrocyte water permeability. Glia 56:587–596
8. Han Z, Wax MB, Patil RV (1998) Regulation of aquaporin-4 water channels by phorbol ester-dependent protein phosphorylation. J Biol Chem 273:6001–6004
9. Kadohira I, Abe Y, Nuriya M, Sano K, Tsuji S, Arimitsu T, Yoshimura Y, Yasui M (2008) Phosphorylation in the C-terminal domain of aquaporin-4 is required for Golgi transition in primary cultured astrocytes. Biochem Biophys Res Commun 377:463–468
10. Madrid R, Le MS, Barrault MB, Janvier K, Benichou S, Merot J (2001) Polarized trafficking and surface expression of the AQP4 water channel are coordinated by serial and regulated interactions with different clathrin-adaptor complexes. EMBO J 20:7008–7021
11. Zelenina M, Zelenin S, Bondar AA, Brismar H, Aperia A (2002) Water permeability of aquaporin-4 is decreased by protein kinase C and dopamine. Am J Physiol Ren Physiol 283:F309–F318
12. Hasegawa H, Ma T, Skach W, Matthay MA, Verkman AS (1994) Molecular cloning of a mercurial-insensitive water channel expressed in selected water-transporting tissues. J Biol Chem 269:5497–5500
13. Jung JS, Bhat RV, Preston GM, Guggino WB, Baraban JM, Agre P (1994) Molecular characterization of an aquaporin cDNA from brain: Candidate osmoreceptor and regulator of water balance. Proc Natl Acad Sci USA 91:13052–13056
14. Moe SE, Sorbo JG, Sogaard R, Zeuthen T, Ottersen OP, Holen T (2008) New isoforms of rat aquaporin-4. Genomics 91:367–377
15. Neely JD, Christensen BM, Nielsen S, Agre P (1999) Heterotetrameric composition of aquaporin-4 water channels. Biochemistry 38:11156–11163
16. Furman CS, Gorelick-Feldman DA, Davidson KG, Neely Yasumura T, JD Agre P, Rash JE (2003) Aquaporin-4 square array assembly: opposing actions of M1 and M23 isoforms. Proc Natl Acad Sci USA 100:13609–13614
17. Rash JE, Yasumura T, Hudson CS, Agre P, Nielsen S (1998) Direct immunogold labeling of aquaporin-4 in square arrays of

astrocyte and ependymocyte plasma membranes in rat brain and spinal cord. Proc Natl Acad Sci USA 95:11981–11986
18. Yang B, Brown D, Verkman AS (1996) The mercurial insensitive water channel (AQP-4) forms orthogonal arrays in stably transfected Chinese hamster ovary cells. J Biol Chem 271:4577–4580
19. Crane JM, Van Hoek AN, Skach WR, Verkman AS (2008) Aquaporin-4 dynamics in orthogonal arrays in live cells visualized by quantum dot single particle tracking. Mol Biol Cell 19:3369–3378
20. Sorbo JG, Moe SE, Ottersen OP, Holen T (2008) The molecular composition of square arrays. Biochemistry 47:2631–2637
21. Strand L, Moe SE, Solbu TT, Vaadal M, Holen T (2009) Roles of aquaporin-4 isoforms and amino acids in square array assembly. Biochemistry 48:5785–5793
22. Suzuki H, Nishikawa K, Hiroaki Y, Fujiyoshi Y (2008) Formation of aquaporin-4 arrays is inhibited by palmitoylation of N-terminal cysteine residues. Biochim Biophys Acta 1778:1181–1189
23. Crane JM, Verkman AS (2009) Determinants of aquaporin-4 assembly in orthogonal arrays revealed by live-cell single-molecule fluorescence imaging. J Cell Sci 122:813–821
24. Hiroaki Y, Tani K, Kamegawa A, Gyobu N, Nishikawa K, Suzuki H, Walz T, Sasaki S, Mitsuoka K, Kimura K, Mizoguchi A, Fujiyoshi Y (2006) Implications of the aquaporin-4 structure on array formation and cell adhesion. J Mol Biol 355:628–639
25. Silberstein C, Bouley R, Huang Y, Fang P, Pastor-Soler N, Brown D, Van Hoek AN (2004) Membrane organization and function of M1 and M23 isoforms of aquaporin-4 in epithelial cells. Am J Physiol Ren Physiol 287:F501–F511
26. Zeidel ML, Nielsen S, Smith BL, Ambudkar SV, Maunsbach AB, Agre P (1994) Ultrastructure, pharmacologic inhibition, and transport selectivity of aquaporin channel-forming integral protein in proteoliposomes. Biochemistry 33:1606–1615
27. Zeuthen T, Belhage B, Zeuthen E (2006) Water transport by Na+-coupled cotransporters of glucose (SGLT1) and of iodide (NIS). The dependence of substrate size studied at high resolution. J Physiol 570:485–499
28. Zampighi GA, Kreman M, Boorer KJ, Loo DD, Bezanilla F, Chandy G, Hall JE, Wright EM (1995) A method for determining the unitary functional capacity of cloned channels and transporters expressed in *Xenopus laevis* oocytes. J Membr Biol 148:65–78
29. Leduc-Nadeau A, Lahjouji K, Bissonnette P, Lapointe JY, Bichet DG (2007) Elaboration of a novel technique for purification of plasma membranes from *Xenopus laevis* oocytes. Am J Physiol Cell Physiol 292:C1132–C1136
30. Moeller HB, MacAulay N, Knepper MA, Fenton RA (2009) Role of multiple phosphorylation sites in the COOH-terminal tail of aquaporin-2 for water transport: evidence against channel gating. Am J Physiol Ren Physiol 296:F649–F657
31. Fenton RA, Brond L, Nielsen S, Praetorius J (2007) Cellular and subcellular distribution of the type-2 vasopressin receptor in the kidney. Am J Physiol Ren Physiol 293:F748–F760
32. Zelenina M, Bondar AA, Zelenin S, Aperia A (2003) Nickel and extracellular acidification inhibit the water permeability of human aquaporin-3 in lung epithelial cells. J Biol Chem 278:30037–30043
33. Zelenina M, Brismar H (2000) Osmotic water permeability measurements using confocal laser scanning microscopy. Eur Biophys J 29:165–171
34. Yang B, Verkman AS (1997) Water and glycerol permeabilities of aquaporin 1–5 and MIP determined quantitatively by expression of epitope-tagged constructs in *Xenopus* oocytes. J Biol Chem 272:16140–16146
35. Moeller HB, Fenton RA, Zeuthen T, MacAulay N (2009) Vasopressin-dependent short-term regulation of AQP4 expressed in *Xenopus* oocytes. Neuroscience 164:1674–1684
36. McCoy ES, Haas BR, Sontheimer H (2009) Water permeability through aquaporin-4 is regulated by protein kinase C and becomes rate-limiting for glioma invasion. Neuroscience (in press)
37. Meinild AK, Klaerke DA, Zeuthen T (1998) Bidirectional water fluxes and specificity for small hydrophilic molecules in aquaporins 0–5. J Biol Chem 273:32446–32451
38. Nagelhus EA, Horio Y, Inanobe A, Fujita A, Haug FM, Nielsen S, Kurachi Y, Ottersen OP (1999) Immunogold evidence suggests that coupling of K+ siphoning and water transport in rat retinal Muller cells is mediated by a coenrichment of Kir4.1 and AQP4 in specific membrane domains. Glia 26:47–54
39. Nagelhus EA, Mathiisen TM, Ottersen OP (2004) Aquaporin-4 in the central nervous system: cellular and subcellular distribution and coexpression with KIR4.1. Neuroscience 129:905–913
40. Binder DK, Yao X, Zador Z, Sick TJ, Verkman AS, Manley GT (2006) Increased seizure duration and slowed potassium kinetics in mice lacking aquaporin-4 water channels. Glia 53:631–636
41. Amiry-Moghaddam M, Williamson A, Palomba M, Eid T, de Lanerolle NC, Nagelhus EA, Adams ME, Froehner SC, Agre P, Ottersen OP (2003) Delayed K+ clearance associated with aquaporin-4 mislocalization: phenotypic defects in brains of alpha-syntrophin-null mice. Proc Natl Acad Sci USA 100:13615–13620
42. Ruiz-Ederra J, Zhang H, Verkman AS (2007) Evidence against functional interaction between aquaporin-4 water channels and Kir4.1 potassium channels in retinal Muller cells. J Biol Chem 282:21866–21872
43. Zhang H, Verkman AS (2008) Aquaporin-4 independent Kir4.1 K+ channel function in brain glial cells. Mol Cell Neurosci 37:1–10
44. Soe R, MacAulay N, Klaerke DA (2009) Modulation of Kir4.1 and Kir4.1-Kir5.1 channels by small changes in cell volume. Neurosci Lett 457:80–84
45. MacVicar BA, Feighan D, Brown A, Ransom B (2002) Intrinsic optical signals in the rat optic nerve: role for K(+) uptake via NKCC1 and swelling of astrocytes. Glia 37:114–123
46. Walz W, Hinks EC (1985) Carrier-mediated KCl accumulation accompanied by water movements is involved in the control of physiological K+ levels by astrocytes. Brain Res 343:44–51
47. Cuevas P, Gutierrez Diaz JA, Dujovny M, Diaz FG, Ausman JI (1985) Disturbance of plasmalemmal astrocytic assemblies in focal and selective cerebral ischemia. Anat Embryol (Berl) 172:171–175
48. Landis DM, Reese TS (1981) Astrocyte membrane structure: changes after circulatory arrest. J Cell Biol 88:660–663
49. Suzuki M, Iwasaki Y, Yamamoto T, Konno H, Yoshimoto T, Suzuki J (1984) Disintegration of orthogonal arrays in perivascular astrocytic processes as an early event in acute global ischemia. Brain Res 300:141–145
50. Neuhaus J, Schmid EM, Wolburg H (1990) Stability of orthogonal arrays of particles in murine skeletal muscle and astrocytes after circulatory arrest, and human gliomas. Neurosci Lett 109:163–168